



HAL
open science

Irradiation creep in materials

Fabien Onimus, Thomas Jourdan, Cheng Xu, Anne A. Campbell, Malcolm Griffiths

► **To cite this version:**

Fabien Onimus, Thomas Jourdan, Cheng Xu, Anne A. Campbell, Malcolm Griffiths. Irradiation creep in materials. R. Konings; R. Stoller. *Comprehensive Nuclear Materials*, 1, Elsevier, pp.310-366, 2021, 978-0-08-102866-7. 10.1016/B978-0-12-803581-8.11645-5 . hal-04065942v2

HAL Id: hal-04065942

<https://hal.science/hal-04065942v2>

Submitted on 13 Apr 2023

HAL is a multi-disciplinary open access archive for the deposit and dissemination of scientific research documents, whether they are published or not. The documents may come from teaching and research institutions in France or abroad, or from public or private research centers.

L'archive ouverte pluridisciplinaire **HAL**, est destinée au dépôt et à la diffusion de documents scientifiques de niveau recherche, publiés ou non, émanant des établissements d'enseignement et de recherche français ou étrangers, des laboratoires publics ou privés.

F. Onimus, T. Jourdan, C. Xu, A.A. Campbell, M. Griffiths (2020) Irradiation creep in materials, Chapter 1.10 in : Comprehensive Nuclear Materials, Elsevier, 2nd Ed., R. Konings, R. Stoller Eds, Vol. 1, pp. 310-366. <https://doi.org/10.1016/B978-0-12-803581-8.11645-5>

Irradiation creep in materials

Fabien Onimus, CEA, Service de Recherches Métallurgiques Appliquées, Université Paris-Saclay, F-91191, Gif-sur-Yvette, France ; fabien.onimus@cea.fr

Thomas Jourdan, CEA, Service de Recherches de Métallurgie Physique, Université Paris-Saclay, F-91191, Gif-sur-Yvette, France ; thomas.jourdan@cea.fr

Cheng Xu, TerraPower, LLC, 15800 Northup Way, Bellevue, WA 98008 USA; cxu@terrapower.com

Anne A. Campbell, Oak Ridge National Laboratory, Materials Science & Technology Division, Oak Ridge, TN 37831, USA; campbellaa@ornl.gov

Malcolm Griffiths, Faculty of Engineering and Applied Science, Queen's University, Kingston, Ontario K7L 3N6, Canada; malcolm.griffiths@queensu.ca

Keywords: creep, irradiation, dislocation, point defects, diffusion, climb, glide, loop, austenitic stainless steel, zirconium alloys, ferritic steel, ferritic-martensitic steel, nickel based alloys, graphite

Synopsis:

A knowledge of the dimensional stability of reactor structural components, under irradiation conditions, is of major importance in the design of thermal, fast, and fusion reactors. When subjected to simultaneous mechanical loading and irradiation, structural materials exhibit a visco-plastic deformation phenomenon, referred to as irradiation creep, which can be more rapid than the deformation occurring out of irradiation. In this chapter, the phenomenology of this peculiar behavior is described after a short history of its discovery. Then, the theoretical mechanisms proposed in the literature during these past 60 years are presented, with a special focus on mechanisms based on stress induced preferred absorption of point defects by dislocation loops, dislocations and grain boundaries and on mechanisms based on climb-enhanced glide of dislocations. These mechanisms are discussed in the light of experimental evidences. Finally, irradiation creep in various materials, such as zirconium alloys, austenitic stainless steels, nickel-based alloys, ferritic-martensitic steels and graphite, is described.

1 Introduction

A knowledge of the dimensional stability of reactor structural components, under irradiation conditions, is of major importance in the design of thermal, fast, and fusion reactors. Out of reactor, materials usually exhibit long-term creep deformation when a small constant load is applied (below the yield stress) at a temperature higher than $T \geq 0.3T_m$ (T_m : melting temperature). This phenomenon is referred to as “thermal creep”. During reactor operation, materials subjected to simultaneous fast neutron irradiation and constant applied load also exhibit creep deformation. Depending on the applied stress, temperature and neutron flux, the in-reactor creep rate can be significantly higher than the out-of-reactor thermal creep rate of the unirradiated material, with the creep rate increasing as the neutron flux increases. This surprising deformation phenomenon, activated by the neutron flux, is called irradiation creep.

1.1 Historical perspective

After the building of the first nuclear reactors during the 1940's and 1950's, the effect of irradiation on the in-reactor creep deformation was discovered on fissionable materials (Konobeevsky, et al., 1955) (Roberts & Cottrell, 1956) and then was studied on a variety of structural materials. However, these studies showed little or no effect of irradiation on their creep behavior, primarily because of the low neutron fluxes employed, the high temperature often used and also the simple instrumentation available (Schoeck, 1958) (Joseph, 1959) (Franklin, et al., 1983). During the early 1960's, the irradiation creep phenomenon was discovered on non-fissile structural materials (Mosedale, 1962) (Hesketh, 1963) (Taylor & Jeffs, 1966) (Lewthwaite, 1967). Then, from this discovery, many studies were dedicated to irradiation creep on various materials. During the 1980's many data became available and review papers were published. From the 1990's up to now, rather few institutes continued to carry on systematic studies of irradiation creep. Only five to ten articles per year were published on this subject from the 1990's, some of them dealing with nanocrystalline materials or other novel materials.

When considering articles published on the subject of irradiation creep, it can be noticed that a large body of papers deal with macroscopic in-reactor measurements, because of industrial needs. A few other experimental papers describe irradiation creep experiments under ion beam irradiation as a way to emulate neutron irradiation. A vast number of papers also describe theoretical models of irradiation creep mechanisms. Sometimes, both experimental and theoretical approaches can be found in the same article. Then, only very few articles describe experimental studies of the deformation mechanisms from a microstructural perspective.

Many non-fissile structural materials have been studied in the past. As graphite (Perks & Simmons, 1964), austenitic stainless steels (Lewthwaite, 1973) (Ehrlich, 1981) and zirconium alloys (Fidleris, 1988) (Franklin, et al., 1983) (Nichols, 1987) (Adamson, et al., 2019) became widely used as structural and cladding materials for high temperature gas-cooled reactors, fast breeder reactors or light and heavy water reactors, respectively, most of the available data concern these three materials. In addition, irradiation creep in nickel-based alloys (Taylor & Jeffs, 1966) and ferritic steels (Toloczko, et al., 1994) were also studied in detail for fast reactors or advanced reactor applications.

It should be emphasized that the number of articles published on this subject is considerable. A thorough review of this topic is thus difficult to achieve. In the following, a short overview of the general phenomenology of irradiation creep, at the macroscopic scale, is described. Then, a discussion on the categorization of irradiation creep mechanisms is provided. Several, but not all, irradiation creep mechanisms are described. Then a discussion along with experimental evidences is provided. In a last part, results concerning irradiation creep of various materials are presented and discussed.

1.2 Phenomenology of creep behavior under irradiation

It is usually considered, for practical purpose, that the in-pile deformation consists of the sum (equation 1) of (i) the classical thermally activated out-of-pile creep, or so-called thermal creep ($\dot{\epsilon}_{thermal-creep}$) and (ii) the irradiation creep ($\dot{\epsilon}_{irradiation-creep}$), strictly speaking. To these two deformation components, a third one can be added, which is the deformation under irradiation without any applied stress, such as swelling or growth ($\dot{\epsilon}_{swelling/growth}$) (Equation 1). This additive approach allows a simple macroscopic definition of each component of the total deformation, although it may not be relevant from the microscopic deformation mechanisms perspective.

$$\dot{\epsilon} = \dot{\epsilon}_{thermal-creep} + \dot{\epsilon}_{irradiation-creep} + \dot{\epsilon}_{swelling/growth} = \dot{\epsilon}_{creep} + \dot{\epsilon}_{swelling/growth} \quad [1]$$

The creep deformation under irradiation ($\dot{\epsilon}_{creep}$), which includes both the irradiation creep and the thermal creep, is the total strain subtracted from the swelling or growth strain ($\dot{\epsilon}_{creep} = \dot{\epsilon} - \dot{\epsilon}_{swelling/growth}$). Practically, the swelling or growth strain is measured on separate samples subjected to the same temperature and neutron flux without applied stress. For low enough stress and/or low enough temperature, the thermal creep remains low, and the creep strain measured under irradiation should only be due to irradiation creep. Some materials, such as austenitic stainless steels, exhibit a very low thermal creep in the temperature range of reactor operation. In that case, in-reactor creep is only the result of

irradiation-creep. However, in general, creep under irradiation is always a combination of thermal creep and irradiation creep.

It is difficult to give a clear definition of what is the thermal creep under irradiation since it is neither the thermal creep of the unirradiated material nor the thermal creep of the as-irradiated material. Indeed, during post-irradiation thermal creep, radiation damage recovery may occur. Because thermal creep under irradiation cannot be clearly defined, although it may be active under irradiation, depending on the material and the temperature and stress range, only the overall creep strain under irradiation is usually computed ($\dot{\epsilon}_{creep} = \dot{\epsilon} - \dot{\epsilon}_{swelling/growth}$).

While pure irradiation creep is activated by the neutron flux, causing the creep rate to increase, the thermal creep rate is strongly reduced by irradiation due to the irradiation-induced hardening. This last phenomenon is often called irradiation-retarded creep as opposed to irradiation creep, which is irradiation induced or irradiation enhanced. The irradiation-retarded creep is evidenced when the neutron flux is too low to induce significant irradiation creep but the accumulated radiation damage decreases or even suppresses the thermal creep (Adamson, et al., 2019) (Holt, 2008) (Singh, et al., 2004). This phenomenon can also be illustrated when out-of-reactor creep test is performed on irradiated samples. In that case, the thermal creep rate is significantly reduced (Soniak, et al., 2002).

In-reactor creep deformation is commonly analyzed by considering that the creep strain rate follows a power law of the stress (σ^n) multiplied by a power law of the neutron flux (φ^p) and multiplied by an Arrhenius term ($\exp(Q/RT)$) to account for the thermal activation of the deformation processes (equation 2) (Franklin, et al., 1983).

$$\dot{\epsilon}_{creep} = K_0 \sigma^n \varphi^p \exp\left(\frac{Q}{k_B T}\right) \quad [2]$$

In equation 2, K_0 is a constant, Q is the activation energy (in eV) and k_B the Boltzmann constant.

It is worth mentioning that this formula is not suitable to describe out-of-flux creep behaviour. Some authors have proposed to use unified phenomenological models to describe both out-of-reactor and in-reactor behaviour. These models assume the sum of the three components described above (equation 1) (Christodoulou, et al., 1996) (Holt, 2008). However, this requires some assumption on the thermal creep behaviour under irradiation.

Several types of mechanical tests (Adamson, et al., 2019), such as uniaxial and biaxial loading devices, are commonly used to assess the in-reactor creep deformation of materials. In the case of multiaxial stress

state tests, such as pre-pressurized closed-ended tubes, the analysis of the measure should be based on the use of stress and strain tensors needed to address the behaviour of a continuum medium in 3D. As with thermal creep, irradiation creep is governed by the deviatoric stress tensor. In the case of an isotropic behaviour, the influence of the biaxial stress state must be addressed by using a Von Mises equivalent stress, or by using a Hill equivalent stress in the case of an anisotropic behaviour (Franklin, et al., 1983). In that last case, the creep deformation along at least two directions for two different stress-states must be measured to deduce the three parameters of the Hill criterion (e.g. for a thin tube, ε_θ and ε_z must be measured during uniaxial creep tests along θ or along z).

Another convenient, but indirect, way to assess creep under irradiation is to use bent strips to measure the stress relaxation under irradiation. The stress in the sample is inhomogeneous; some parts are in tension and other in compression. From stress relaxation, the irradiation creep law can be deduced by using simple approach described by Causey et al. (Causey, et al., 1988) assuming that the stress exponent is equal to one. This technique is particularly useful for low ductility materials such as graphite.

From in-reactor tests, creep parameters such as the stress exponent, the flux exponent and the creep activation energy have been measured for various materials. Details concerning the in-reactor behavior of different materials are given at the end of this chapter. It is often acknowledged that for low applied stress a stress exponent close to $n = 1$ is relevant for most of materials. In the case of zirconium alloys, it is shown that as the applied stress increases the stress exponent increases. Because of the limited neutron flux range available in material testing reactor, the flux exponent is often difficult to determine accurately. However, a flux exponent close to $p = 1$, or slightly lower, is often deduced from the data. Concerning the activation energy Q , it is usually acknowledged that it is low, at least for low temperature and low applied stress, showing that irradiation creep is a nearly athermal phenomenon. In this situation, the irradiation creep constitutive law reduces to equation 3. In equation 3, the proportionality coefficient (B_0), which can be slightly temperature dependent, is called the irradiation creep compliance.

$$\dot{\varepsilon}_{creep} = B_0 \varphi \sigma \quad [3]$$

From a macroscopic perspective, irradiation creep thus appears to be rather simple (at least from the schematic picture provided above) as pointed out by Garner et al. (Garner, et al., 2011). But the microscopic mechanisms at the origin of this behavior are far from being well understood.

2 Irradiation creep deformation mechanisms

Detailed research or review articles, presenting several possible irradiation creep mechanisms, can be found in the literature. Some of them are listed in Table 1.

Table 1: Review or research articles presenting several possible irradiation creep mechanisms.

1975	Gittus (Gittus, 1975)
1980	Holt (Holt, 1980)
1980	Wolfer (Wolfer, 1980)
1980	Mansur and Reiley (Mansur & Reiley, 1980)
1983	Franklin et al. (Franklin, et al., 1983)
1987	Nichols (Nichols, 1987)
1988	Matthews and Finnis (Matthews & Finnis, 1988)
2007	Was (Was, 2007)
2008	Holt (Holt, 2008)
2015	Borodin et al. (Borodin, et al., 2015)
2016	Borodin (Borodin, 2016)

The reader willing to learn more on this complicated topic should go back to these early reviews. In the following, a concise overview of irradiation creep deformation mechanisms is presented, focusing on the basic processes with the help of a limited number of equations and some schematics.

2.1 Categorization of creep mechanisms

Under irradiation, incident particles, such as fast neutrons, induce atomic displacements. This creates a high concentration of point defects, vacancies and self-interstitial atoms, that are free to migrate. These point defects can cluster together creating various types of point defect clusters such as dislocation loops, stacking fault tetrahedra or cavities. These point defect clusters are usually very small, of the order of 5 to 10 nm and in very high density, from 10^{21} m^{-3} to 10^{23} m^{-3} . The point defects can also be annihilated on sinks, which are all microstructural features in the crystalline material where the point defects disappear. These sinks can be grain boundaries, dislocations or precipitates.

Many mechanisms have been proposed in the literature to explain irradiation creep deformation. All these mechanisms agree on the fact that irradiation creep deformation is related to the production of vacancies

and self-interstitial atoms (referred to as interstitials in the following) by incident radiation and how they redistribute under an applied stress. However, they differ in their descriptions of the detailed fate of these point defects. Indeed, at the very fine scale of crystalline defects, there are several ways to achieve mass redistribution under stress. Possibly several of these mechanisms could be active at the same time and they may be coupled. Several categorizations of creep mechanisms can be found in the literature.

In the case of thermal creep, the usual categorization is illustrated on a temperature-stress Ashby deformation map (Gittus, 1975) (Franklin, et al., 1983). On these maps, three domains are shown: i) the high temperature and low stress domain where so-called “diffusional creep” mechanisms bring a higher strain rate than other creep mechanisms. The medium stress and medium to high temperature domain, where ii) “dislocation creep” mechanisms overwhelm other mechanisms. At higher stress, above the yield stress, iii) conventional yielding visco-plasticity occurs by dislocation glide. The creep mechanisms are thus categorized into mechanisms involving dislocations (dislocation creep) and mechanisms that do not involve dislocation (diffusional creep).

Concerning irradiation creep, Franklin et al. (Franklin, et al., 1983) proposed to distinguish i) radiation-retarded creep mechanisms, ii) radiation-enhanced mechanisms and iii) radiation-induced mechanisms. Irradiation-induced creep mechanisms are those which operate in addition to thermal creep mechanisms. Irradiation-enhanced creep mechanisms are those which promote an acceleration of a normally operating thermal creep mechanism. Irradiation-retarded creep mechanisms result in an inhibition of thermal creep mechanisms.

In their thorough review, Franklin et al. (Franklin, et al., 1983) also provide a nice historical perspective of the theory of irradiation creep mechanisms (see also (Adamson, et al., 2019)). They point out that the theoretical work has mainly proceeded along two different paths. The radiation-enhanced climb-glide mechanism has been considered initially for zirconium alloys, whereas stress-induced preferred absorption (SIPA) mechanisms have been mostly explored for austenitic stainless. Then, as the theory improved, the mechanisms proposed for zirconium alloys have been applied to austenitic stainless steels and conversely.

The predominance of these two successful families of irradiation creep mechanisms in the literature suggests a new categorization of the mechanisms, depending on the main origin of the strain: i) the mass-transport-based mechanisms (essentially SIPA) when the strain is mainly the result of point defects diffusion, including dislocation climb; ii) the glide-based mechanisms, when the strain is mostly the result

of dislocation glide, including climb-assisted glide. This is the categorization that we will adopt in the following.

2.2 Mass-transport based mechanisms:

In this section, we review the irradiation creep mechanisms for which the strain results from point defect diffusion and their absorption on sinks. These mechanisms are all based on the difference of absorption rates of point defects by sinks, depending on their orientation with respect to stress. The strain may result from the flow of point defects to various elements of the microstructure: dislocations, dislocation loops, grain boundaries and surfaces. All these phenomena will be referred to as stress induced preferred absorption (SIPA) creep or mass-transport-based creep. Before reviewing these mechanisms, we focus on a very classical mechanism based on differential emission of vacancies, which is not a SIPA mechanism.

2.2.1 Differential emission of vacancies and radiation effects

This mechanism, often described in textbooks for high temperature thermal creep and low stress, is referred to as the Nabarro-Herring mechanism (Gittus, 1975). Within this model, it can be shown that the equilibrium vacancy atomic fraction (n_+) on a grain boundary perpendicular to a tensile applied stress (σ) (Figure 1a) is increased $n_+ = n_0 \exp(\frac{\sigma\Omega}{k_B T})$, whereas the equilibrium vacancy atomic fraction (n_-) close to the grain boundary perpendicular to a compressive applied stress is decreased $n_- = n_0 \exp(-\frac{\sigma\Omega}{k_B T})$. n_0 is the vacancy atomic fraction at thermodynamic equilibrium, which is equal to $n_0 = \exp(-\frac{\Delta G_f}{k_B T})$ where ΔG_f is the formation energy for a vacancy. Ω is the atomic volume, k_B is the Boltzmann constant. The vacancy concentration (per unit volume) at thermodynamic equilibrium is $C_0 = n_0/\Omega$. The vacancy concentration gradient $((n_+ - n_-)/d\Omega$ where d is the grain size) results in a vacancy flux which results in turn into a strain by mass-transport.

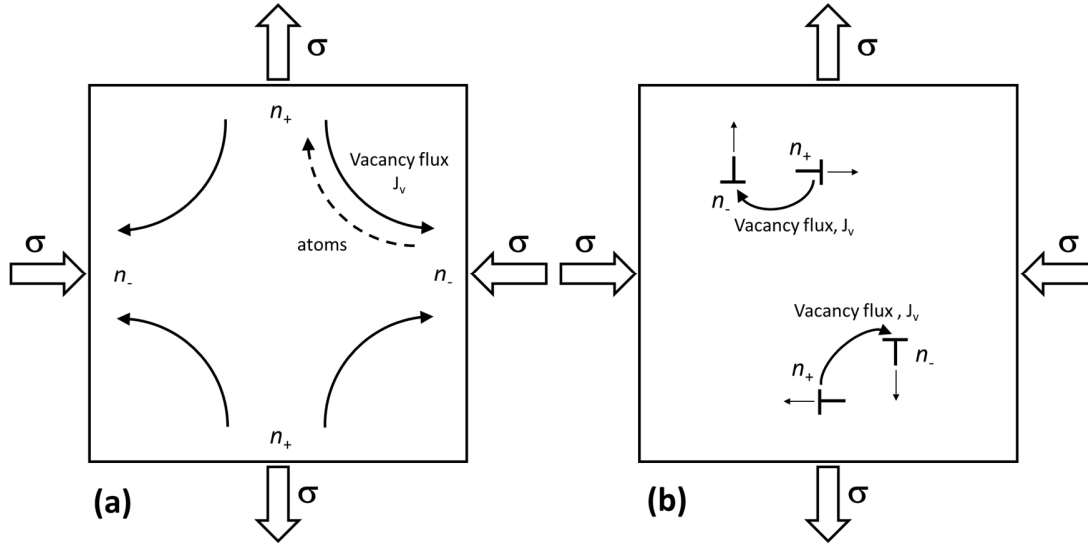


Figure 1: (a) The textbook case of Nabarro-Herring high temperature creep mechanism, (b) pure thermal climb of dislocations under stress by the Nabarro mechanism.

The net flux of vacancies per unit time and unit area (J_v) from one grain boundary to the other is given by Equation 4, where D_v is the diffusion coefficient of vacancies.

$$J_v = \frac{D_v n_0}{d\Omega} \left[\exp\left(\frac{\sigma\Omega}{k_B T}\right) - \exp\left(-\frac{\sigma\Omega}{k_B T}\right) \right] \quad [4]$$

The strain rate of the polycrystal is thus equal to

$$\dot{\epsilon} = \frac{J_v \Omega}{d} \quad [5]$$

For usual values of applied stress, we have $\sigma\Omega/k_B T \ll 1$, leading to a strain rate which is a linear function of the stress (Equation 6). In equation 6, D_{SD} is the self diffusion coefficient which is equal to $D_{SD} = D_v n_0$. A geometrical prefactor B is often added to this formula.

$$\dot{\epsilon} = 2 \frac{D_v n_0 \sigma \Omega}{d^2 k_B T} = 2 \frac{D_{SD} \sigma \Omega}{d^2 k_B T} \quad [6]$$

Very similar arguments can be applied to dislocations (Figure 1b) instead of grain boundaries. The vacancy concentration is increased around an edge dislocation with Burgers vector parallel to the tensile applied stress and is decreased around an edge dislocation with Burgers vector parallel to the compressive applied stress (and perpendicular to the tensile applied stress). This vacancy gradient results in vacancy flux from

one dislocation to the other leading to pure climb of edge dislocations (Nabarro creep) resulting in strain. The climb velocity of dislocations is given by Equation 7 (Gittus, 1975) (Was, 2007). In equation 7, R is the outer cut-off radius used in classical dislocation theory (with $R = 1/\sqrt{\pi\rho}$) and r_c is the inner cut-off radius which corresponds to the radius of the dislocation core.

$$v_c = \frac{2\pi D_{SD} \sigma \Omega}{bk_B T \ln\left(\frac{R}{r_c}\right)} \quad [7]$$

Since the strain rate is proportional to the mean dislocation velocity (v_c) and to the mobile dislocation density (ρ_m), owing to Orowan's law, the thermal creep strain rate is expressed as Equation 8.

$$\dot{\epsilon} = \rho_m b v_c = \rho_m \frac{2\pi D_{SD} \sigma \Omega}{k_B T \ln\left(\frac{R}{r_c}\right)} \quad [8]$$

If a dependence of the dislocation density as square of the stress is assumed ($\rho \propto \sigma^2$), as it is often done in the literature (Gittus, 1975), the Nabarro thermal creep model based on dislocation pure climb yields strain rate given by Equation 9, where A is a constant coefficient.

$$\dot{\epsilon} = A \frac{D_{SD} \sigma^3 \Omega}{k_B T} \quad [9]$$

Because irradiation increases the vacancy concentration by several orders of magnitude, it has been originally thought (Schoeck, 1958) that this could be the reason for radiation-enhanced creep. However, since in these models the creep rate is proportional to the vacancy concentration gradient only which is due to the difference in the equilibrium concentration near dislocations, it has rapidly been recognized (Mosedale, 1962) (Duffin & Nichols, 1973) that irradiation does not affect the vacancy gradient between various sinks subjected to stress but only the overall vacancy concentration. Irradiation creep is thus not due to the increase of vacancy concentration only.

Irradiation creep based on mass transport is in fact due to the presence of both interstitials and vacancies in very high supersaturation and how they are absorbed, under stress, on the various sinks present in the microstructure. One important class of mechanisms is based on the fact that the applied stress affects the differential absorption (Stress Induced Preferential Absorption or SIPA) of vacancies and interstitials on various sinks. To understand the origin of this differential absorption under stress we need to go back to the fundamentals of the interaction of point defects with elastic fields.

2.2.2 Interaction of point defects with elastic fields – flow of defects to sinks

For our purpose, a point defect is conveniently represented, from an elastic point of view, as a distribution of point forces localized on the neighboring atoms. The associated dipole tensor P_{ij} is in general a sufficient approximation for the modeling of interaction energies with slowly varying elastic fields (Siems, 1968). To this lowest order, the interaction energy with a strain field ε_{ij} reads

$$E(\mathbf{r}) = -P_{ij}\varepsilon_{ij}(\mathbf{r}), \quad [10]$$

where \mathbf{r} is the location of the defect. Summation on repeated indexes is implied in all equations.

Values of dipole tensors of point defects are now routinely obtained by atomistic calculations (Varvenne & Clouet, 2017). Dipole tensors of point defects are in general different at stable and at saddle positions. For example, a vacancy in bcc and fcc metals is isotropic at stable position but anisotropic at saddle position. The components of its dipole tensor at saddle position depend on the jump direction.

In the case where the point defect is isotropic, the dipole tensor can be simply expressed by a single value which is proportional to the relaxation volume (ΔV). For cubic materials, this dipole tensor is expressed as $P_{ij} = K\Delta V\delta_{ij}$ where K is the bulk modulus and δ_{ij} is the Kronecker symbol. In general the relaxation volume of interstitials is significantly higher, in absolute value, than that of vacancies ($|\Delta V_i| > |\Delta V_v|$). Therefore, the interaction energy between a dislocation, or more generally a strain field, and an interstitial is higher than with a vacancy. This effect will be referred to as the elastic interaction difference (EID) in the following (Woo, 1988).

A defect can be polarized by the elastic field, so that more generally, its dipole tensor is given by

$$P_{ij}(\boldsymbol{\varepsilon}(\mathbf{r})) = P_{ij} + \alpha_{ijkl}\varepsilon_{kl}(\mathbf{r}), \quad [11]$$

where α_{ijkl} is the diaelastic polarizability of the defect (Trinkaus, 1975) (Leibfried & Breuer, 1978). The associated interaction energy is

$$E(\mathbf{r}) = -P_{ij}\varepsilon_{ij}(\mathbf{r}) - \frac{1}{2}\varepsilon_{ij}(\mathbf{r})\alpha_{ijkl}\varepsilon_{kl}(\mathbf{r}). \quad [12]$$

Polarizabilities are still poorly known. Qualitative estimates based on the Eshelby inclusion were first proposed (Heald & Speight, 1974). Only a few calculations with empirical potential calculations have been performed (Dederichs, et al., 1978) (Schober, 1984) (Woo & Puls, 1985) (Ackland, 1988).

Dederichs and Schroeder have shown that the flux of point defects can be written as a function of a renormalized diffusion tensor (Dederichs & Schroeder, 1978). For example, in the simple case of a defect with only one stable configuration (such as a vacancy) in a cubic material, the components of this diffusion tensor are

$$\tilde{D}_{ij}(\mathbf{r}) = \frac{1}{2} \nu \sum_{\mathbf{h}} h_i h_j \exp\left(-\frac{E_{\mathbf{h}}^{\text{sad}}(\mathbf{r})}{k_B T}\right), \quad [13]$$

where ν is the jump frequency in the absence of any elastic field, \mathbf{h} is the jump vector, $E_{\mathbf{h}}^{\text{sad}}$ is the interaction energy at saddle position for jump \mathbf{h} (Eqs 10 and 12). The dependency of the saddle point energy on the jump vector comes from the anisotropic character of the dipole tensor: under certain stress conditions, Eq. 10 leads to different values for different jump directions. This lowering of the symmetry gives rise to anisotropic diffusion, a phenomenon often referred to as elasto-diffusion. For example, in bcc and fcc metals under uniaxial tensile stress, a vacancy preferentially migrates in a plane orthogonal to the tensile direction (Woo, 1984).

2.2.3 SIPA-I mechanisms

SIPA-I was the first diffusional model to explain steady state irradiation creep. It is due to polarizability effects (Heald & Speight, 1974) (Bullough & Willis, 1975) (Wolfer & Ashkin, 1976). Initially this model was simply called SIPA, but it was renamed SIPA-I (Savino & Tomé, 1982) as other sources of preferential absorption were identified. Within this model, dislocations absorb more or less defects, depending on the orientation of their Burgers vector with respect to stress. A schematic picture of this mechanism can be proposed by considering a dislocation population with a random distribution of Burgers vector orientations in the crystal (Fig. 2a). Edge dislocations absorb more interstitials than vacancies because of the EID effect, leading to an isotropic climb of all dislocations ($v_2 = v_1$). This produces no net strain. However, this requires the presence of other sinks with smaller EID effect, such as grain boundaries (GB) or cavities, in order to absorb vacancies in excess (Duffin & Nichols, 1973). If there is no other sink, edge dislocations absorb as many vacancies as interstitials and there is no dislocation climb.

Under an applied stress, the interaction between dislocations and point defects is modified. For dislocations with Burgers vectors parallel to the tensile applied stress (Fig. 2b), the net flux of interstitial is increased, whereas it is decreased for dislocations with Burgers vector parallel to the compressive direction. The difference of climb velocities ($v_2 - v_1$) gives rise to a positive creep strain rate in the

direction of the tensile applied stress ($\dot{\epsilon} = \rho b(v_2 - v_1)$, assuming equal density for both types of dislocations) and to a negative strain in the direction of the compressive stress since $v_2 > v_1$.

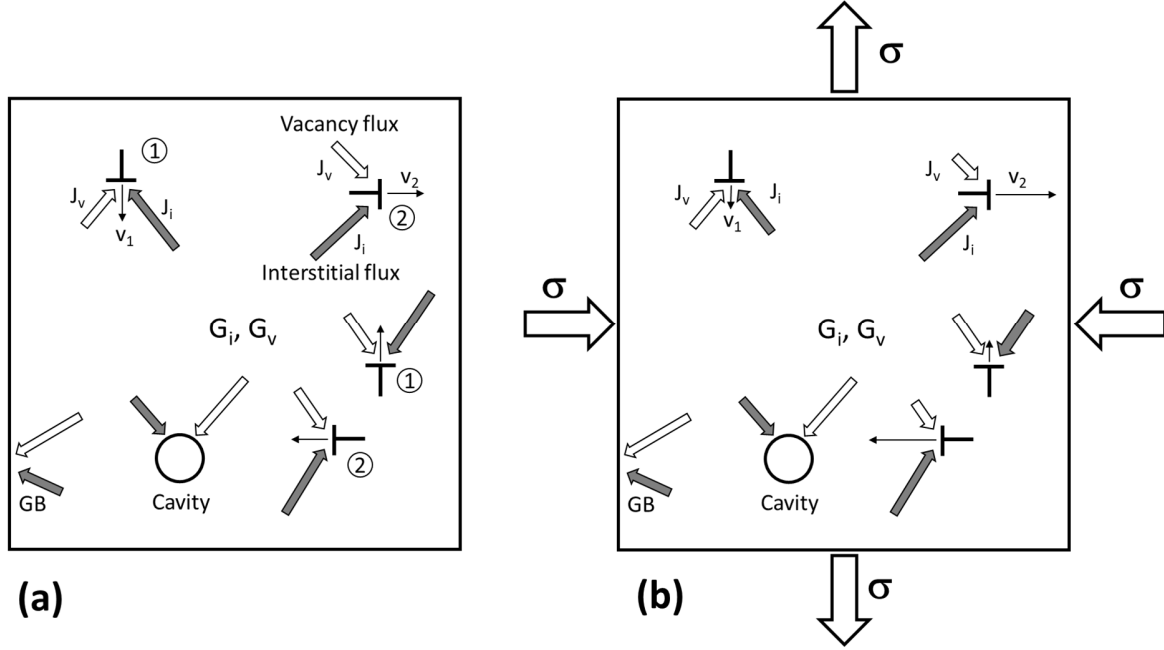


Figure 2: a) flux of point defects to dislocations and neutral sinks (grain boundaries and cavities) under irradiation, b) influence of the applied stress on the flux of point defects under irradiation (SIPA-I mechanism), explaining irradiation creep. The length of the arrows is proportional to the flux of point defects to the sinks. G_i and G_v are respectively the creation rates of interstitials and vacancies due to irradiation.

From a more detailed theoretical point of view, SIPA-I phenomenon arises in the formula when expressing the saddle point energy to second order in strain. The local strain is the sum of the applied external field (ϵ^e) and the internal field created by dislocations (ϵ^d). The interaction energy is thus

$$E_h^{\text{sad}}(\mathbf{r}) = -P_{h,ij}^{\text{sad}} \left(\epsilon_{ij}^e(\mathbf{r}) + \epsilon_{ij}^d(\mathbf{r}) \right) - \epsilon_{ij}^e(\mathbf{r}) \alpha_{h,ijkl}^{\text{sad}} \epsilon_{ij}^d(\mathbf{r}) + \text{other terms in } (\epsilon^e)^2 \text{ and } (\epsilon^d)^2 \quad [14]$$

One sees that the second term, in $\epsilon_{ij}^e(\mathbf{r}) \epsilon_{ij}^d(\mathbf{r})$, introduces a coupling between the external field and the dislocation field. In other words, under stress the diffusion coefficient, so the flux of point defects, may be different close to dislocations with different Burgers vector orientations. The term responsible for SIPA-

Γ is proportional to polarizabilities at saddle point position, which have been rarely calculated (Schober, 1984).

2.2.4 SIPA-AD (elasto-diffusion) mechanisms

Later it was proposed that anisotropic flow of point defects towards dislocations could be explained without resorting to polarizabilities (Dederichs & Schroeder, 1978) (Savino, 1977). Indeed, by expanding the exponential in Eq. 13 up to first order in ε^e , a term proportional to $\varepsilon^e \varepsilon^d$ and to the product of dipole tensor components arises, which can therefore bias the diffusion depending on the coupling between the external and the dislocation stress fields.

Additional studies (Tomé, et al., 1982) (Skinner & Woo, 1984) revealed that there was in fact another contribution to the absorption bias, which is larger than this mechanism. This is the actual SIPA-AD mechanism. As discussed previously, for a uniaxial tensile stress state vacancies tend to diffuse preferentially in the plane orthogonal to the stress direction, whereas interstitials behave the opposite way. This diffusion anisotropy is responsible for the higher absorption rate of vacancies by dislocations whose line direction lies along the stress direction (the opposite is obtained for interstitials). To understand how this phenomenon can lead to a net strain in the appropriate direction, it has to be kept in mind that only edge dislocation segments can climb (including edge kinks on a mixed dislocation). With this knowledge, it can be noticed that the lines of edge dislocations with Burgers vector parallel to the tensile direction (indicated as 1 in Fig. 3), which will produce the strain along the tensile direction, all lie in the plane perpendicular to the applied tensile stress (Fig. 3). On the other hand, the lines of edge dislocations with Burgers vectors perpendicular to the tensile direction, which will produce a strain in directions orthogonal to the tensile direction, can be either along the tensile direction (denoted as 2 on Fig. 3), perpendicular to the tensile direction (denoted as 3 on Fig. 3), or along intermediate positions. The applied stress increases the vacancy flow towards the dislocations with lines along the tensile direction (dislocations 2) because of the cylindrical symmetry of this configuration. The climb velocity of this dislocation (v_2) is thus reduced compared to the case with zero applied stress, where only EID is effective (Woo, 1984). As the dislocation line is tilted away from the tensile direction, this effect is reduced and vanishes to zero when the dislocation line is perpendicular to the applied stress (dislocation 3). For dislocations 1, there is also no influence of the applied stress. As a consequence, the climb velocity of dislocations 1 is equal to that of dislocations 3 and is higher than that of dislocations 2 ($v_1 = v_3 > v_2$). Because dislocations 2 have Burgers vectors perpendicular to the applied stress, whereas dislocations 1

have Burgers vectors parallel to the applied stress, the overall effect, considering a random distribution of dislocation lines, is a strain along the tensile direction (Woo, 1984).

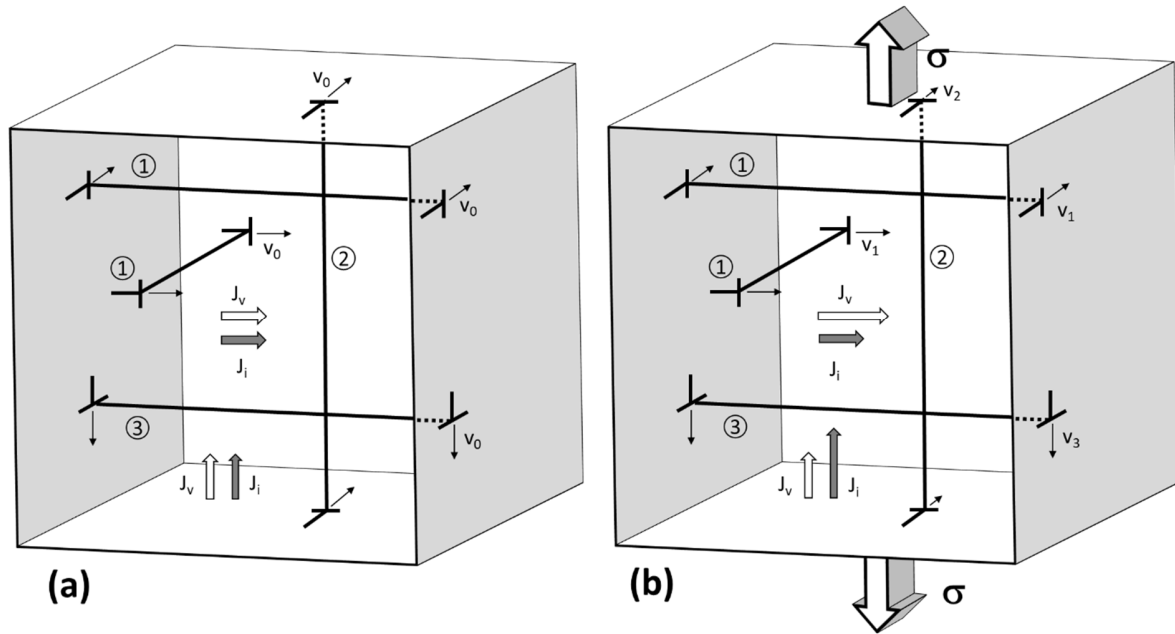


Figure 3: a) Random distribution of dislocations that climb isotropically under irradiation without applied stress resulting in zero net strain; b) Reduced climb of dislocations with lines parallel to the stress direction resulting in a net positive creep strain along the tensile direction.

The application of the SIPA-AD mechanism to grain boundaries is straightforward. The grain boundaries perpendicular to the applied stress receive a net interstitial flux higher than the vacancy flux because of the anisotropic diffusion induced by the applied stress, whereas the grain boundaries parallel to (containing) the tensile direction receive a higher net flux of vacancies than interstitials. This induces a positive strain along the tensile direction and a negative strain perpendicular to the tensile direction.

Similar models, based on the differential anisotropic diffusion (DAD) of interstitials vs. vacancies in hcp structure, have been developed to explain irradiation growth in zirconium (Woo & Gösele, 1983). In this latter case, anisotropic diffusion is related to the low symmetry of the hcp lattice and is not induced by stress; in the context of creep of cubic materials, the symmetry is lowered by the coupling between the anisotropic dipole tensor at saddle point and the external stress. The SIPA-AD model gives creep rates more than one order of magnitude larger than the creep rates produced by the SIPA-I model (Savino & Tomé, 1982) (Woo, 1984). It must be noted that estimations of SIPA-AD creep rates are based on

approximations of point defect properties and should be taken with care. In addition, it has been shown that the flow of vacancies to dislocations is not necessarily perpendicular to the dislocation line, which may modify the effect of stress on absorption bias by the SIPA-AD mechanism (Carpentier, et al., 2017).

2.2.5 Example: strain rate due to the climb of straight dislocations

The strain rate arising from the climb of straight dislocations through SIPA mechanisms can be calculated theoretically. Following the work of Woo (Woo, 1984) and Borodin (Borodin, 1995) a general approach is described below.

We consider a set of edge dislocations of N different types, with Burgers vectors \mathbf{b}^k ($k = 1, \dots, N$) of the same magnitude b , i.e. $\mathbf{b}^k = b\hat{\mathbf{b}}^k$. Their density is noted ρ_k . No other sinks are present in the material. The creep rate is given by Orowan's law (Borodin & Ryazanov, 1992)

$$\varepsilon_{jl} = b \sum_k \rho_k \hat{b}_j^k \hat{b}_l^k v^k, \quad [15]$$

where v^k is the climb velocity of dislocations of type k . Assuming that only interstitials and vacancies migrate to dislocations, the climb velocity is given by

$$v^k = \frac{\Omega}{b} (J_i^k - J_v^k), \quad [16]$$

where Ω is the atomic volume and J_α^k ($\alpha = i, v$) is the flow of point defects of type α per unit line of dislocation. This flux is different from one dislocation type to another one due to the SIPA-I and SIPA-AD mechanisms. In a rate theory approach, it is often written under the following form (the temperature is assumed to be low enough to neglect thermal emission of point defects):

$$J_\alpha^k = Z_\alpha^k D_\alpha C_\alpha. \quad [17]$$

In this equation D_α is the diffusion coefficient of point defects α without any effect of elastic interactions, C_α is the concentration of point defects and Z_α^k is an absorption efficiency. The dependency of the fluxes on stress is entirely contained in this factor and gives rise to SIPA effects (I and AD). For a uniaxial stress of magnitude σ , regardless of the underlying SIPA mechanism it can be expanded up to first order in σ (Borodin & Ryazanov, 1992):

$$Z_\alpha^k(\sigma) = Z_\alpha^0 \left(1 + \beta_\alpha^k \frac{\sigma}{\mu} \right), \quad [18]$$

with μ the shear modulus. The coefficient β_α^k takes different forms, depending on the SIPA mechanism considered and on the assumptions made to render the calculation tractable, in particular on the symmetry of dipole and polarizability tensors (Woo, 1984) (Borodin, 1995). For SIPA-AD, it depends on elastic dipoles, while for SIPA-I it depends on polarizabilities. From the rate theory model, point defect concentrations are determined as a function of the point defect creation rate G , recombination coefficient K_{iv} , total sink strengths $k_i^2 = \sum_k Z_i^k \rho_k$ and $k_v^2 = \sum_k Z_v^k \rho_k$, and diffusion coefficients D_i and D_v . Using Eqs 15, 16, 17 and 18 the creep rate can be written as

$$\varepsilon_{jl} = a\Omega G C_{jl} \frac{\sigma}{\mu} \quad [19]$$

with

$$C_{jl} = \langle \hat{b}_j \hat{b}_l (\beta_i - \beta_v) \rangle - \langle \hat{b}_j \hat{b}_l \rangle (\langle \beta_i \rangle - \langle \beta_v \rangle) \quad [20]$$

$$a = \frac{2}{1 + \sqrt{1 + \xi}} \quad [21]$$

$$\xi = \frac{4K_{iv}G}{k_i^2 k_v^2 D_i D_v} \quad [22]$$

In the expression of C_{jl} , the average $\langle \dots \rangle$ is performed on the dislocation types; for a quantity f^k it reads $\langle f \rangle = 1/\rho \sum_k \rho_k f^k$. One sees that the creep rate is proportional to the applied stress. In the recombination regime, $\xi \gg 1$ and the creep rate is proportional to \sqrt{G} , while in the sink dominated regime, $\xi \ll 1$ so the creep rate is proportional to G . The dependency on temperature, at fixed microstructure, is mostly given by the variation of C_{jl} with T . For both SIPA-AD and SIPA-I it is inversely proportional to T . However, the influence of the temperature on the microstructure evolution may also have an indirect influence on the creep rate yielding to a more complex temperature dependency.

2.2.6 Remarks concerning the SIPA mechanism on dislocations

The SIPA mechanism has been extensively described in the literature. However, in order to have a complete theory based on a SIPA mechanism, two other issues must be addressed.

The issue of the overcoming of the high loop density by climbing dislocations

The numerous loops, or more generally point defect clusters, created under irradiation act as obstacles against dislocation climb. Within the usual SIPA theory for dislocation climb, this pinning effect of

dislocations during their motion is not explicitly taken into account. A complete theory for this mechanism should include the interaction between dislocations and loops and how the dislocations overcome loops.

The issue of the formation and regeneration of the dislocation network in the frame of SIPA mechanisms

Because in Solution Annealed (SA) austenitic stainless steels or in recrystallized zirconium alloys the initial dislocation density is very low, typically $\rho_m \approx 10^{12} \text{ m}^{-2}$, the strain resulting from the climb (or glide) of these dislocations cannot account for the creep strain. Indeed, assuming a mean free path, by climb (or glide), for the dislocations of the order of the grain size, typically $\lambda \approx 10^{-5} \text{ m}$, and a Burgers vector of $b \approx 3 \times 10^{-10} \text{ m}$, the resulting strain is $\varepsilon = \rho_m b \lambda \approx 3 \times 10^{-3}$. This clearly shows that dislocation multiplication is needed to account for strain of the order of several percent, as it is also found in the usual dislocation theory applied to the plasticity of metals. During thermal creep, new mobile dislocations are generated from sources operating by the interaction between existing mobile dislocations, such as Frank-Read sources or spiral source, or from favourable sites on grain boundaries or sub-boundaries (Gittus, 1975).

Under irradiation, dislocation sources, such as Frank-Read sources, that are activated by climb also exist. They are called Bardeen-Herring sources (Hull & Bacon, 2001). They could explain the irradiation creep strain. It is also often considered that the dislocation loops, such as Frank loops in austenitic stainless steels, as they grow unfault and coalesce, creating a dislocation network (Wolfer, 1980) which climbs via the SIPA mechanisms described above resulting in strain. As loops are continuously created and coalesce, a steady state is reached, explaining the steady state secondary irradiation creep rate. The formation of the dislocation network has also been considered for zirconium alloys (Holt, 1980).

2.3 Glide-based irradiation creep mechanisms

The glide-based irradiation creep mechanisms are all the mechanisms for which strain arises primarily from glide, although the strain rate can be controlled by climb. The strain rate is proportional to the mean dislocation velocity (v) and to the mobile dislocation density (ρ_m) according to Equation 19.

$$\dot{\varepsilon} = \rho_m b v \quad [23]$$

The expression of the mean dislocation velocity depends on the mechanism considered.

2.3.1 Irradiation-retarded thermal creep mechanisms

In the temperature range of reactor operation, thermal creep is the result of dislocation glide, possibly assisted by climb. The high density of small point defect clusters created by irradiation act as obstacles to

dislocation glide. Therefore, the thermal creep component, that should also take place in reactor, is significantly reduced by irradiation. This is the mechanism at the origin of the radiation-retarded creep.

The increase of yield stress or hardness is often accounted for using the dispersed barrier hardening model where the critical stress to overcome obstacles is inversely proportional to the mean distance (\bar{l}) between obstacles in the dislocation glide plane (Foreman & Makin, 1966) (Singh, et al., 1997) (Was, 2007). In the case of loops the mean distance between obstacles is approximately $\bar{l} = 1/\sqrt{Nd}$, where N is the loop number density and d is the mean loop diameter (Fig. 4).

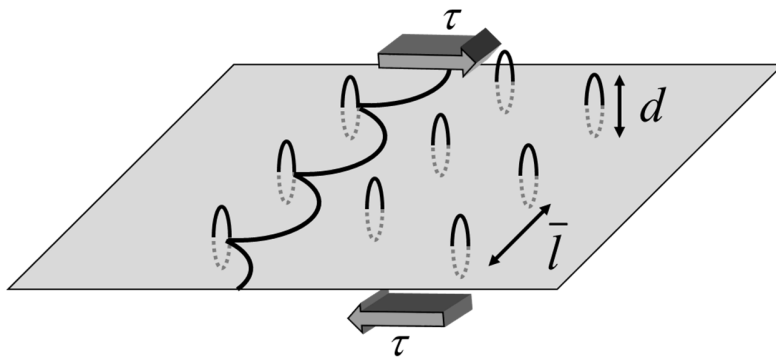


Figure 4: Schematic showing the pinning of a dislocation, submitted to an applied shear stress τ , by loops with diameter d separated by a mean distance \bar{l} .

Following this model, the increase in yield stress ($\Delta\sigma_c = \sigma_c - \sigma_0$, with σ_0 the yield stress of the unirradiated material and σ_c the yield stress of the irradiated material) can thus be expressed as Equation 24

$$\Delta\sigma_c = M\alpha_l\mu b\sqrt{Nd} \quad [24]$$

where M is the Taylor factor relating the yield stress and the critical resolved shear stress (τ_c) ($\sigma_c = M\tau_c$), α_l is a coefficient characteristic of the strength of obstacles, μ is the shear modulus.

The effect of forest dislocations (ρ) on the strength of the material can also be taken into account, using the square root of the sum of the two contributions, leading to an expression for the increase in yield stress as

$$\Delta\sigma_c = M\mu b \sqrt{\alpha_f^2 Nd + \alpha^2 \rho} \quad [25]$$

In this formula, α is a coefficient characteristic of the strength of forest dislocations.

There are several ways to express the secondary creep strain rate due to dislocation glide in the viscoplastic regime to account for thermal creep of materials (Gittus, 1975) (Caillard & Martin, 2003). A detailed description of thermal creep theories is beyond the scope of this review. A simple and rather empirical way is to express the strain rate as a power law where the applied stress is divided by a mechanical threshold stress, or reference stress (σ_c). This reference stress represents the stress required for a gliding dislocation to overcome localized obstacles in its glide plane in the absence of thermal activation (Estrin, 2007).

$$\dot{\epsilon} = \dot{\epsilon}_0 \left(\frac{\sigma}{\sigma_c} \right)^n \quad [26]$$

The stress exponent n is the Norton coefficient and $\dot{\epsilon}_0$ is a reference strain rate which depends on the temperature. Within this framework, the irradiation-induced hardening can be simply introduced in the reference stress (σ_c) according to Equation 25.

A more physically based expression for the strain rate can be derived according to Equation 27 (Gittus, 1975) (Caillard & Martin, 2003). In this expression $\dot{\epsilon}_0$ depends on the temperature and on the mobile dislocation density and V_a is the activation volume which may depend on the applied stress and on the temperature.

$$\dot{\epsilon} = \dot{\epsilon}_0 \exp\left(\frac{(\sigma - \sigma_c)V_a}{kT}\right) \quad [27]$$

From these equations, it can be seen that as the loop density increases under irradiation, the critical, or reference, stress (σ_c) increases and the secondary thermal creep strain rate ($\dot{\epsilon}$) decreases, accounting for the radiation-retarded creep effect.

Another phenomenon could also explain radiation-retarded creep. Under irradiation, dislocations absorb point defects, which create many jogs on the dislocation lines originally present in the material. More precisely, a pure screw dislocation cannot climb by absorption of point defects, but kinks or jogs of edge character, on screw or mixed dislocations can absorb point defects and climb out of the glide plane of the

dislocation, creating jogs such as helical jogs (Fig. 5) by helical climb. These jogs are obstacles to dislocation motion. The initial dislocations are thus pinned by these jogs and cannot act as dislocation sources. New dislocations must therefore be created which requires a high applied stress explaining the suppression of thermal creep observed in some materials such as zirconium alloys. A similar mechanism has been proposed by Singh et al. (Singh, et al., 1997) where the dislocations are decorated by atmosphere of small point defect clusters. By acting in the same way as Cottrell atmosphere, the dislocations are locked in their initial configuration. This mechanism is referred to as source hardening.

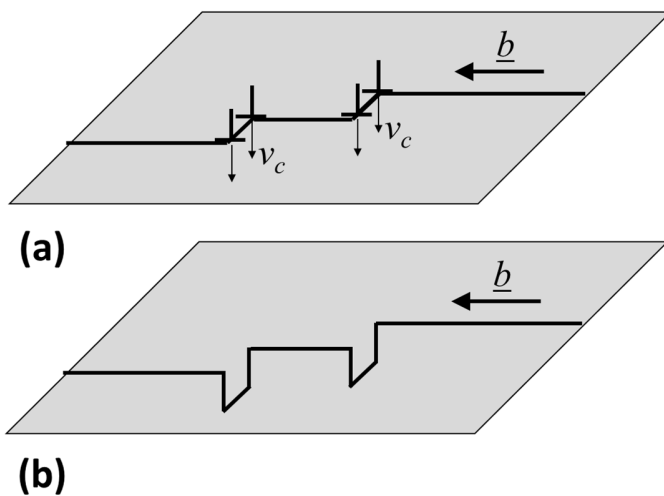


Figure 5: Schematic showing the climb of kinks of edge character on a screw dislocation. This results in the formation of helical jogs on the screw dislocation that are strong pinning points to dislocation glide.

2.3.2 Climb-assisted glide irradiation creep mechanisms

In the mechanism of climb-assisted glide, also referred to as climb-plus-glide or stress induced climb and glide (SICG), the cumulated strain is the result of the glide of dislocations, but the strain rate is controlled by their climb to overcome obstacles since the climb velocity (v_c) is much lower than the glide velocity ($v_c \ll v_g$). The dislocation velocity can thus be expressed as the mean distance between obstacles (L) divided by the duration (t_c) to climb over these obstacles. This duration ($t_c = h/v_c$) corresponds to the height of the obstacle (h) divided by the climb velocity of the dislocation (v_c) (Fig. 6). The obstacles can be precipitates, small point defect clusters created by irradiation or even solute atoms.

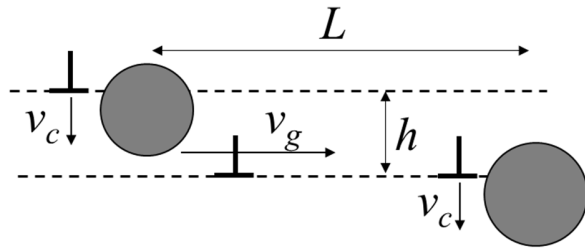


Figure 6: Schematic describing the climb-assisted glide mechanism under irradiation.

The dislocation velocity is thus expressed as

$$v = \frac{L}{h} v_c \quad [28]$$

And the creep rate is given by

$$\dot{\epsilon} = \rho_m b \frac{L}{h} v_c \quad [29]$$

It should be pointed out that the categorization proposed earlier (pure climb vs climb-assisted glide) is based on the fact that $L/h \gg 1$. Thus, there is a continuity between the two families of mechanisms when $L/h \approx 1$.

The climb-controlled glide mechanism can occur in the absence of irradiation. Because the equilibrium concentration of vacancies around a dislocation is affected by an applied stress, depending on the orientation of its Burgers vector with respect to the stress, the dislocation absorbs (or emits) vacancies leading to its climb over obstacles. Neighboring dislocations oriented differently could be vacancy sources (or sinks). A classical climb-controlled glide mechanism, often described in textbooks, has been derived by Weertman (Weertman, 1955) (Weertman, 1957). In this model dislocations are piled up in front of obstacles, the overcoming of obstacles being enabled by climb.

As discussed earlier, the vacancy gradient is not modified by irradiation. It is only the overall vacancy and interstitial concentrations which are increased by irradiation. Therefore, the climb of dislocations under irradiation is the result of the differential absorption of interstitials and vacancies. This differential absorption first arises because of the Elastic Interaction Difference (EID) effect for interstitials and vacancies interacting with dislocations. Provided that there is another sink, such as a neutral sink, which can absorb a net quantity of vacancies, interstitials preferentially eliminate on dislocations leading to their

climb. In this model the dislocation climb velocity only depends on the net flux of interstitials (interstitial flux minus vacancy flux) reaching the dislocation and does not depend on the applied stress, which is problematic for a creep mechanism.

Some authors, as reviewed in (Matthews & Finnis, 1988), have discussed that the dependency on the stress can arise from the mobile dislocation density (ρ_m). Indeed, in the frame of thermal creep it is often considered that the mobile dislocation density is proportional to the square of the applied stress. This argument finds its origin in the early work of Taylor (Taylor, 1934) who considered a single-crystal of a pure metal containing only line dislocations. Because the stress field resulting from the presence of dislocations has a long range ($\mu b/2\pi r$ for a screw dislocation), any dislocation in the middle of a random dislocation network experiences a stress equal to $\mu b/2\pi r_s$, where r_s is the mean distance between adjacent dislocations which equals to $r_s = 1/\sqrt{\rho}$ with ρ the dislocation density. A mechanical equilibrium is assumed between the external applied stress σ on the crystal and the internal stress applied on this dislocation, by the other dislocations, to maintain a steady state dislocation network (Gittus, 1975). This analysis bears some similarities with the one usually done for dislocation pile-up. The equilibrium distance between dislocations is thus related to the applied stress ($r_s = \mu b/2\pi\sigma$) yielding to $\rho \propto \sigma^2$. In this model, the dislocation glide is activated by the applied shear stress on the slip planes and the rate controlling step, which is climb, is dependent on the stress through the overall dislocation density.

In the case of a crystal containing dislocation lines and a high density of small dislocation loops, this analysis is probably not valid since the numerous loops affect the stress field experienced by the dislocations and this relationship should not be used.

Other authors proposed that the dependency on the stress arises from the L/h ratio. The model by Gittus (Gittus, 1972) (Gittus, 1975) considers a dislocation network where segments (of length l) are pinned. Under the applied stress, the segments bow out by glide until the force due to the applied stress is balanced by the line tension forces. Because of the EID effect, the dislocation will, in the presence of more neutral sinks, absorb more interstitials than vacancies leading to its climb. Gittus envisages that each dislocation, which is immobile after its bowing, climbs a height (approximately equal to half the dislocation spacing) to a position where it is free to bow out again and repeat the whole process (Heald & Harbottle, 1977). The area swept by glide during the bow out process can be calculated using the formula derived by Mott (Mott, 1952) followed by Friedel (Friedel, 1953). In this formula, the area swept during the glide process is proportional to the applied stress ($A = \sigma l^3/6\mu b$) leading to a linear dependence of the creep

strain with stress. This model is referred to as I-creep. It has however been recently criticized by Barashev et al. (Barashev, et al., 2016).

The stress dependence of the strain rate may come from another origin. Indeed, because the equilibrium position of a bowed dislocation within a random array of obstacles depends on the applied stress, the area swept by the dislocation during its glide between two climb events, until finding a new equilibrium position, depends on the applied stress (Kelly & Nicholson, 1971). The area swept by the dislocation is related to the mean distance between obstacles along the dislocation line which is stress dependent because more strongly curved dislocations interact with a higher density of obstacles (Caillard & Martin, 2003).

Foreman and Makin (Foreman & Makin, 1966) have used computer simulation to deduce the stress required for a dislocation to overcome an array of obstacles through the Orowan process. Later, Kelly and Foreman (Kelly & Foreman, 1974) applied this computer simulation to assess the irradiation creep deformation mechanism of a dislocation pinned by an array of obstacles that can be destroyed at random by the neutron irradiation. A pinning lifetime, related to the incoming neutron flux, is attributed to obstacles. No dependence on stress concerning the overcoming process of obstacles is assumed. The dislocation velocity is determined from the time taken to traverse the array. Quite remarkably, it is shown that the dislocation velocity depends on the applied stress, linearly for low applied stress, and non-linearly with a stress exponent higher than unity, for higher applied stress. This approach has also been used by Kirsanov et al. (Kirsanov, et al., 1981) to study climb-enhanced glide deformation under irradiation.

The dependence on the applied stress can also directly come from the climb velocity (v_c), according to Mansur (Mansur, 1979) and Mansur and Reiley (Mansur & Reiley, 1980). Indeed, as discussed earlier, the differential absorption of interstitials and vacancies by dislocations can be affected by the applied stress. Combining this linear dependence on stress with the dependence on the glide distance obtained in the frame of the I-creep model, the model by Mansur and Reiley results in a quadratic stress dependence for the creep rate. This is the SIPA mechanism (either SIPA-AD or SIPA-I) applied to the climb-enhanced glide model, which is referred to as preferred absorption glide (PAG or SIPAG) by Mansur and Reiley. However, this effect is probably very low because the stress induces only a small correction to the dislocation climb velocity which remains essentially due to the EID effect.

It is also interesting to mention the work done by Nichols (Nichols, 1969) (Nichols, 1987) because of its historical importance, who also discussed in great detail the enhanced-climb glide past obstacles. This

author adopts a pragmatic and empirical approach and considers the thermal creep strain rate expressed by Weertman (Weertman, 1957), which is proportional to σ^4 , since it assumes dislocation pile-ups, and to the self-diffusion coefficient. In his model, Nichols assumes the same stress dependence under irradiation, because it agrees well with experimental data for zirconium alloys, and replace the self-diffusion coefficient by an “effective” diffusion coefficient since it is recognized that under irradiation both interstitials and vacancies diffuse towards dislocations thus lowering the induced climb rate past obstacles thanks to the EID effect. It must however be underlined that the use of a stress exponent of 4 has no theoretical basis and that it is not justified, from a mechanistic point of view, to replace the self-diffusion coefficient by an effective diffusion coefficient.

2.3.3 Enhanced jog dragging mechanism

In the mechanisms described above, an edge dislocation, as it encounters an obstacle, climbs over it. Because the obstacle is limited in size, jogs are created on the sides of the dislocation. These jogs can easily glide, dragged by the dislocation, because the glide plane defined by the Burgers vector and the line is along the dislocation motion (Fig 7a). This type of jog can also be created by the absorption of a perfect loop by an edge dislocation.

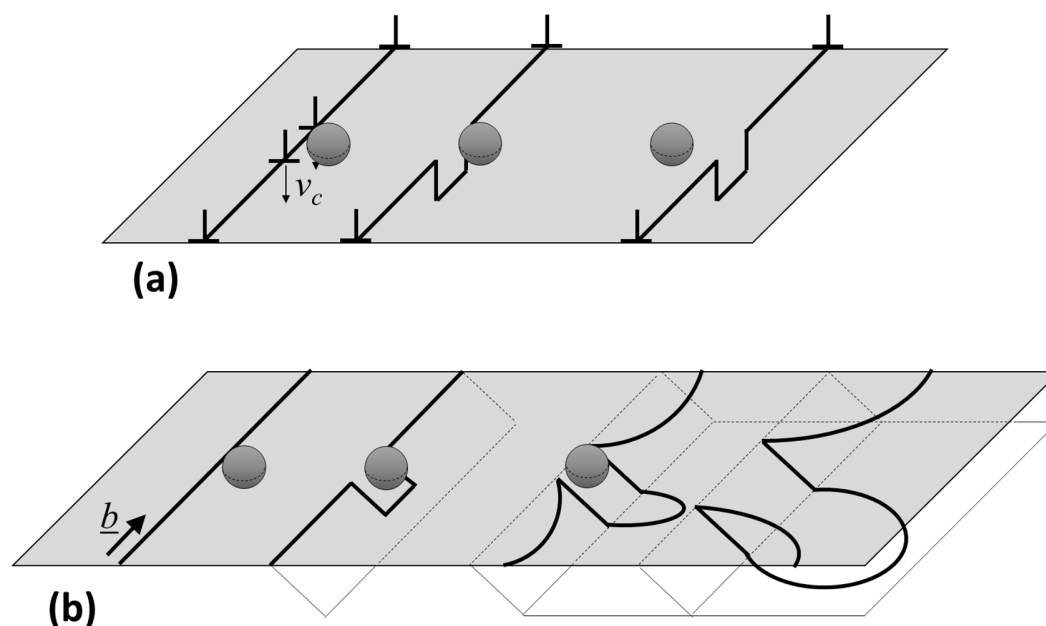


Figure 7: a) climb under irradiation of a part of an edge dislocation to overcome an obstacle leading to the formation of a jog; b) double cross-slip of a part of a screw dislocation to overcome an obstacle creating two jogs that must climb to be dragged by the gliding dislocation.

On the other hand, a screw dislocation, encountering an obstacle, can cross-slip to overcome the obstacle, however jogs are created on the sides. In that case, the jogs cannot glide in the direction of the gliding dislocation motion. Indeed, the glide direction of these jogs is perpendicular to the motion of the gliding dislocation (Fig7b). This type of jog can also be created by the absorption of a perfect loop by a screw dislocation. These jogs can only move by climb in the glide direction of the dislocation, which in turns requires the absorption/emission of vacancies in the case of thermal creep. This can be the controlling mechanism of thermal creep (Gittus, 1975). Under irradiation, because of the high concentration of vacancies and interstitials, the jog mobility may be enhanced, provided that the net flux of point defects toward the jogs is appropriate to help the jog move in the right direction, considering the Burgers vector of the jog. Because of the high density of loops along the glide plane, the dislocations are heavily jogged so that the enhanced dragging mechanism could be a relevant mechanism for irradiation creep.

2.3.4 Enhanced recovery mechanism

It is often considered that secondary thermal creep results from a balance between a strain hardening phenomenon and a recovery phenomenon. At the microscopic scale the strain hardening phenomenon is the result of dislocation multiplication, dislocations acting as obstacles against each other. Because two dislocations with opposite Burgers vector can annihilate each other, a recovery process also occurs. The annihilation can be the result of cross-slip or climb, which are temperature dependent. Other mechanisms, such as the coarsening of the dislocation network can also be found in the literature to explain the recovery phenomenon (Gittus, 1975).

There are several ways to express the evolution of the forest dislocation density evolution. The usual formula is given by equation 30 (Gittus, 1975) (Estrin, 2007).

$$\dot{\rho} = \frac{\dot{\epsilon}}{b} \left[\frac{k_1}{L} - k_2 \rho \right] \quad [30]$$

In equation 30, L is the dislocation mean free path which can be related to the dislocation density but also to the density of other obstacles such as precipitates or irradiation-induced loops. The coefficient k_2 depends on the strain rate and on the temperature since it is related to dislocation climb (or cross-slip).

Under irradiation, the high concentration of interstitials and vacancies will be absorbed on dislocations. Because of the Elastic Interaction Difference (EID) which induces a bias for interstitial absorption and

provided that there is another sink with a lower bias to absorb the excess vacancies, the dislocation climb under irradiation results in an enhanced recovery (increase of the coefficient k_2). This enhanced recovery decreases the steady-state dislocation density yielding to an increased secondary creep rate.

In this model, it is assumed that it is the presence of dislocations which brings the strength of the metal. However, in an annealed metal, under irradiation the density of loops ($Nd \approx 10^{14} \text{ m}^{-2}$) can be several orders of magnitude higher than the original dislocation density ($\rho \approx 10^{12} \text{ m}^{-2}$). In that case, the enhanced recovery of line dislocation does not decrease significantly the strength (see equation 25), and cannot thus explain the enhanced creep under irradiation.

2.3.5 Mobile dislocation production

As pointed out earlier, to produce a strain of the order of several percent from a mechanism involving dislocations, dislocation multiplication is required. This can be achieved by the classical Frank-Read mechanism or thanks to spiral sources. Under irradiation, it has been proposed (Piercy, 1968) that mobile dislocations are produced thus explaining the enhanced creep rate under irradiation. Indeed, under irradiation a high density of small prismatic loops are created. These loops, if they are perfect, after unfauling for instance, can glide on their cylinder, defined by the Burgers vector (\underline{b}) and the loop line. However, under an applied shear stress, the upper part of the loop glides in one direction and the lower part glides in the other direction, because of the inverse Peach-Koehler force due to the reverse line direction. The only way for a dislocation loop to glide on its cylinder across the crystal is the result of its dragging by a gliding dislocation. When the loop reaches the grain boundary, a dilatational strain is produced, but this strain is the same as the one resulting from the formation of this loop (Fig. 8). There is therefore no net strain resulting from the glide of prismatic dislocation loops on their cylinder, dragged by gliding dislocations.

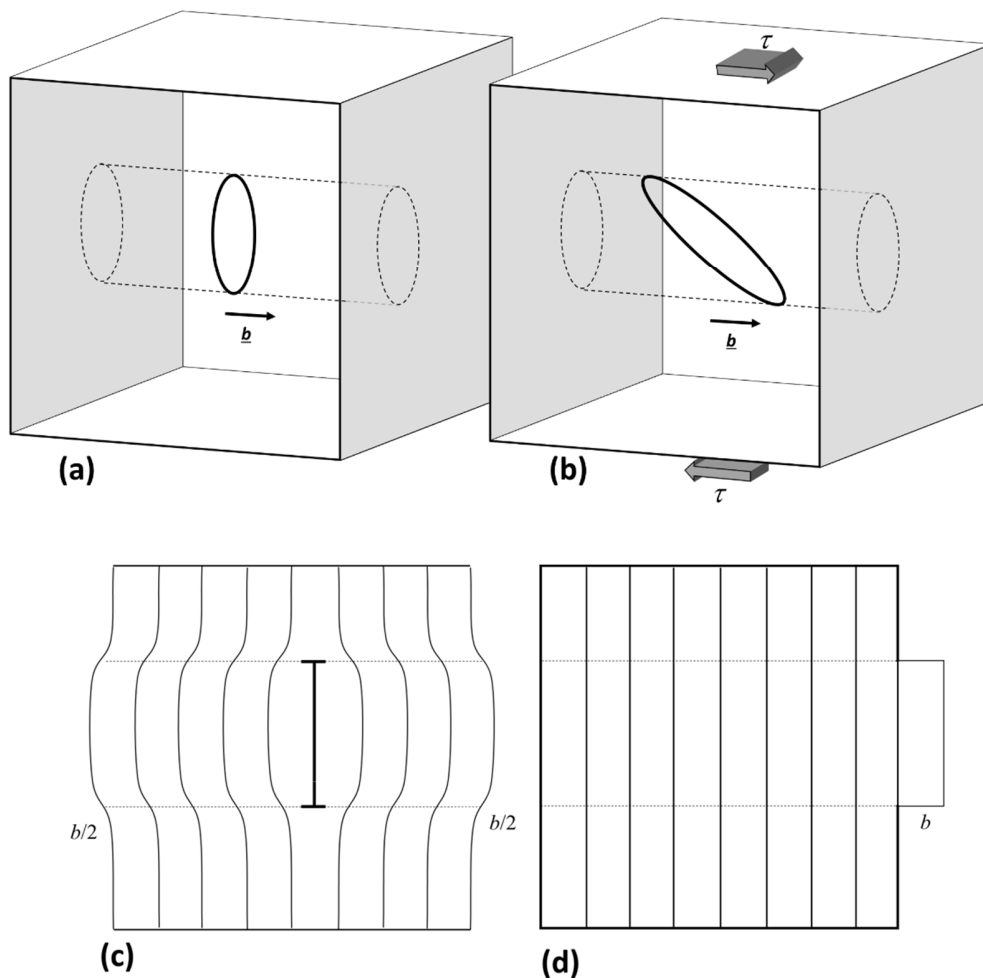


Figure 8: a) A perfect interstitial loop, able to glide on its cylinder, in the middle of a crystal is tilted (b) under an applied shear stress. c) The formation of the interstitial loop creates a dilatational strain. For simplicity, it is considered here that it creates a step of $b/2$ on each side of the crystal. d) If the loop is pushed or dragged on its cylinder, a step of size b appears on one surface of the crystal. There is no net strain resulting from the glide of the loop on its cylinder.

However, if coalescence of loops occurs, then line dislocations are created which can glide under the applied shear stress resulting in a net shear strain. Let's consider a schematic case where a row of perfect interstitial loops with the same Burgers vector are all aligned in the same habit plane in the crystal (Fig 9a). Because of the formation of these loops, the crystal already exhibits a strain (Fig 10a). When these loops grow, they coalesce creating a long dislocation dipole represented schematically on Figure 9a. For an applied stress high enough to activate these sources, both edge dislocations glide through the crystal

in opposite directions. The strain resulting from the glide of these dislocations can be analysed by drawing sketches (Figure 10).

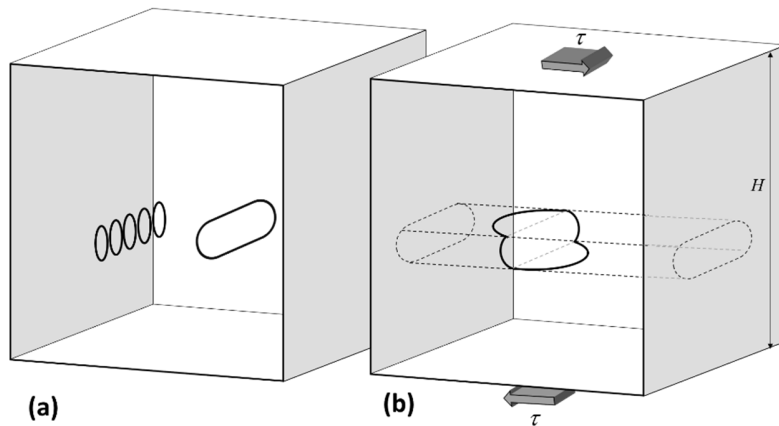


Figure 9: a) The coalescence of perfect interstitial loops leads to the formation of a dislocation dipole; b) under an applied shear stress the dislocation lines glide according to the Peach-Koehler force.

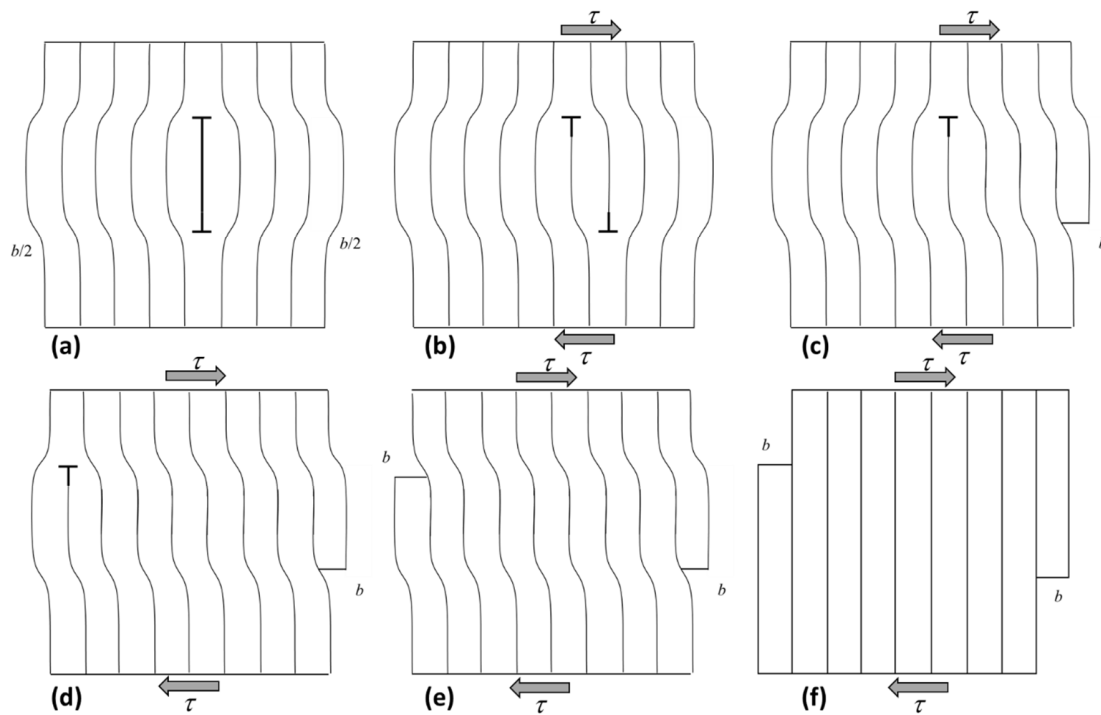


Figure 10: a) Dilatational strain resulting from the formation of the loop. b)-f) Under an applied shear stress, the two dislocations of the dipole glide in reverse directions. c) and d) When the dislocations reach the surfaces, steps of magnitude b are created, resulting in a shear strain in addition to the dilatational strain due to the formation of the loop.

In Figure 10, it is shown that the two dislocations of the dipole of interstitial character can glide in opposite directions under the applied shear stress. When the dislocations reach the surfaces of the crystal, steps of magnitude b are created, resulting in a shear strain. This shear strain adds up to the dilatational strain resulting from the formation of the loop (Fig 10f).

From these sketches, it can be concluded that indeed a net shear strain results from the glide of the line dislocations created by the coalescence of loops. This conclusion can be generalized to a more complex network resulting from the coalescence of loops with different Burgers vectors, which can indeed produce a net shear strain as a result of its glide.

This argument, assuming only dislocation glide, does not explain why creep rate under irradiation is higher than the creep rate after irradiation since in this last case a high dislocation density is also present. This shows that it is not an actual mechanism in itself. Climb-enhanced glide mechanism is also needed along with the phenomenon of the formation and regeneration of the dislocation network to explain the higher creep rate under irradiation.

2.3.6 Dislocation unpinning models

Another class of irradiation creep models considers that the strain is the result of the glide of dislocations through an array of obstacles and the strain rate is controlled by the rate at which the dislocation unpins itself from obstacles. The release from the pinning point can be achieved by the direct effect of the incoming particle which destroys the pinning point, as proposed in the original model by Kelly and Foreman (Kelly & Foreman, 1974). It is also possible that if the cascade falls on the pinning point, such as a small loop, the dislocation can be released from the loop, as suggested by Gaumé et al. (Gaumé, 2018). The pinning points can also be bypassed by dislocation climb or penetration by combination of stress and thermally activated cutting (Dollins & Nichols, 1974) (Dollins, 1971). As described earlier, Kelly and Foreman have been able to assess the stress dependency of such a mechanism by using computer simulation. Although there is no dependency on stress of the unpinning mechanism, because the number

of pinning points along the dislocation depends on the applied stress, a stress dependency arises, which is linear for low applied stress.

2.3.7 Intergranular stress driven creep or “yielding creep”

A last mechanism, sometimes referred to as “Cottrell” creep or “yielding creep”, that may be worth mentioning because of its historical significance (Hesketh, 1968) (Gittus, 1975) (Matthews & Finnis, 1988) concerns materials exhibiting stress free growth under irradiation. Indeed, because at the grain scale the growth is anisotropic and because the grains are mechanically constrained by the neighboring grains, intergranular stresses arise under irradiation without external applied stress. These intergranular stresses can become very high, close to the yield stress, if they are not relieved by a visco-plastic deformation process. The simplest form of this model assumes that the only possible deformation process is the dislocation glide when the yield stress is reached. If the intergranular stress is just below the yield stress, applying a small additional external stress increases the local stress up to the yield stress which in turn induces plastic deformation, thus explaining the enhanced deformation under irradiation.

2.3.8 Remarks concerning the dislocation glide based mechanisms

The issue of the overcoming of the high loop density by dislocations

As for the SIPA mechanisms, a complete theory of enhanced-climb and glide of dislocations under irradiation must take into account the details of the interactions between dislocations and loops, and how dislocations overcome the loops. This is not done explicitly in all mechanisms described above.

The issue of the nature of the obstacles to overcome

Furthermore, in the climb-enhanced glide theory, it is not clear what are the obstacles controlling the dislocation motion. If loops are considered as the controlling obstacles to be overcome by climb, in that case an interaction should occur leading to various reactions, such as jog formation. The obstacle cannot be considered as fixed and the result of the reaction has to be taken into account.

Besides, if loops are considered as the controlling obstacles, it is not possible to explain how the creep rate under irradiation can be higher than the creep rate of the unirradiated material which does not contain any loop. Other types of obstacles, such as solute atoms, must be considered.

On the role of the applied stress range

Nichols (Nichols, 1970) (Nichols, 1987) proposed that these various deformation mechanisms occur in series, explaining the evolution of the stress dependency as the stress increases. For a low applied stress

loop alignment occurs (SIPA on loops), leading to anisotropic distribution of loops depending on the orientation of the habit plane with respect to the applied stress. For higher stress, the climb of line dislocations via the SIPA mechanism takes place, and then the dislocation climb and glide process occurs at even higher stress.

3 Experimental evidences of irradiation creep mechanisms

3.1 Experimental evidences of SIPA-based mechanisms

Although in the previous part SIPA mechanisms have been mainly discussed in the case of differential dislocation climb, they can operate in the presence of many sink types: dislocation loops, grain boundaries and surfaces. For the two latter sinks, SIPA-AD mechanism is generally invoked, due to the short range of their strain field. However, for dislocation and dislocation loops both mechanisms (SIPA-I and SIPA-AD) can operate.

3.1.1 Stress dependency and magnitude

A common feature of SIPA models is that the strain rate is proportional to the applied stress (Heald & Speight, 1975) (Savino & Tomé, 1982). This is in good agreement with measurements of steady state creep (stage II) for moderate applied stress, which partly explains why such models are still popular.

Following the discovery of SIPA-I, a few authors obtained satisfactory agreement on creep rates using this model, at least in the steady state regime (Wolfer, 1975) (Bullough & Hayns, 1975) (Wolfer, 1980). Other studies have shown that creep strain rates predicted by SIPA-I were far too low (Nichols, 1979) (Simonen & Hendrick, 1979) (Kishimoto, et al., 1988). The difficulty, when assessing the magnitude of SIPA-I creep, is to use the correct value for the fraction of freely migrating defects which are the only ones to participate to creep strain in SIPA models (Nichols, 1979), and to use correct values for defect polarizabilities. A recent study based on cluster dynamics confirmed the too low magnitude of SIPA-I effect (Garnier, et al., 2011b).

To solve the discrepancy between experimental creep rates and SIPA-I predictions, taking into account the effect of anisotropic diffusion (SIPA-AD) seems promising (Wassilew, et al., 1987). However, the uncertainties concerning the precise relative amplitude of the two effects, which still prevail in the absence of reliable simulation results, make SIPA-I still largely invoked in the literature (Garnier, et al., 2011b) (Xu & Was, 2015). It is indeed difficult, from an experimental point of view, to distinguish between SIPA-I and SIPA-AD mechanisms. SIPA-AD has a strong dependence on the load direction with respect to the lattice. This could possibly permit to conclude as to the relative amplitudes of SIPA-I and SIPA-AD (Borodin & Ryazanov, 1994).

3.1.2 Dependency on dislocation density

Another argument in favour of SIPA mechanisms is the dependency of creep rate on dislocation density. There is some evidence that the creep rate of cold-worked (CW) materials is larger than the one of solution annealed (SA) materials, at least at low dose (Mosedale, et al., 1972) (Straalsund, 1977) (Walters, et al., 1977). However, in the secondary creep regime there is often no significant difference between CW and SA materials, especially for austenitic stainless steels (Mosedale, et al., 1977) (Holt, 1980). Concerning zirconium alloys, there is a low dependency on dislocation density, the creep rate being higher when the dislocation density increases. SIPA models lead to creep rates which are essentially independent on dislocation density in the sink-dominated regime (Bullough & Hayns, 1975) (Woo, 1984), *i.e.* at not too low temperature. In this regime the only dependency comes from the dependency of the bias factors on dislocation density, which is usually considered as logarithmic and is therefore small (Nichols, 1979). We note that similar creep rates during stage II in CW and SA materials are not a definite argument in favour of SIPA models, since microstructures of SA and CW tend to become similar as the dose increases.

3.1.3 Evidence for the formation and regeneration of the dislocation network

As pointed out earlier, the formation of a dislocation network by the coalescence of loops is considered necessary to explain the creep strain, induced by dislocation climb, reached under irradiation. Nevertheless, there are not so many evidences of this dislocation network under neutron irradiation (Stoller & Odette, 1987) (Zinkle & Stoller, 1993). This dislocation network has been observed mainly under high temperature irradiation as reported by Wolfer (Wolfer, 1980) (Fig. 11). Based on rather few data, it is shown that as the irradiation dose increases the dislocation density in solution annealed steel increases. For the same doses, and same irradiation temperature, the dislocation density of a 20% cold worked austenitic stainless steel decreases (because of enhanced recovery under irradiation due to enhanced climb) and both materials tend to reach similar values for the dislocation density at higher doses.

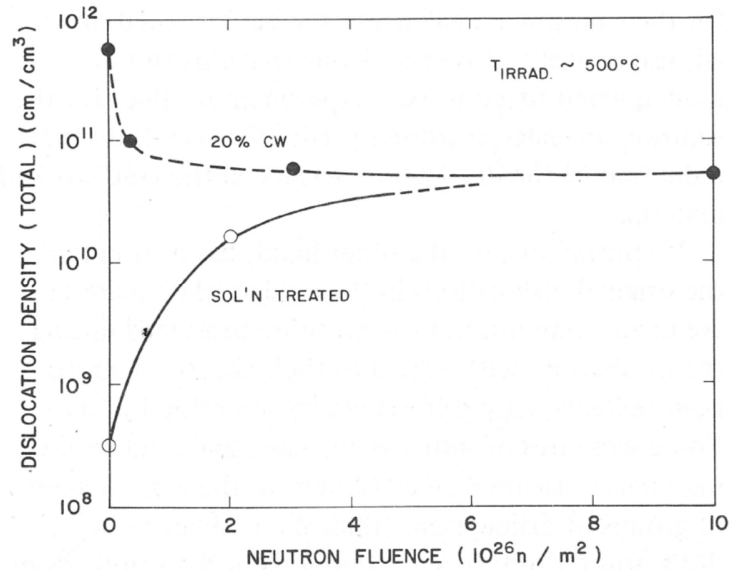


Figure 11: The evolution of the measured dislocation density for solution annealed and 20% CW stainless steel as a function of fluence for an irradiation temperature of 500°C. From M.L. Bleiberg, J.W. Bennett (Eds.) Radiation effects in breeder reactor structural materials, TMS-AIME, New York, 1977, pp. 727-755 and given in Wolfer, W. G., 1980, J. Nucl. Mater. 90, p. 175.

In the case of zirconium alloys, this dislocation network is seldom observed. Only Jostsons et al. (Jostsons, et al., 1977) report the observation of a dislocation network after neutron irradiation at a temperature of 400°C.

For temperatures typical of PWR, between 300 to 350°C, it is very difficult to distinguish this dislocation network, because of the high density of small Frank loops in austenitic stainless steels or perfect loops in zirconium alloys. Renault et al. (Renault-Laborne, et al., 2016) managed to observe small dislocation segments in between of dense loop arrangement.

3.1.4 Dislocation climb velocity

A direct evidence of SIPA models could be provided by comparing the climb velocities of dislocations with different orientations with respect to the load direction. To the authors' knowledge, a correlation between climb rate and dislocation orientation has never been observed. More evidences have been given concerning the formation and growth of dislocation loops.

3.1.5 Evidences of SIPA effect on dislocation loops

Effect of stress on loop density depending on the loop habit plane

There are some experimental evidences that an applied stress induces an anisotropic loop microstructure in ferritic and austenitic steels, with a dependency of the loop density on the normal stress to the loop plane, without significant effect on the loop size (Okamoto & Harkness, 1973) (Brager, et al., 1977) (Garner, 1979) (Caillard, et al., 1980) (Gelles, et al., 1981) (Xu & Was, 2014). This phenomenon is also observed in non-metallic materials (Zinkle, 1992). In particular some results were obtained at low doses, to avoid any effect of the dislocation network on loop distribution (Atkins & McElroy, 1987). It was initially thought that a model based on classical nucleation under stress would explain the effect of stress on the loop density. This model, called stress-induced preferred nucleation (SIPN) (Brailsford & Bullough, 1973) (Wolfer, et al., 1972), proved to be irrelevant for interstitial dislocation loops. Binding energies of self-interstitials are in general so large that no nucleation barrier exists (Garner, et al., 1979). It was then proposed that small clusters would reorient under stress, which would lead to anisotropic loop distribution (Wolfer, 1980). This is a more plausible mechanism than SIPN but atomistic data to support this phenomenon are still lacking. The effect of stress has been studied on single point defects (Chen, et al., 2010) but not on clusters. A more in-depth investigation of the detailed atomic processes driving the formation of small clusters under stress is necessary (Tanigawa, et al., 1996). Finally, it was suggested that SIPA could explain the anisotropic dislocation loop microstructure. Using a cluster dynamics model, Wolfer et al. (Wolfer, et al., 1977) have shown that SIPA could also change the loop density. This is an indirect evidence, however, since SIPA is expected to have a larger effect on loop growth. The effect on loop density would result from the modification of the growth rate of small interstitial clusters. If confirmed, the effect of SIPA on loop microstructure would be conceivably stronger at low doses, where loops are essentially the only sinks in SA materials. At larger doses, other sinks with lower biases can be present (voids, c-loops for Zr within DAD model), so there is a net flux of interstitials to all types of loops and the differences in loop distributions would then be less visible.

A peculiar feature of the creep models based on anisotropic loop distribution, whether it is induced by SIPA mechanism or not, is that the stress only has an influence during the formation of clusters. Nucleation of interstitial loops is large at low doses for SA materials and then decreases as the dislocation density increases, since dislocations absorb a large part of the defects. It means that the strain levels due to the anisotropic distribution of loops are mostly determined by the initial stress state, and that if the stress is subsequently removed, anisotropic deformation should occur (Brailsford & Bullough, 1973) (Wolfer,

1980), a behaviour akin to the irradiation growth in hcp materials. This has indeed been observed experimentally (Garner & Gelles, 1988). That is why the strain rate is sometimes seen to be proportional to swelling (Brailsford & Bullough, 1973) but not to stress. It has been shown that the anisotropic microstructure can persist at higher doses by anisotropic loop unfauling (resulting also in creep strain (Lewthwaite, 1973)) and the formation of an anisotropic dislocation network (Zuppiroli, et al., 1977) (Gelles, 1993) (Gelles, et al., 2000) (Ando, et al., 2007). However, as irradiation proceeds the microstructure eventually becomes isotropic, whatever the stress levels (Zuppiroli, et al., 1977). Although loops still nucleate and feed the dislocation network, anisotropic loop formation may be hindered by the large internal stresses created by the network dislocations. Interactions between network dislocations also cancel the anisotropic character of the microstructure. Therefore it seems reasonable to invoke anisotropic loop formation as a creep mechanism in the low dose, primary transient stage of creep (Zuppiroli, et al., 1977) (Caillard, et al., 1980), which fades away as the dose increases.

It must also be pointed out (Xu & Was, 2014) that the anisotropy in the loop density distribution can only explain a small amount, less than 10%, of the overall creep strain. The stress effect on loops is thus evidence that a stress effect on dislocations should also occur (but it has never been observed). The effect of stress on dislocation climb is actually the relevant mechanism to explain irradiation creep rather than the effect of stress on loops which contribute only marginally to the creep strain.

Effect of stress on loop growth rate and loop size

SIPA models may also be assessed by comparing growth velocities of loops with different orientations. Experiments exhibiting differences in growth velocities or loop size are scarce, compared to those showing an effect on loop density (Brager, et al., 1974) (Faulkner & McElroy, 1979) (Garner & Gelles, 1988) (Jitsukawa, et al., 1992). In general the effect has been inferred from a few loop measurements and remains small. Given the poor statistics, differences in loop growth rates may also be a sign of internal stress or local increase of sink strength due to neighbour loops and dislocations. Indeed, significant differences in loop growth rates have been observed in unstressed materials (Jitsukawa & Hojou, 1994). The results also may not be conclusive if samples are observed at high dose, since in ferritic and austenitic steels the loop size is limited by the interaction of loops with the network dislocations (Brager, et al., 1977) (Stoller & Odette, 1987). Saka *et al.* have shown that under stress, loops were elongated in the direction of the tensile stress, and that the results were not consistent with SIPA-I effect (Saka, et al., 1989). It has been argued that the small effect of stress on loop size may not rule out a SIPA effect (Garner & Gelles, 1988), since the effect of SIPA-I has been shown to be maximum at intermediate loop size and then to

decrease (Garner, et al., 1979). This theoretical result is worthy of more investigation given the underlying assumption of infinitesimal loops (Wolfer & Ashkin, 1975). It seems questionable, in addition, to explain creep with a mechanism which produces the same loop size on all planes, except if the loops unfault and become part of the network before reaching the size where their growth rate is independent of stress.

Finally, it should be mentioned that in some cases, no effect of stress on either density or size could be measured. For example, some recent works (Garnier, et al., 2011a) (Renault-Laborne, et al., 2016) have attempted to analyse the loop density and size per habit plane in stainless steels deformed under neutron irradiation up to high doses. No significant differences between loop size and density were observed depending on the loop habit plane. Nevertheless, it appears that the overall Frank loop density decreases when the applied stress increases and the mean loop size tends to slightly increase, at least for SA 304L and for CW 316. In Zr alloys, the role of an applied stress on $\langle c \rangle$ -loop has also been investigated using heavy ion irradiation up to high doses (Gharbi, et al., 2015). Only a small effect of stress, probably within the scatter of experimental data, is noticed, proving that the SIPA effect on $\langle c \rangle$ -loops is very small. It should be noted, however, that in this case both $\langle c \rangle$ - and $\langle a \rangle$ -loops are present, which may reduce the effect of stress on the $\langle c \rangle$ -loop microstructure. All these recent results shed some doubts on the relevance of the SIPA phenomenon on loops.

3.1.6 Evidences of SIPA effect on grain boundaries

SIPA mechanism is also used to explain creep in materials with small grains and nano-structures such as nano-pillars, where dislocations are not present in sufficient density to produce significant strain. As such it bears some resemblance to Nabarro-Herring creep, but the driving force is not the difference in equilibrium concentration (which would rule out any effect of irradiation); it is the anisotropic diffusion of point defects produced by irradiation (SIPA-AD) which leads to different fluxes of point defects to the different grain boundaries or surfaces. For example, a dependency of creep rate on grain aspect ratio and grain size has been shown in Zr-2.5Nb (Walters, et al., 2015). In Zr alloys, other aspects of the deformation points to an effect of SIPA especially in the case of submicronic grains (Adamson, et al., 2019). SIPA mechanism at interfaces and grain boundaries has also been shown to be relevant in metallic nanolaminates (Dillon, et al., 2017). We note that in this kind of materials, other mechanisms have been proposed, depending on the grain size and stress level (Ashkenazy & Averbach, 2012)

3.2 Experimental evidences of glide-based mechanisms

In the case of zirconium alloys, climb-enhanced glide has long been the preferred explanation for the observed irradiation creep whereas it is less favored for austenitic stainless steel. The main reasons for this is the stress dependence of irradiation creep in these different materials.

3.2.1 Stress and temperature dependency

In general, when a stress exponent higher than one is obtained, it is considered that dislocation glide enhanced by climb must be activated. In the case of zirconium alloys, it is observed that the stress exponent increases from 1 up to 2 to 3 as the stress or temperature increase (Fidleris, 1988) suggesting that dislocation glide is more activated in these conditions under irradiation. It was also shown that the activation energy increases as the temperature increases, proving that dislocation climb is more activated in-reactor at higher temperature. Furthermore, according to Holt (Holt, 1980) the irradiation creep anisotropy is consistent with glide in the case of zirconium alloys. These observations have been considered to be strong evidence in favor of the climb-enhanced glide mechanism for zirconium alloys.

3.2.2 Evidences of dislocation glide under irradiation

In order to assess that dislocation glide has occurred during a mechanical test, conducted on an unirradiated material, classical studies, using transmission electron microscopy, rely on the fact that dislocation density increases with plastic strain. In the case of irradiated sample, because of the high loop density, dislocation density increase is not observed but white cleared bands, called dislocation channels, where dislocation loops have been cleared by gliding dislocation, are often observed. This can be used to prove that dislocation glide has occurred during testing after irradiation. Another very interesting method is to use scanning electron microscopy to observe slip traces on the surface of the sample or use digital image correlation. These techniques have been employed on neutron or ion irradiated materials. Using in situ straining experiment inside a TEM, it is also possible to assess, by direct observation of the dislocation motion and the analysis of the traces, that dislocation glide occurs. This last technique enables to see the pinning of gliding dislocations on irradiation defects. A review of these experiments done after irradiation is beyond the scope of this review.

However, it is difficult to assess experimentally that dislocations have glided in a material during irradiation creep based only on post-irradiation examinations. Because of the high density of loops usually present after irradiation and because of the potential formation of a dislocation network by coalescence of loops, it is difficult to observe the dislocations that have glided. In the case of zirconium alloys, some

authors have been able to observe dislocation channels after in-reactor creep experiment (MacEwen & Fidleris, 1977). Parakinen et al. (Parakinen et al., 2013) have studied OFHC copper tested under low strain rate tensile tests either inside a nuclear reactor or after irradiation. They have compared the microstructures obtained after these two different experiments. They observe that while during testing done after irradiation, the dislocation glide was highly localized inside defect free channels, under irradiation only few defect free channels were observed and the matrix between the channels contained homogenous distribution of linear dislocations. These observations of defect free channels under irradiation deformation prove that in these conditions dislocation glide can occur. It is however not clear whether the homogenous distribution of linear dislocations has undergone glide or climb under irradiation. Renault et al. (Renault-Laborne, et al., 2016) also observed a dislocation network after in-reactor creep but again it is not known whether these dislocations have undergone glide or climb.

Recently, Gaumé et al. (Gaumé, et al., 2018) have been able to observe in situ, in a TEM under an applied stress, the dislocation glide activated by the ion beam in a zirconium alloy. A mechanism of pinning-unpinning, similar to that proposed by Kelly and Foreman (Kelly & Foreman, 1974) where irradiation helps to unpin the dislocation from irradiation defects, was observed in situ.

Concerning the technique based on slip traces, to the author's knowledge there is no observation reported in the literature of slip traces on the surface of sample subjected to irradiation creep test.

4 Irradiation creep in zirconium alloys

In-reactor, zirconium alloys subjected to an applied stress deform by irradiation creep. Furthermore, zirconium alloys are unique in comparison to most other engineering alloys in that they deform anisotropically during irradiation in the absence of an applied stress by the growth phenomenon.

The history of the development of irradiation creep concepts for Zr-alloys has been described in detail by (Adamson et al., 2019). Stress induced preferred nucleation (SIPN) and Stress induced preferred absorption (SIPA) have been largely dismissed as major contributors to irradiation creep in Zr-alloys (Woo, 1988; Christodoulou et al., 1993, Woo et al., 1999), leaving stress induced climb and glide (SICG) as the more prominent mechanism in the past 30 years. Whereas stress-induced climb and glide was the mainstay of earlier modelling efforts, recent evidence shows that the grain structure has a large effect on irradiation creep when the grain sink strengths are large (i.e. grain dimensions are small) (Griffiths et al., 2002a; Griffiths et al., 2002b; Bickel et al., 2010; Walters et al, 2013; Griffiths et al., 2017a), suggesting that the SIPA-AD (due to elasto-diffusion) mechanism (Woo, 1984), involving point defect diffusion to grain boundaries, could be important..

Just as with thermal creep, irradiation creep is often described as being comprised of distinct phases: primary, secondary and tertiary. The tertiary phase is one of accelerating creep caused by the changing dimensions of the sample, e.g. necking in a tensile test, and will not be considered here as in-reactor strains are often not large enough for accelerating tertiary creep to be applicable. Primary creep can be considered as a transient stage at the beginning of irradiation that is characterised by a high initial strain rate that slows to the secondary strain rate after a certain transient time. The primary stage includes the same hardening effects as thermal creep and also includes the effects of an evolving irradiation microstructure. Although the initial primary transient is often complete after 1000 - 2000 hours of irradiation (depending on the temperature and irradiation damage rate) the transition to the secondary, so-called steady-state, may still last a long time (depending on the temperature and damage rate) until the initial microstructure evolution involving dislocation loops slows and becomes more-or less constant. At that time one can consider the creep to be secondary, although it may never be completely steady-state because changes in the microstructure (such as cavity and phase structure evolution) may still be occurring over long times.

4.1 Primary Irradiation Creep

4.1.1 Effect of sulphur on primary creep

Primary irradiation creep is important for stress relaxation and during power transients. Mechanistically, one of the more interesting observations concerning primary creep in the past twenty years involves the work on the effect of sulphur first reported by (Soniak et al., 2002). Soniak et al. demonstrated that the primary irradiation creep of Zr-1%Nb (M5) cladding was sensitive to the presence of as little as 10 ppm sulphur. They showed how the sulphur effect on primary creep was consistent with the effect of sulphur in reducing thermal creep as seen in laboratory tests (Mardon et al., 1994). It is noteworthy that Soniak et al.'s data showed that only primary creep was affected with little apparent effect on steady state creep behaviour, Figure 4-1. The work by Soniak et al. demonstrated two important things: (i) that sulphur is an important element in reducing primary creep; (ii) that the effect of sulphur is not apparent in the steady-state irradiation creep regime. The results can be understood if one assumes that primary creep is governed by dislocation slip. The effect of sulphur appears to be one where it segregates to dislocation cores and thus reduces dislocation mobility, which is apparent in laboratory tests and also during primary creep. As the material hardens from the accumulation of radiation damage, the slip-based creep is suppressed and there is then a transition to the secondary irradiation creep regime. In steady-state irradiation creep there is little apparent effect of sulphur, which supports the notion that irradiation creep, in the steady-state is not dominated by dislocation slip.

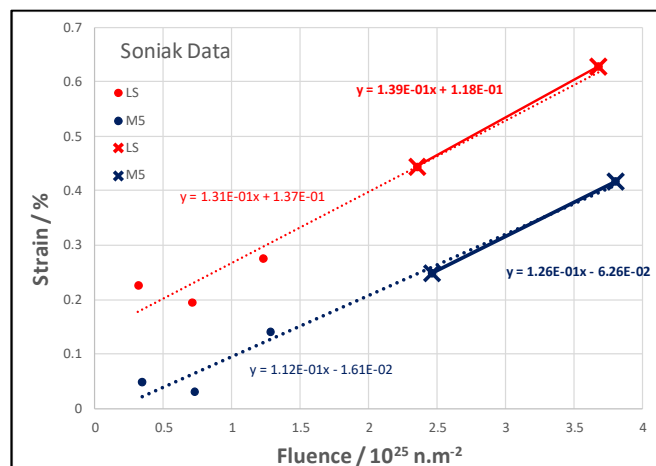


Figure 4-1. Irradiation creep of low sulphur (LS) and M5 alloy (containing 10 wt ppm S) from (Soniak et al. 2002).

4.1.2 Evidence of thermal creep suppression and influence of dislocation density

For most observations of irradiation creep deformation, there is a high strain rate (as a function of time) in the primary stage that is complete after about 3000 hours, and coincides with primary thermal creep.

The time for this stage appears to be relatively insensitive to neutron fluxes $<10^{17} \text{ n.m}^{-2}.\text{s}^{-1}$ (Adamson et al., 2019). As the damage rate (neutron flux) increases, the primary creep due to dislocation glide is suppressed and at high neutron fluxes, in OSIRIS for example, the effect of the hardening is manifested as the complete suppression of primary strain at the beginning of irradiation (Adamson et al., 2019). Figure 4-2 shows the creep strain as a function of time in out-of-flux laboratory tests for unirradiated and pre-irradiated (to a fluence of about $9 \times 10^{25} \text{ n.m}^{-2}$ in OSIRIS) creep capsules (DeAbreu et al., 2018). It shows that whereas the primary creep occurs over a long period in the unirradiated case it is non-existent for the pre-irradiated material, in keeping with the lack of a primary transient for the in-reactor high flux irradiation in OSIRIS. This can be explained by effect of hardening due to radiation damage.

Also plotted are the diametral strain data for 27% and 12% cold-worked creep capsules during irradiation in the NRU reactor at two different fluxes (two and three orders of magnitude lower than the OSIRIS irradiation) for the same temperature and hoop stress (about 280 °C and 125 MPa). The data indicate that the steady-state creep rates are similar for the 12% compared with 27% cold-worked material. However the offset strain, due to the primary creep, is higher for the 27% cold-worked material. The unirradiated material exhibits a continuously decreasing creep rate with time with no evidence of saturation up to 7000 hours. After 7000 hours the creep rate (per unit time) of the unirradiated material lies between the creep rate for the low flux and higher flux specimens, in keeping with the suppression of creep at low fluxes that is observed for pressurized tubing (DeAbreu et al., 2018).

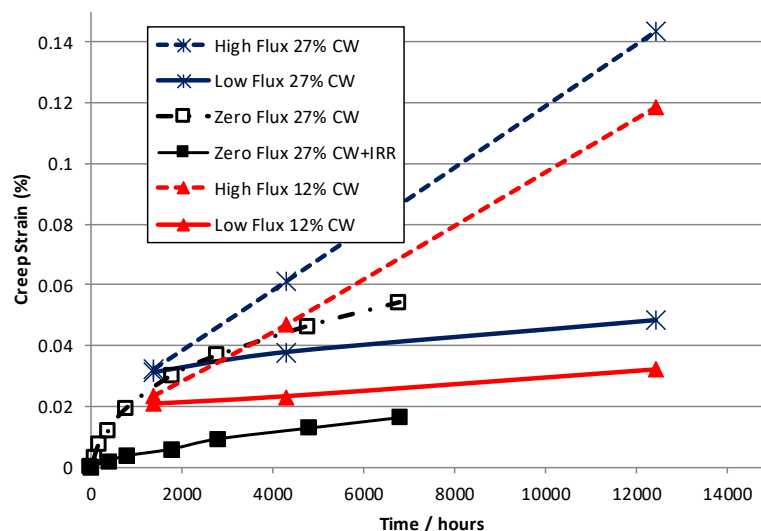


Figure 4-2. Diametral creep for internally pressurised creep capsules (125 MPa hoop) at 280 °C. Identically-made capsules were tested out of flux in the unirradiated and pre-irradiated ($16 \times 10^{25} \text{ n.m}^{-2}$, $E > 1 \text{ MeV}$, at 280 °C) states, in a low flux ($\text{LF} \sim 10^{16} \text{ n.m}^{-2}.\text{s}^{-1}$), and in a high flux ($\text{HF} \sim 10^{17} \text{ n.m}^{-2}.\text{s}^{-1}$). The zero flux 27%CW + IRR sample corresponds with a pressurized tube that has been previously irradiated to a high dose ($>8 \times 10^{25} \text{ n.m}^{-2}$, $E > 1 \text{ MeV}$) at the same temperature as the out-reactor (zero neutron flux) test, 280 °C.

Although a transition from primary to secondary creep is not apparent for the unirradiated material up to 7000 hours in Figure 4-2, a primary creep transient appears to be mostly complete for the irradiated materials at times <1400 hours based on the almost linear creep rate at longer times. Although a primary to secondary transition is apparently occurring at short irradiation times, the ongoing secondary creep at longer times is not constant and is still evolving as the microstructure evolves. As the microstructure is a function of accumulated dose (dpa) and as irradiation enhances creep through the climb and glide process, the evolution of the creep rate with irradiation time is a function of both the neutron flux and fluence.

4.2 Secondary, Steady-State Irradiation Creep

Unlike most other engineering alloys that are mostly isotropic in their creep response, the steady-state secondary creep rate of Zr-alloys is anisotropic and is strongly dependent on the texture and grain structure of the material. Even with this additional complication, the irradiation creep of Zr-alloys can be compared with other materials when tests are conducted under identical conditions of temperature and damage rate. The fundamental parameter that characterises the steady-state irradiation creep response is the creep compliance (strain rate per unit atomic displacement per unit stress). The creep compliances of different annealed materials tested in the NRU reactor are compared in Table 4-1 (Causey et al., 1980). The compliance data in Table 4-1 were originally reported as a function of neutron fluence. The fluence has been converted to dpa assuming the $1 \text{ dpa} = 0.7 \times 10^{25} \text{ n.m}^{-2}$, $E > 1 \text{ MeV}$ in the NRU reactor and a threshold displacement energy of 40 eV for all materials (Walters et al., 2018). This is different from the conversions applied in the paper by (Causey et al., 1980), for which it was assumed that $1 \text{ dpa} = 0.45 \times 10^{25} \text{ n.m}^{-2}$, $E > 1 \text{ MeV}$. To maintain consistency with current standards of dpa, the new dpa rates, obtained using the SPECTER code, will be applied in this case (Walters et al., 2018). The data in Table 4-1 show that the irradiation creep compliance is higher at lower temperatures for austenitic stainless steels and Ni-alloys whereas there is little discernible effect of temperature for Zr-alloys. The irradiation creep compliance of different Zr-alloys in either the annealed or cold-worked metallurgical state is illustrated in

Table 4-2 using data reported by (Causey et al, 1988). The data show the anisotropy of creep in cold-worked Zr-alloy components. Based on the known texture of these tubes it is clear that the creep rate is faster when there are fewer basal poles oriented in the measurement direction. In the same publication (Causey et al, 1988) showed that cold-working (unspecified amount) had a large effect on the irradiation creep of various Zr-alloys at temperatures of 320 K (47 °C), resulting in increased creep rates between 2 and 4 times the rate for annealed material. A comparison of the creep compliance for the annealed (Table 4-1) and cold-worked alloys (Table 4-2) at 570 K indicates little effect of cold-working for Zr-2.5Nb but a strong effect for Zircaloy-2 and Excel alloys.

Table 4-1

Creep constants for various annealed materials derived from stress relaxation tests at 340 K (67 °C) and 570 K (297 °C) for fast neutron fluxes ($E > 1$ MeV) of 1.5×10^{25} and 2.1×10^{25} n.m.s⁻¹ respectively (Causey et al., 1980).

Creep Compliance / 10^{-6} dpa ⁻¹ .MPa ⁻¹			
Material	340 K	570 K	Ratio ($\frac{340\text{ K}}{570\text{ K}}$)
Ni	16.80	12.60	1.33
X-750	9.10	3.50	2.6
304 SS	1.96	1.75	1.1
403 SS	1.89	1.40	1.4
410 SS	1.40	0.70	2
4140 steel	4.20	1.40	3
Zircaloy-2	2.80	2.80	1
Zr-2.5Nb	16.10	18.90	0.85
Zr ₃ Al	7.00	5.60	1.25

Table 4-2

Relative creep compliance for various stress relaxation samples extracted as strips from the longitudinal and transverse directions of as-fabricated tubing made from various Zr-alloys at 570 K (297 °C) for fast neutron fluxes ($E > 1$ MeV) of 2×10^{17} n.m.s⁻¹ (Causey et al., 1988).

Material ^d	Orientation ^a	Creep Compliance / 10^{-6} dpa ⁻¹ .MPa ⁻¹	Relative to 27% CW Zr-2.5Nb
25% CW Zr-2.5Nb	L	19.44	1.00
25% CW Zr-2.5Nb	T	10.23	1.00
25% CW Zr-2	L	21.88	1.13
25% CW Zr-2	T	14.58	1.43
Zr-1.1Cr-0.2Fe ^b	L	23.09	1.19

Annealed Excel ^c	L	7.29	0.38
Annealed Excel ^c	T	4.09	0.40
25% CW Excel ^c	L	12.15	0.63
25% CW Excel ^c	T	7.16	0.70

a) L =longitudinal, T=transverse directions in tube.

b) Small tube material.

c) Excel alloy composition Zr-3.5Sn-0.8Mo-0.8Nb.

d) Amount of cold-work not specified - assumed to be about 25%, which is standard for full-size pressure tubing.

4.2.1 Influence of flux on in-reactor secondary creep

Data obtained from pressurized tubing irradiated in the NRU reactor at 300 °C with a hoop stress of about 120 MPa are shown in Figure 4-3. The zero flux data are taken from a sister tube in the out-of-flux sections ($\text{flux} < 10^{12} \text{ n.m}^{-2}.\text{s}^{-1}$) of the same assembly at the same pressure and temperature. The neutron fluxes are shown in the figure legend in units of $10^{15} \text{ n.m}^{-2}.\text{s}^{-1}$ and extending to neutron flux levels two orders of magnitude lower than the low flux data shown in Figure 4-2. The results show that:

- 1) The primary creep is higher for the in-flux compared with the out-of flux material, but decreases with increasing flux.
- 2) The magnitude of the primary creep and the secondary creep rate decrease slightly as the flux increases between 0.3 and $4.6 \times 10^{15} \text{ n.m}^{-2}.\text{s}^{-1}$. They are nearly independent of flux in this range.
- 3) The primary creep is suppressed and the secondary creep rate increases as the flux increases above $6 \times 10^{15} \text{ n.m}^{-2}.\text{s}^{-1}$. The steady-state creep rate is assumed to be proportional to fast neutron flux based on historical in-pile experiments and assessments (Franklin et al., 1983; Fidleris, 1988).

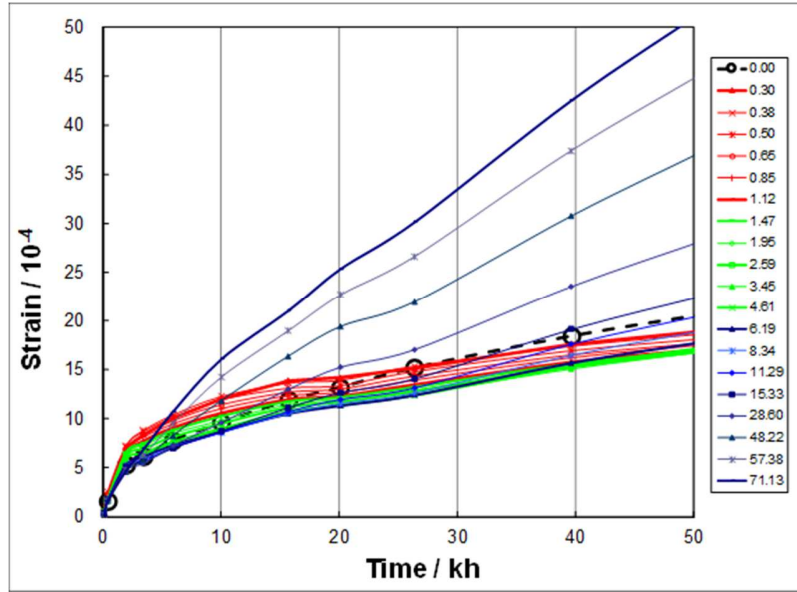


Figure 4-3. Diametral strains for 27% CW Zr-2.5Nb pressurized tube assembly 50206 in the vicinity of the creep suppression zone at the outlet (300°C). The strain data correspond to diameter gaugings between 170 and 51,570 hours of operation. Each curve corresponds to a different neutron flux, given in the legend in units of $10^{15} \text{ n.m}^{-2}.\text{s}^{-1}$.

4.2.2 Influence of dose on in-reactor secondary creep

The creep rate is not constant and decreases with increasing time (dose) becoming linear with dose as the fast fluence increases. This is best illustrated by plotting the strain per unit fluence in Figure 4-4. It is clear that the strain rate decreases rapidly with increasing dose and achieves a steady-state condition after a fast neutron fluence of $2\text{-}4 \times 10^{24} \text{ n.m}^{-2}$ corresponding to a dpa level of about 0.3 dpa. The same response is exhibited by plotting the NRU creep capsule data, shown in Figure 4-2, in Figure 4-5. Also included in the plot are the OSIRIS in-reactor creep data (red diamonds, OSIRIS 27% CW). Data for CANDU reactor pressurized tubes that had multiple gaugings are also shown. The latter data are comprised of standard pressurized tubes (G-series tubes) and some experimental pressurized tubes (TG3 RT1). The TG3 RT1 tubes were specially fabricated to minimise dislocation density. To compensate for the lower work-hardening the tubes were designed to have smaller grains in order to maintain their strength (Fleck et al., 1984). It is clear that the TG3 RT1 tubes, having smaller grains and low dislocation densities, exhibit the highest steady-state creep rate when plotted as a function of dose.

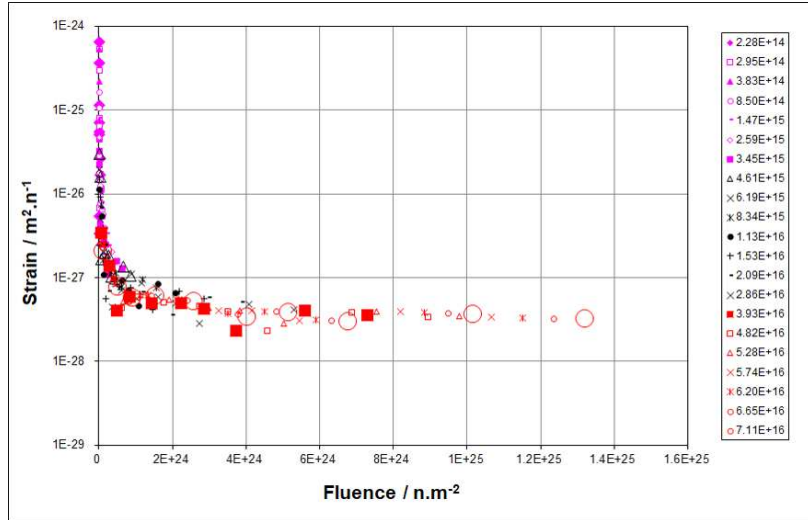


Figure 4-4. Diametral strain per unit neutron fluence for 27% CW Zr-2.5Nb pressurized tube assembly 50206 in the vicinity of the creep suppression zone at the outlet (300°C). The data correspond to diameter gaugings between 170 and 51,570 hours of operation. Each curve corresponds to a different neutron flux, given in the legend in units of $n.m^{-2}.s^{-1}$.

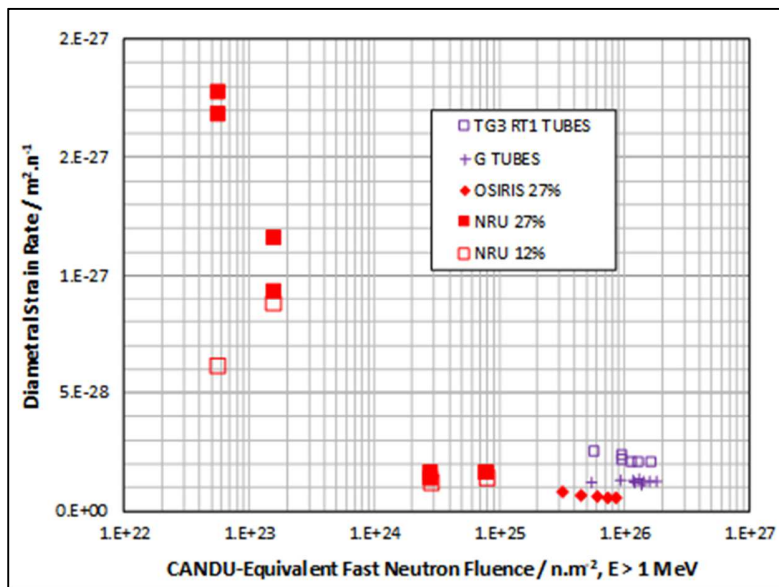


Figure 4-5. Irradiation creep and growth rates (per unit fluence) as a function of CANDU-equivalent fast neutron fluence for Zr-2.5Nb having similar textures but made by different manufacturing routes and therefore having different dislocation and grain structures.

The transition to steady-state behaviour after a fluence of about $10^{24} n.m^{-2}$ ($E > 1 MeV$), i.e. about 0.1 – 0.2 dpa, shown in Figures 4-4 and 4-5 corresponds with the saturation in a-type dislocation density, Figure 4-6. The a-type loops evolve and saturate at a low fluence (Griffiths, 1988). The c-type loop structure, however, evolves over a much larger dose range. The increase in c-loops, which are vacancy in nature,

results in a lower diametral creep strain because the texture has a large basal pole component in the transverse (hoop) direction. The negative slope of the creep compliance as a function of dose is consistent with the evolution of the vacancy c-loop density.

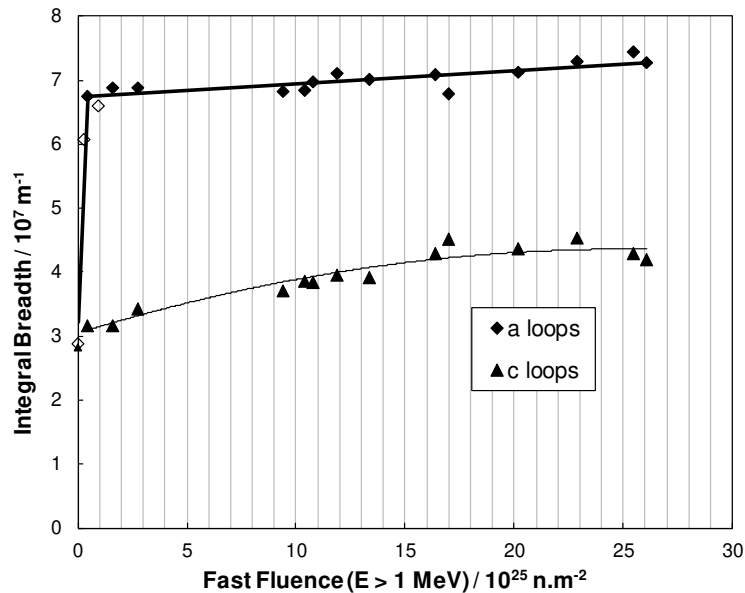


Figure 4-6. Dislocation densities (a- and c-type) for CANDU pressurized tubing irradiated in the OSIRIS reactor, represented by prism and basal plane X-ray diffraction line broadening respectively, as functions of fast neutron fluence, $E > 1$ MeV, at 250 °C (Pan et al., 2004).

4.2.3 Influence of temperature on in-reactor secondary creep

The temperature dependence of in-reactor creep has components based on thermal and irradiation processes. It is generally considered that pure irradiation creep has only a weak temperature dependence (often the process is called “athermal”) but thermal processes play an increasingly large role above about 300 °C (573 K). Above about 350 °C (623 K), thermally produced vacancies compete with irradiation-produced defects, and by 400 °C (673 K) thermal processes dominate in-reactor creep. In all cases, increasing temperature results in increasing irradiation and thermal creep rates. An example of the temperature effect that can be assumed to be steady-state irradiation creep (fast fluence $> 2 \times 10^{24}$ n.m⁻², $E > 1$ MeV) for cold-worked Zircaloy-2 is given in Figure 4-7 (Fidleris, 1988).

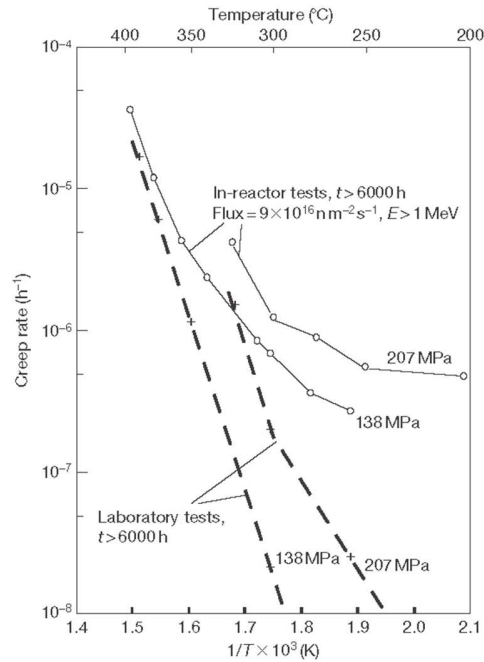


Figure 4-7. Temperature dependence of laboratory and in-reactor creep rates of cold-worked Zircaloy-2, (Fidleris, 1988).

4.3 Effect of Microstructure and Chemistry Variables

The main mechanism that has been considered in the past to explain the steady-state irradiation creep of cold-worked materials such as Zr-2.5Nb pressurized tubing is stress-induced climb and glide (SICG). A number of the early models included this mechanism implicitly to account for irradiation creep, i.e. it was the dislocation structure and the anisotropy of dislocation slip, albeit possibly modified during irradiation, that governed the creep process (Christodoulou et al., 1993, Tome et al., 1993; Christodoulou et al., 1996, Woo et al., 1994; Woo et al., 1999; Woo et al., 2000). In more recent years, data have increasingly been accumulated indicating that grain boundary sinks are very important, especially when the grain dimensions are sub-micrometer. The alloy chemical content has also a significant effect on the in-reactor creep behavior.

4.3.1 Influence of chemistry

Just as sulphur has an impact on primary creep through its likely effect on dislocation mobility, other elements (Sn, Nb and O) are known to have an effect on irradiation creep. Researchers and reactor engineers use an empirical SNO parameter, derived from the composition of Sn, Nb and O, to correlate with the steady-state creep response. The data plotted in Figure 4-8 show that steady-state irradiation creep is reduced with increase in SNO. The data also show that cold-worked (CW) and stress-relieved

annealed (SRA) Zr-alloys exhibit higher steady-state creep rates compared with recrystallised annealed (RXA) materials. The increased diametral creep for the cold-worked material in this case could reflect the higher c-component dislocation density. Because these data correspond with textures typical of fuel cladding (high radial basal poles texture parameter), the effect of the enhanced helical climb of c-component dislocations will be to preferentially increase the diametral creep rate (as compared to axial creep rate). For material with a strong basal texture in the transverse direction the diametral creep rate decreases with increasing c-dislocation density (Figures 4-5 and 4-6).

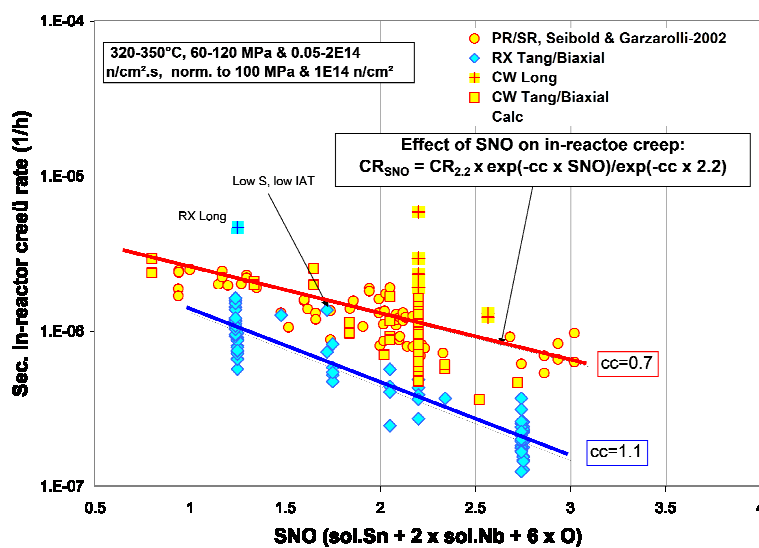


Figure 4-8. Correlation between SNO and secondary in-reactor creep rates at 320 °C – 350 °C. All data normalized as indicated. Upper solid line (red) for CW and SRA materials, lower solid line (blue) for RXA materials (Adamson et al., 2019).

4.3.2 Influence of cold-work and dislocation density

A weak dependence on dislocation density has been demonstrated at high doses (Holt, 1979). In contrast to this, the creep rate is directly proportional to the dislocation density in the primary creep regime (**Erreur ! Source du renvoi introuvable.**) as illustrated in Figure 4-2. This can be explained by the fact that dislocation slip dominates until the microstructure has evolved to its maximum hardness. More recent analyses have shown that the dependence of steady-state diametral irradiation creep on cold-working is weak for Zr-2,5 Nb pressurised tubing at about 305 °C (Walters et al., 2015; Griffiths et al., 2017a), Figure 4-9. There is a trend of increasing creep compliance with increased cold-work for the axial direction of pressurised tubing. In this case the irradiation was performed in the OSIRIS reactor for which 0.73 dpa corresponds with a fast neutron fluence of $1 \times 10^{25} \text{ n.m}^{-2}$, $E > 1 \text{ MeV}$ (Walters et al. 2018). Under these

conditions a creep compliance of $1 \times 10^{-31} \text{ m}^2 \cdot \text{n}^{-1} \cdot \text{MPa}^{-1}$ is equivalent to a creep compliance of $1.4 \times 10^{-6} \text{ dpa}^{-1} \cdot \text{MPa}^{-1}$

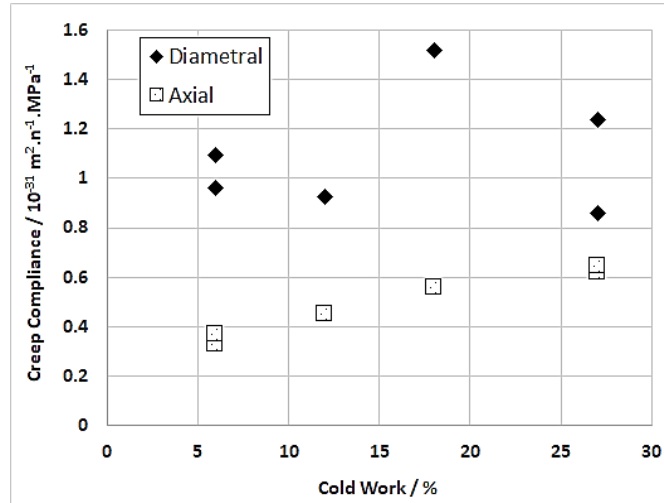


Figure 4-9. Creep compliance of cold-worked Zr-2.5Nb creep capsules normalized to a temperature of 585K and a texture of $f_R=0.4$ versus % cold-work (Walters et al., 2015).

(DeAbreu et al., 2018) showed that, depending on the neutron flux, the amount of cold-work can have a strong effect, not only on the primary creep but also on the steady-state irradiation creep. It is observed that diametral creep rates exhibited by Zr-2.5Nb creep capsules cold-worked to 27% are higher compared with 12% CW at doses up to $1 \times 10^{25} \text{ n} \cdot \text{m}^{-2}$ for temperatures of 280 °C, 320 °C and 340 °C, at neutron fluxes $> 1 \times 10^{17} \text{ n} \cdot \text{m}^{-2} \cdot \text{s}^{-1}$ (Figure 4-10) (DeAbreu et al., 2018). Unfortunately, the rates were determined assuming a single constant creep rate, rather than an evolving rate, after the initial primary creep. The effect of both temperature and cold-work are therefore confounded by the effect of fluence, and the strain rate data are compromised by the assumption of a single constant rate from low fluences. Detailed analysis on the effect of cold-work is available, however, for the data at low temperatures (280 °C) and is shown in Figure 4-5. Whereas cold work has a large effect on the primary diametral creep, any effect on secondary diametral creep is weak at 280 °C, consistent with the data shown in Figure 4-9. Even with the assumption of linearity in creep rate from low doses, the effect of cold-work on the secondary creep rate is more apparent at higher temperatures (340 °C), see Figure 4-10. The effect of cold-work is apparent at higher temperatures because thermal creep is expected to be more dominant (see Figure 4-7) and, even though the data are “high flux”, i.e. $\sim 1 \times 10^{17} \text{ n} \cdot \text{m}^{-2} \cdot \text{s}^{-1}$, the fluences for the data ($10^{23} \text{ n} \cdot \text{m}^{-2}$ to $10^{25} \text{ n} \cdot \text{m}^{-2}$) span the range where hardening from the radiation damage may not be suppressing dislocation slip as much as at the lower temperatures. Further analysis is required before any conclusions can be made

regarding the relative contributions of dislocation slip and mass transport (SIPA-I, SIPA-AD on dislocations or grain boundaries) and the effect of temperature and cold-work on secondary diametral creep.

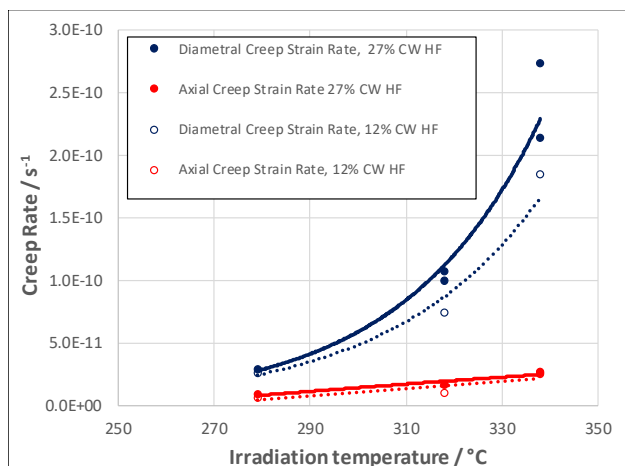


Figure 4-10. Axial and diametral creep rates for 12% and 27% cold-worked pressurised creep capsules irradiated in the NRU reactor at temperatures from 280 °C to 340 °C. Data reported by DeAbreu et al. (DeAbreu et al., 2018) for a fast neutron flux is $1.52 - 1.63 \times 10^{17} \text{ n.m}^{-2}.\text{s}^{-1}$ and a hoop stress $\sim 125 \text{ MPa}$ and for fluences between about 10^{23} n.m^{-2} and 10^{25} n.m^{-2} .

4.3.3 Influence of grain size and shape

Grain boundaries are important because they can serve as sinks for irradiation-produced defects, thereby influencing the mechanisms of both creep and growth. Isolating them as an independent variable is difficult due to the variety of thermo-mechanical processes that affect both size and shape of grains. For Zircaloy, (Franklin et al., 1983) and (Holt, 1979), report only small effects on creep, with grain shape (aspect ratio) having a stronger influence than the mean size. Kreyms and Burkhart (Kreyms and Burkhart, 1968) report larger relaxation creep rates in Zircaloy for fine grained, cold-worked and recrystallized microstructure than for larger grained hot-rolled microstructures, but the influence of fabrication variables was not clear. For Zr-2.5Nb pressurized tubes, (Griffiths et al., 2002a; Griffiths et al., 2002b) found the radial grain thickness to be an important variable, with creep rate increasing with increasing thickness. Garzarolli in (Adamson et al., 2009) has analyzed a large amount of data on Zircaloy. There appears to be a minimum creep rate in the grain size range 5-10 μm . Grain size of most commercial Zircaloy products are in this range.

(Walters et al., 2015) reported that diametral creep of cold-worked Zr-2.5Nb creep capsules increased

with a higher ratio of width/thickness, i.e. that creep was very sensitive to the grain aspect ratio, Figure 4-11. In that case the data were normalised for operating conditions using an empirical model derived by (Jyrkhama et al., 2016). Regressing out the operating conditions using the same model it was possible to derive another model for the normalised creep rate as a function of texture, grain aspect ratio, dislocation density and grain thickness. Applying this model to experimental and production pressurized tubes it was possible to show that the absolute grain dimensions are also important (Griffiths et al., 2017a). In the latter case it was shown that the creep rate of pressurized tubing was highest for the TG3 Rt1 experimental tubes, (Figure 4-12). The TG3 Rt1 tubes were specially fabricated to have a low dislocation density to minimise the axial elongation, which was perceived to be dependent on dislocation density at that time. To compensate for the reduced strength, the tubes were fabricated to have smaller grains (Fleck et al., 1984). The fact that the creep is sensitive to both the grain aspect ratio and grain dimensions is consistent with a creep mechanism dominated by diffusional mass transport. Although diffusional mass transport would be insensitive to absolute dimensions if the only sinks were the grain boundaries, the presence of dislocations (either from cold-working or radiation damage) means that the grain boundaries have to compete for point defects with other sinks. In such circumstances, the creep is sensitive to both the absolute grain dimensions and the aspect ratio.

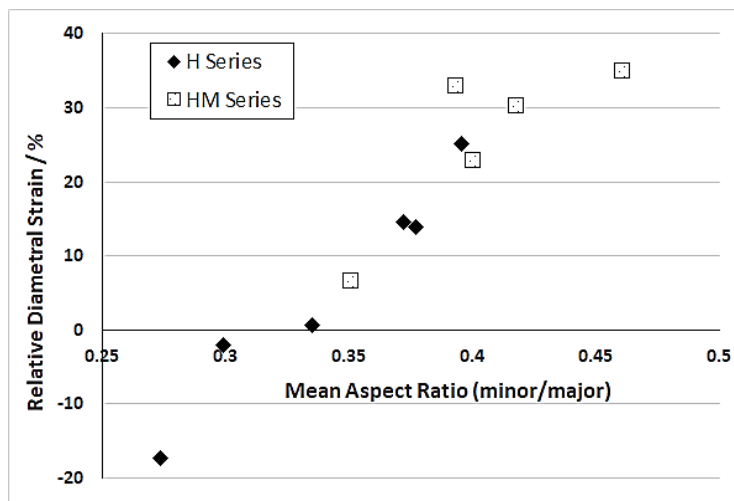


Figure 4-11. Relative diametral strain as a function of grain aspect ratio for Zr-2.5Nb pressurized tubes irradiated in CANDU reactors (Walters et al., 2015).

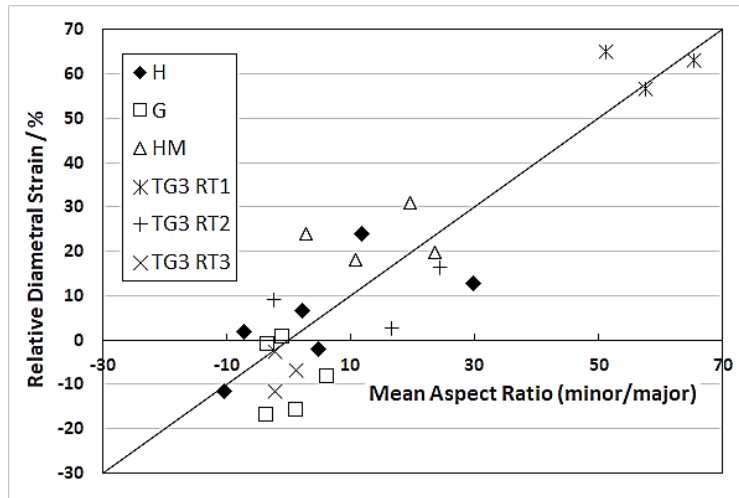


Figure 4-12. Relative back-end diametral strain vs. grain aspect ratio in production and experimental Zr-2.5Nb pressurized tubes irradiated in CANDU reactors (Griffiths et al., 2017a).

4.3.4 Influence of texture and temperature on in-reactor creep anisotropy

Texture controls the anisotropy of irradiation creep. Measured as the ratio of axial and transverse strain rates, the irradiation creep anisotropy for Zr-2.5 Nb pressurized tubing is shown in Figure 4-13 (Adamson et al., 2019). Also shown is the output for a semi-empirical model developed to match these data (Christodoulou et al., 1993; Christodoulou et al., 1996 ; Holt, 2008).

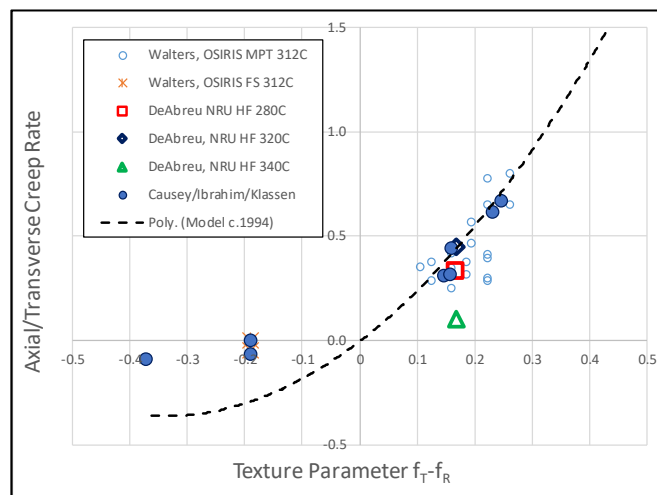


Figure. 4-13. Dependence of the ratio of biaxial in-reactor creep compliance in the transverse and axial directions of Zr-2.5Nb pressurized tubing on the texture parameter, $f_T - f_R$, and comparison with a semi-empirical model (dotted line).

Comparing the NRU data with those obtained from irradiation of similar creep capsules in OSIRIS reactor at a much higher fast neutron flux, i.e. about $2 \times 10^{18} \text{ n.m}^{-2}.\text{s}^{-1}$, the effect of temperature on the irradiation creep anisotropy is very much the same. In OSIRIS the temperature dependence of diametral creep is much stronger compared with the axial creep, Figure 4-14. The data in Figure 4-14 show that the creep anisotropy changes with temperature.

The strong effect of temperature on diametral creep, as opposed to axial creep, is an indication that the temperature dependence of irradiation creep is anisotropic. Given that the anisotropy of slip is not expected to change significantly over the temperature range of interest and given the weak dependence of creep on dislocation density in OSIRIS (Figure 4-9), the anisotropy and temperature dependence of creep could best be explained if the effect of stress on point defect diffusion, SIPA-AD (due to elasto-diffusion), was also temperature dependent.

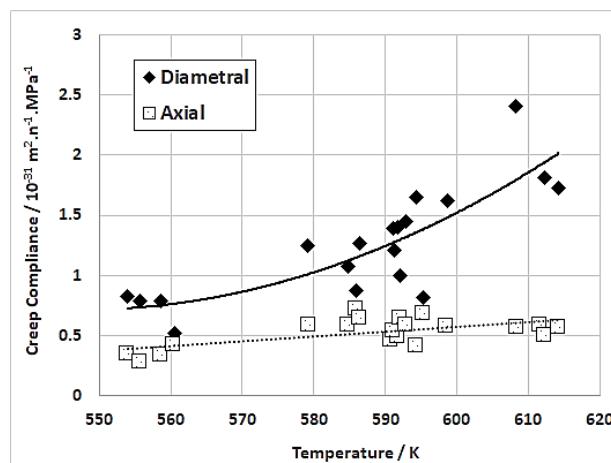


Figure 4-14. Creep compliance normalized to $f_r = 0.4$ versus temperature (Walters et al., 2015).

4.4 Discussion on irradiation creep mechanisms in Zr-alloys

Irradiation creep has a different anisotropy to thermal creep occurring by dislocation slip (Christodoulou et al., 1993; Christodoulou et al., 1996). The difference in anisotropy response to a given stress state is probably because irradiation creep and thermal creep are dominated by different mechanisms. Whereas thermal creep in the temperature and stress ranges of interest is clearly dependent on dislocation slip, there is strong evidence that irradiation suppresses dislocation slip due to formation of defect clusters (loops) that act as barriers to dislocation motion (DeAbreu et al., 2016; Griffiths et al., 2005; Griffiths et al., 2009; Griffiths et al., 2017a). Although the stress-induced climb and glide mechanism assumes that

climb of dislocations over obstacles more than compensates for the hardening effect of irradiation, there are few data to indicate whether this is the dominant mechanism in most power reactor conditions. At low fluences, high temperatures or high stresses one might expect slip to be dominant. In the reactor core, one must assume that dislocation slip and diffusional mass transport are both potential mechanisms for irradiation creep; the important question is how much of each contributes to the observed strain and under what circumstances. Clearly at the beginning of irradiation one can expect thermal creep to start out the same as in laboratory tests for unirradiated material, quickly transitioning to secondary irradiation creep as the material hardens from the accumulation of radiation damage. Likewise, with increasing temperature the material is increasingly less influenced by the effects of irradiation and more of a contribution to the creep strain due to thermal creep by dislocation slip can be expected, unless the temperature is so high that other diffusional creep mechanisms start to be important. At intermediate conditions, where most reactors operate, it is difficult to determine exactly what mechanisms are operating. However, one can infer which mechanisms are the most applicable from the data in many cases.

The difference between the irradiation creep and thermal creep anisotropy is likely due to the effect of stress on the intrinsic anisotropic diffusion of irradiation-induced point defects, the effect of so-called elasto-diffusion (Woo, 1984). Once one incorporates the effect of stress on mass-transport, one effectively links the processes of irradiation creep and growth, the transition from growth to creep being a continuous evolution as a function of stress (DeAbreu, 2017). It could be argued that the mechanisms of irradiation creep are applicable to deformation even in the absence of an applied stress due to: (i) the grain interaction stresses that exist from fabrication, and (ii) stresses that are induced by the intrinsic irradiation growth in individual grain of a textured poly-crystal. However, especially for high irradiation growth rates, the irradiation deformation in the absence of an applied stress can be understood simply based on the intrinsic deformation of the material (irradiation growth). Irradiation creep then represents the extrinsic effect of the applied stress on the growth behaviour.

The mechanisms of irradiation creep include the direct accumulation of strain from diffusional mass transport as well as dislocation glide, the relative proportion of each being dependent on the neutron flux, fluence and irradiation temperature (DeAbreu, 2017; Griffiths et al., 2005; Griffiths et al., 2017a; Bickel et al., 2010). Thus, irradiation creep can be considered as a combination of thermally-activated slip, which is enhanced by the additional climb that occurs in an irradiation environment due to the higher steady-state point defect concentrations, and diffusional mass transport, Figure 4-15.

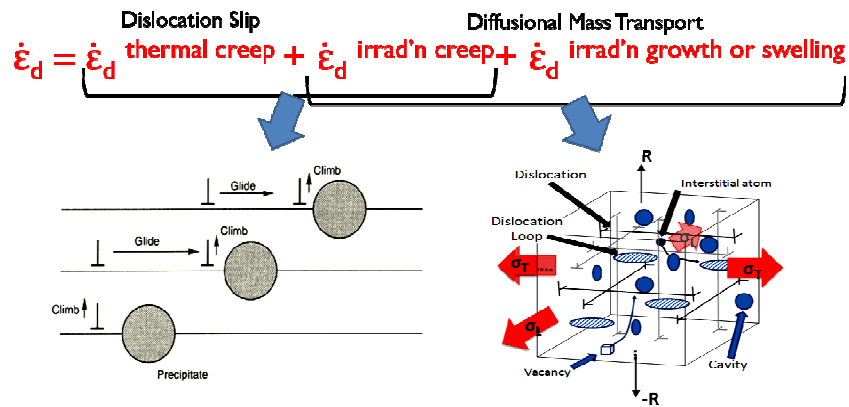


Figure 4-15. Schematic outlining the two main mechanism contributing to irradiation deformation, dislocation slip and diffusional mass transport.

Assuming that the out-reactor creep of pre-irradiated material represents the in-reactor thermal creep contribution, at power reactor temperatures (below 350 °C) the thermal creep contribution is small, at least for the moderate stresses of interest for long time behaviour of fuel components and pressurized tubes (Griffiths et al., 2005; Griffiths et al., 2009). Thermal creep at such low temperatures is often assumed to be dominated by dislocation slip. If irradiation creep would be also dictated by dislocation slip it would be reasonable to assume that irradiation creep is simply enhanced thermal creep. However, there are no data to show that irradiation and thermal creep are governed by the same physical mechanism, although elements of thermal creep, i.e. dislocation glide, do seem to be operating at lower neutron fluxes and fluences and high temperatures (DeAbreu et al., 2017). From this perspective primary creep may be regarded as the transition from thermal creep of unirradiated material to irradiation creep of irradiated material as the material hardens due to radiation damage at the beginning of irradiation. The transition from thermal to steady-state irradiation creep is often represented as an offset (or intercept) strain at time zero in empirical models. Irrespective of whether irradiation creep is determined by dislocation slip, or mass transport, or a combination of both, it is not possible to differentiate between thermal and irradiation creep in the analysis of the in-reactor creep data in the temperature range from 60 °C to 400 °C unless one has already assumed the value of one or other from a mechanistic model. Thus, empirical models for steady-state in-reactor creep implicitly contain the combined effect of irradiation and thermal creep, the latter being subsumed into the former.

5 Irradiation creep of austenitic stainless steels

5.1 Introduction

Austenitic stainless steels are used in Sodium Fast Reactors (SFR) as structural components and fuel cladding tubes and in Light Water Reactors (LWR) for internal structures. Operation temperatures in the SFRs vary from 400°C to 550°C for the structures and up to 650°C for the fuel cladding. The internal structures of LWRs are irradiated at lower temperatures between 300°C and 400°C.

In austenitic stainless steels, the thermal creep occurring without irradiation, due to dislocation slip, exhibits a minimum at intermediate temperature between 200°C and 500°C (Couvant, 2005). This phenomenon is due to dynamic strain ageing (DSA) (Hahn, 1988; Kashyap, 1987; deAlmeida, 1998; Choudhary, 2001). Furthermore, under irradiation, pinning of dislocations by radiation damage occurs. Thus, the creep strains measured during in pile creep testing when DSA and irradiation hardening are prominent are likely to be dominated by irradiation creep caused by diffusional mass transport rather than dislocation glide.

The history of the development of irradiation creep concepts that apply to austenitic stainless steels until 1983 has been described and discussed in detail by (Franklin et al., 1983). At that time, the main focus was on mechanisms that relied on the effect of stress on dislocation loop nucleation (SIPN), diffusion to dislocations (SIPA) and the enhancement of climb of gliding dislocations over obstacles (SICG). Reviews of irradiation creep mechanisms by (Matthew & Finnis, 1988) have indicated how mechanistic understanding has evolved. In more recent reviews of irradiation creep by Garner (Garner, 2010; Garner, 2012) the role of swelling was discussed extensively. In that case the swelling (when present) is deemed an important factor in the dimensional changes observed during irradiation. This is due to the direct impact on the volume change of the material and because the voids created under irradiation, associated with swelling, increase the density of sinks for vacancy point defects (neutral sinks) and this results in a higher flux of interstitials to network dislocations and dislocation loops, thus inducing an enhanced irradiation creep rate.

The irradiation creep of stainless steels exhibits primary and secondary stages. There are few data on primary creep but extensive data on secondary creep under varying material and operating conditions extending to high doses.

5.2 Primary Irradiation Creep

Contrary to what is observed for Zr-alloys, primary creep in austenitic stainless steels is very much larger than the primary creep observed in thermal creep tests (Figure 5-1). Densification, caused by aging effects, results in a shrinkage in specimen dimensions and confounds the observation of primary creep (Figure 5-2). The primary transient strain sometimes observed in creep tests may be affected also by other factors such as relaxation of residual stresses. Irradiation growth could also potentially confound the interpretation of the creep or densification response (Bates, 1981), although the magnitude of irradiation growth is generally small in cubic materials.

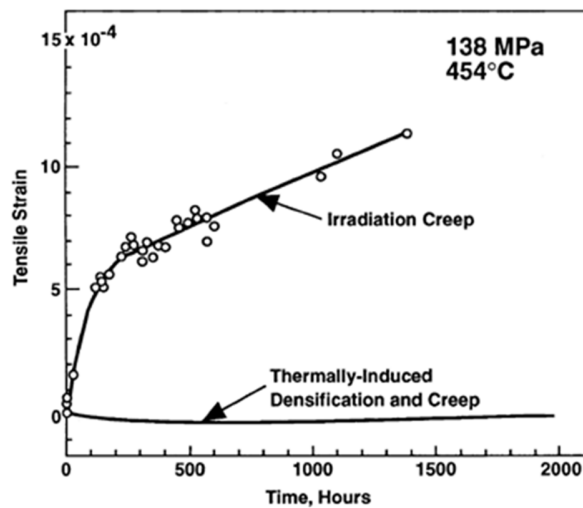


Figure 5-1. Comparison of creep rates observed in 20% cold worked 316 stainless steel in uniaxial tests during thermal aging or neutron irradiation in EBR-II (after Gilbert et al., 1973).

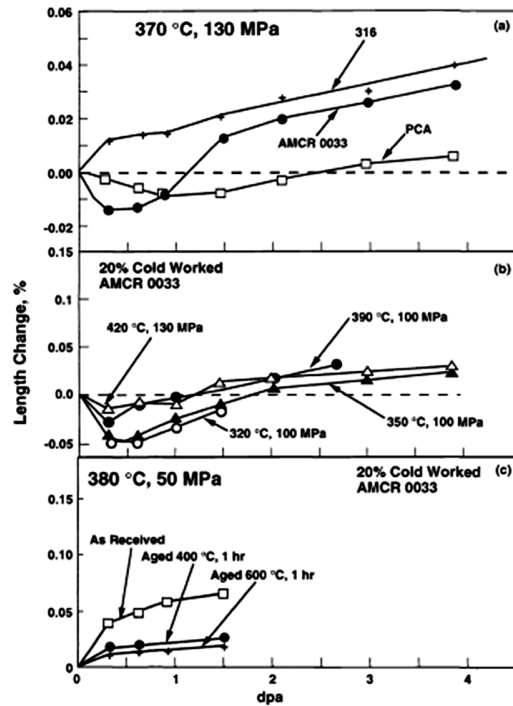


Figure 5-2. Length changes observed in HFR during uniaxial creep tests of (a) three different cold worked steels at 370 °C; (b) 20% cold worked AMCR 0033 at different irradiation temperatures; (c) 20% cold worked AMCR 0033 in different starting conditions (after Hausen et al., 1988).

5.3 Secondary Steady-State Irradiation Creep

5.3.1 Stress Dependence

As with other materials, irradiation creep of austenitic stainless steels exhibits a nearly linear dependence on stress. At low stress, the equivalent strain, ϵ , is proportional to the equivalent stress σ and the dose ϕt .

$$\epsilon = B_0 \sigma \phi t$$

At high temperature, above 400°C, and high doses when the swelling is significant (swelling rate is noted $\dot{S} = d(\frac{\Delta V}{V})/d\phi$), the irradiation creep compliance is enhanced. A simplified empirical law is often given by an equation of the type described below (Garner, 2012).

$$\epsilon = (B_0 + D\dot{S})\sigma\phi t$$

The irradiation creep compliance has been measured by many authors and are reported in Table 1. The temperature, stress and dose range are indicated in this Table. An example of measurements, in the

temperature range between 384°C and 406°C, reported by (Garner and Puigh, 1991) are shown on Figure 5-3.

Table 5-1: List of irradiation creep compliance B_0

Reference, first author	Steel	T (°C)	B_0 (10^{-6} MPa ⁻¹ .dpa ⁻¹)	σ (MPa)	Dose (dpa)
(McSherry, 1978) (Puigh, 1982)	CW316	410 - 425	1-2		12
(Hausen, 1988)	CW316	370	0.7	130	4
(Garner, 1992)	CW316	475 - 600	3.5 – 8	0 – 217	1 -10
(Krasnoselov, 1987)	CW316	350 - 500	1.0 – 3.0		4 - 28
(Mosedale, 1977)	CW316	280	2		
(Gilbert, 1978)	CW316	500	5	<200	
(Causey, 1980)	SA304	300	1.7	160 – 190	2
(Wire, 1977)	SA304	410 – 437	1.6	0 – 200	1
(Foster, 1998a)	CW316	380 – 460	1.5 – 2	80 – 327	2 - 60
(Foster, 1998a)	CW316	454	0.95		
(Foster, 1998b)	CW316	380 – 400	1.4	80 - 330	
(Williams, 1997)	CW316	430	0.8 – 1.9	50 – 350	1
(Gilbert ,1973)	CW316	454	0.95	138	3
(Lewthwaite, 1980)	316	370 – 305	1 – 2	20 – 60	25
(Porter, 1991)	SA304	380 – 415	0.5 – 1	0 – 190	85
(Grossbeck, 1988)	CW316	300 – 600	2.	20 – 470	12
(Grossbeck, 1990)	CW316 SA316	60 – 400	2	100 – 350	8
(Grossbeck, 1990)	US PCA 15Cr/15Ni	330 - 400	1.5	50 – 350	8
(Grossbeck, 1990)	US PCA 15Cr/15Ni	60	6.5	50 – 200	8
(Grossbeck, 1996)	SA316, CW316	330	1.3 – 2.7	100 - 300	19
(Garner, 1988)	CW316	385 - 400	1	0 – 343	130
(Lehmann, 1979)	CW316, SA316,	400 – 430	1.3		
(Foster, 2003)	SA304	390	0.38	69 – 188	93.3
(Grossbeck ,1996)	CW316, SA316	330	2.8	300	7 - 20
(Foster, 1999)	CW316	200 – 585	1.1 – 1.5	40 – 400	2 – 60
(Foster, 1999)	CW316	60	2.2	40 – 400	7 - 20
(Neustroev, 2000)	15Cr/15Ni	420	1.0 – 1.7	0 – 320	100
(Uehira, 2001)	PNC316		1.1 – 3.0		107
(Simonen, 2005)	300-series	250 – 500	1	<250	

The data in Figure 12 include both swelling and creep. This figure shows that the stress dependence is linear although there is some non-linearity apparent in the plots that may simply reflect changes in swelling as the stress changes.

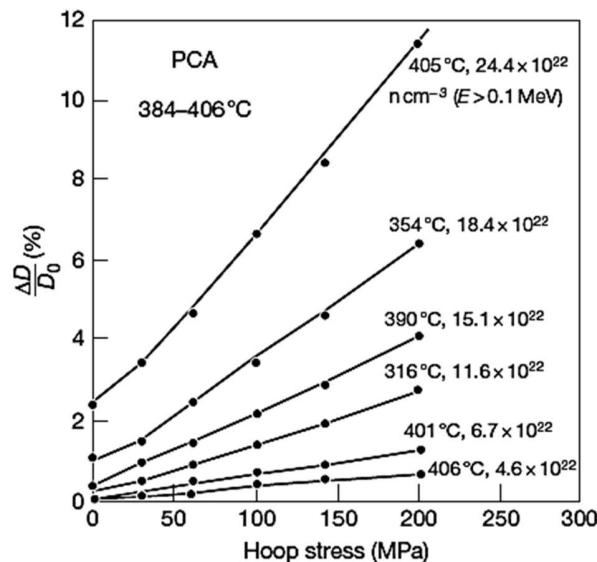


Figure 5-3. Linear stress dependence of total diametral strain (creep and swelling) for 20% cold-worked PCA (Ti-modified 316 stainless) pressurized tubes irradiated in FFTF at 400°C. Reproduced from. Stress-free swelling is approximately three times the Y-intercept value with the largest swelling at 8%.

It is remarkable that despite the fact that metallurgical states and tensile or thermal creep properties are different, all the austenitic stainless steels of varying thermo-mechanical treatments exhibit a similar compliance, B_0 , for a given temperature, typically between 0.7 to $3 \times 10^{-6} \text{ MPa}^{-1} \cdot \text{dpa}^{-1}$. This is usually explained by the evolution of the dislocation network under irradiation, as reported by Wolfer et al. (JNM 1980). Indeed, the dislocation network of the cold-worked material partly recovers under irradiation whereas the dislocation network in the solution-annealed material increases, the two materials having a similar dislocation network after doses $\sim 10 \text{ dpa}$.

It must also be mentioned that according to Garner (Garner, 1994) the derivation of B_0 is confounded by the effect of differences in swelling in different alloys and the difficulty in separating the swelling strain and the irradiation creep strain. Anisotropic swelling (Flinn, 2007) and the dependence of swelling on the stress (because the flux of point defects to different sinks is also affected by the stress) complicates the partitioning between swelling and irradiation creep strains (Séran, 1990; Porter, 1991; Foster, 2003; Toloczko, 2004). Differences between the definitions of strain and stress in different studies also makes it difficult to compare data from different sources.

More recently, experiments have been conducted using pressurized tubes irradiated in three different material testing reactors (OSIRIS at 300°C, EBR-II at 375°C and BOR-60 at 330°C) to study the creep behaviour of cold-worked and solution-annealed 304 and 316 austenitic stainless steels under irradiation (Garnier, 2011a). Diametric deformation of tubes was measured at regular intervals after unloading. When swelling occurs the irradiation creep strain is deduced assuming that the strain due the swelling is isotropic. The diametral strain from swelling in the absence of stress is deduced by using the diametric evolution of a non-pressurized tubes or by performing density measurements. Diametric evolution of four tubes machined in SA 304 austenitic stainless steels pressurized at different hoop stress levels is presented in Figure 5-4 (a). The irradiation creep compliance per MPa per dpa, *i.e.* $(B_0 + D\dot{S})$, can be extracted by plotting the strain rate per dpa against stress in Figure 5-4(b). The results show that the compliance is $2.99 \times 10^{-6} \text{ MPa}^{-1} \cdot \text{dpa}^{-1}$. The plot also shows that the hoop strain is zero for an extrapolated hoop stress of $\sim 50 \text{ MPa}$ assuming a linear stress dependence for steady-state irradiation creep up to 200 MPa. This implies that there may be a growth component giving a negative strain rate of $1.6 \times 10^{-4} \text{ dpa}^{-1}$ at zero hoop stress or some other phenomenon such as residual fabrication stresses that need to be overcome before positive creep is possible. The compliance $(B_0 + D\dot{S})$ of pressurized tubes can also be assessed by plotting the strain as function of dose times stress.

The results obtained on both cold-worked and solution-annealed 304 and 316 stainless steels are plotted in Figure 5-5 where the strain is shown as a function of dose times stress. The slight difference between OSIRIS and BOR-60 is likely due to errors in calculating dpa due to differences in the spectra. This data set shows that the cold-worked materials exhibits a slightly lower creep compliances compared with solution-annealed materials. The fact that irradiation creep compliances are similar for solution-annealed and cold-worked materials is consistent with earlier findings. The intercept at zero strain may be indicative of either a residual stress effect or other non-irradiation-creep dimensional changes similar to that illustrated in Figure 5-4(b). However the processed data are not in a form that would allow further detailed analysis.

Considering the scatter in the experimental data set, the bolt relaxation of the French PWR internals has been simulated with good agreement with in-reactor measurements (Lemaire2004; Massoud2002).

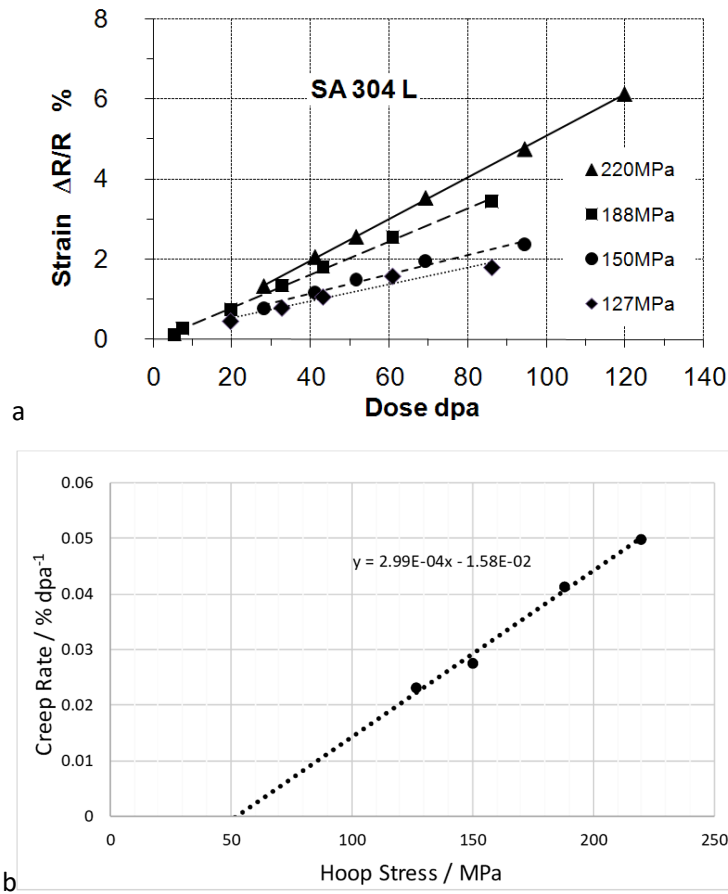


Figure 5-4. Evolution of in-reactor creep as a function of dose for SA 304 at different stress levels irradiated in BOR-60 at 330°C (Garnier, 2011a)

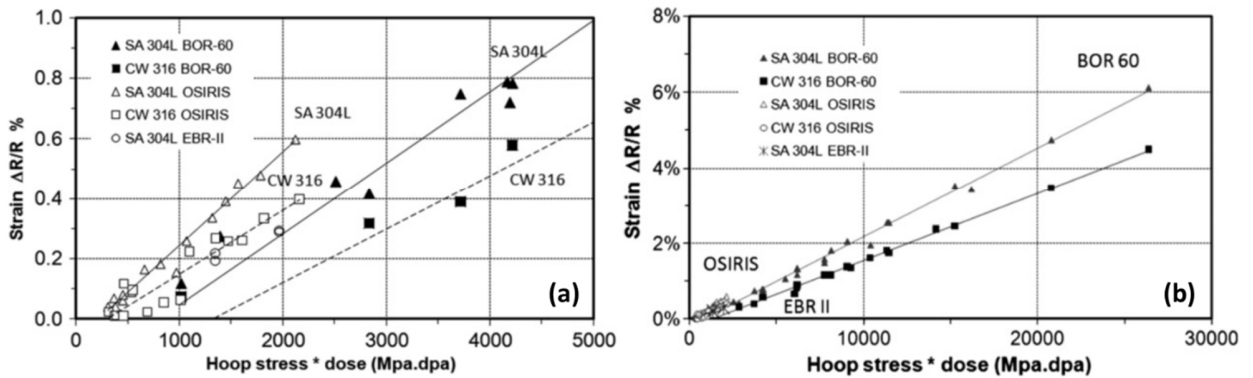


Figure 5-5. Evolution of in-reactor creep as a function of dose for SA 304L and CW 316 BOR-60 at 330°C, OSIRIS at 330°C and EBR-II at 375°C. (a) up to low doses, (b) up to higher doses (Garnier, 2011a).

5.3.2 Temperature dependence

Overall, there is only a weak temperature dependence for irradiation creep in austenitic steels. At temperatures as low as 60 °C it is reported by Grossbeck (Grossbeck 1990) that the irradiation creep compliance is high, around $6.5 \times 10^{-6} \text{ MPa}^{-1} \cdot \text{dpa}^{-1}$, whereas it is only $1.5 \times 10^{-6} \text{ MPa}^{-1} \cdot \text{dpa}^{-1}$ between 330°C and 400 °C. Above 300°C, it is usually considered that the compliance B_0 is essentially athermal (Hausen 1988) (**Erreur ! Source du renvoi introuvable.**). However, some authors show a slight decrease from 3 to $1 \times 10^{-6} \text{ MPa}^{-1} \cdot \text{dpa}^{-1}$ as the temperature increases from 330°C to 500°C (Figure 5-6). The trend in this case is likely driven by the fact that the dislocation density is lower at higher temperatures (Figure 5-7). The dislocation structure here includes both the network dislocations and dislocation loops. Other authors report a slight positive temperature dependence between 400 and 600°C as shown on figure 5-8.

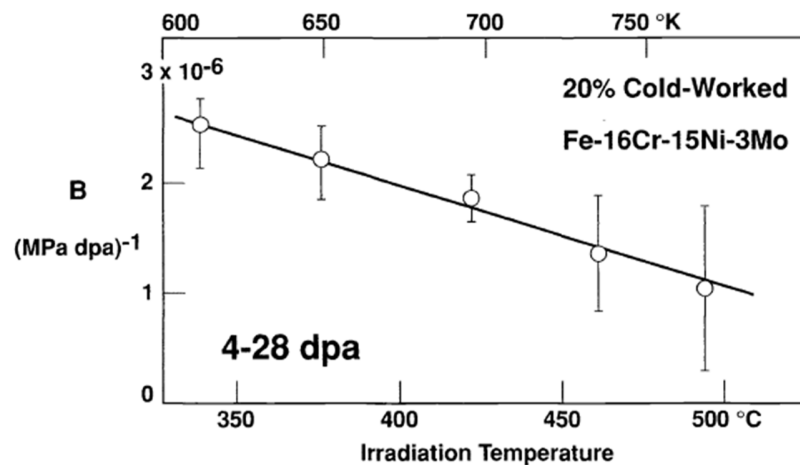


Figure 5-6. Temperature dependence of creep compliance in cold worked 0X16H15M3b, measured across flats of a helium-pressurized hexagonal lattice element irradiated in BOR-60. No swelling was observed at these exposures (after Krasnoselov et al, 1987).

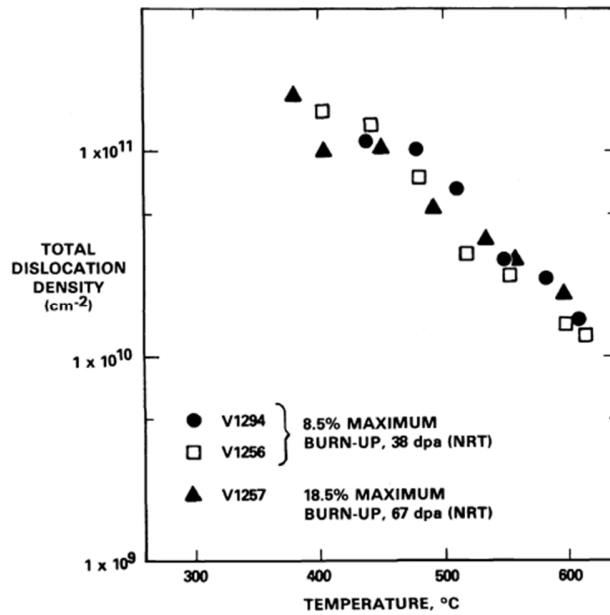


Figure 5-7. Total of network and loop dislocation density observed in M316 cladding from three fuel pins irradiated in DFR (after Brown and Fulton, 1979; Brown et al, 1983).

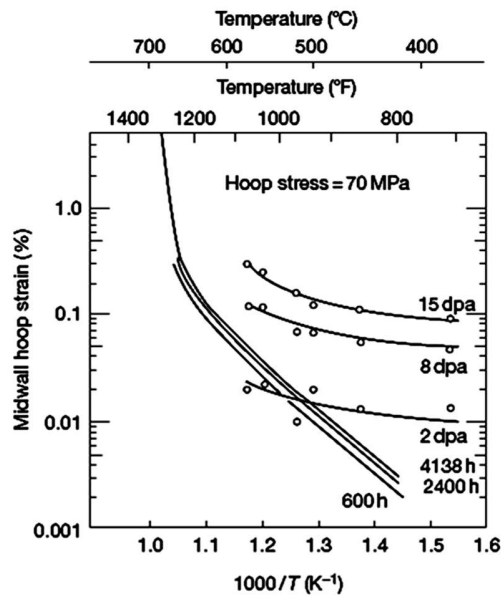


Figure 5-8. Thermal creep and irradiation creep in EBR-II of 20% cold-worked 316 pressurized tubes at various dpa levels at 70 MPa hoop stress. Reproduced from Gilbert, E. R.; Bates, J. F. J. Nucl. Mater. 1977, 65, 204–209.

5.3.3 Flux dependence

The steady state irradiation creep is primarily a linear function of the neutron flux (Figure 5-9). The flux and temperature dependence are difficult to separate experimentally because high flux generally

corresponds with more nuclear heating and higher temperatures. The data shown in Figure 5-9 are therefore confounded by the fact that the temperature is also higher at the higher neutron flux. Indeed, some data have shown that, over the same range of temperatures applicable to Figure 5, there is a weak negative temperature dependence, Figure 5-6.

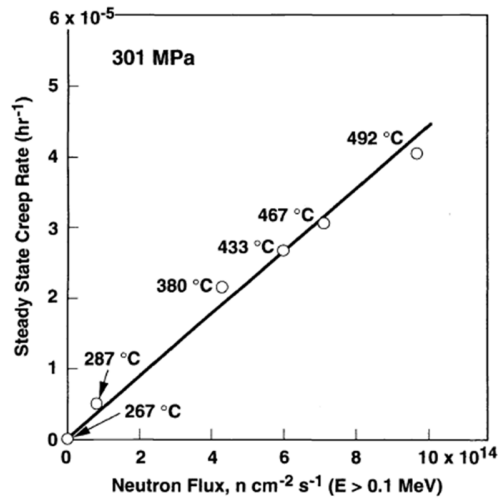


Figure 5-9. Secondary creep rates observed in annealed 09KM6N15M3B irradiated in BR-10 (after Kruglov et al., 1980).

There is evidence that, at very low fluxes and low irradiation temperatures, there is a negative flux dependence of the irradiation creep compliance, i.e. the creep strain per unit stress per unit fluence. This basically means that a low fluxes there is a higher creep rate per unit time. The negative flux dependence is illustrated in Figure 5-10.

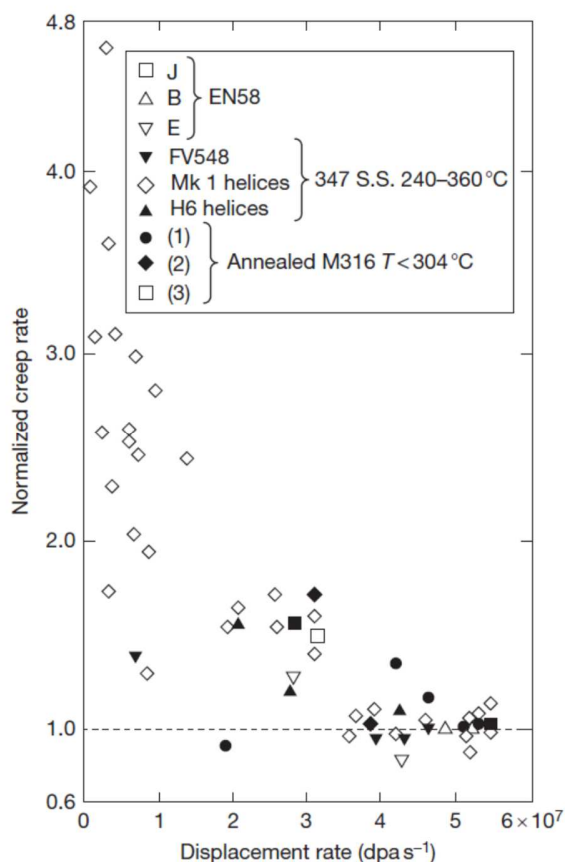


Figure 5-10. Dependence of irradiation creep rate (per unit dpa) of springs made from various austenitic steels on dpa rate in and below the DFR core, normalized to the highest displacement rate studied. Reproduced from Garner, F., *Compr. Nucl. Mater.* 1st Ed, 2012 based on data given by Lewthwaite, G. W.; Mosedale, D. J. *Nucl. Mater.* 1980, 90, 205–215.

A re-examination of the Lewthwaite and Mosedale data shows that the flux dependence is confounded by the effect of fluence. This arises because, over the duration of creep tests, the lower fluxes correspond with lower fluences. If there is a fluence dependence of creep that slows the secondary creep rate then this change in the material response may show up as an apparent higher creep rate at low fluxes.

5.3.4 Fluence dependence

Secondary irradiation creep is generally assumed to be linear with dose until swelling becomes significant. At that time the irradiation creep is a combination of swelling and non-swelling compliances. The data reported by (Garner et al. 1992), Figure 5-11, show that the strain rate is non-linear with increasing dose and the increasing creep rate can be attributed to a combination of strain from swelling and increased creep. These data also show that there is only a small difference between the irradiation creep for various levels of cold-working (10%, 20% and 30%).

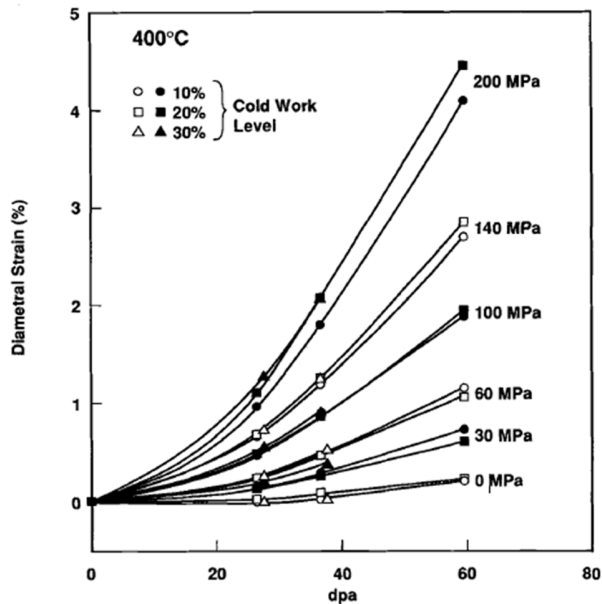


Figure 5-11. Deformation induced by irradiation creep and swelling at 400 C for three cold work levels in D9 austenitic stainless steel. Open and closed data points are identical and are used only to differentiate closely spaced data. Reproduced from Garner, F. A., Hamilton, M. L., Eiholzer, C. R., Toloczko, M. B., & Kumar, A. S. (1992). Irradiation and thermal creep of a titanium-modified austenitic stainless steel and its dependence on cold work level. *Journal of nuclear materials*, Vol. 191, pp. 813-817.

The creep strain responses for various batches of three austenitic stainless steels (FV548, EN58 and 316) were reported and plotted by (Lewthwaite and Mosedale, 1980) assuming that the creep strain for a given stress increased linearly with increasing dpa (or time at a constant flux) given an initial transient. Although the trend with dose and dose rate is confounded by variations in temperature and stress, Lewthwaite and Mosedale reported that the irradiation creep rate (creep strain per unit dpa) was negatively correlated with dose rate, i.e. the strain per unit dpa was larger at low dose rates. Given that the low dose rate data also corresponds to low doses, the dose rate effect may simply reflect a dose/fluence effect as noted by (Garner and Toloczko, 1997). Selecting data at approximately the same temperature, then normalising for stress, the strain rate per unit dpa plotted as a function of dpa shows that in each case the creep per unit dpa decreases monotonically over a dose of about 5-10 dpa and tends to a constant value at high doses (>10 dpa). The raw strain data are plotted together with the derived creep compliances (strain per unit dpa normalised for stress) in Figure 5-12 for EN58E SS, Figure 5-13 for FV548 SS and Figure 5-14 for 316 SS.

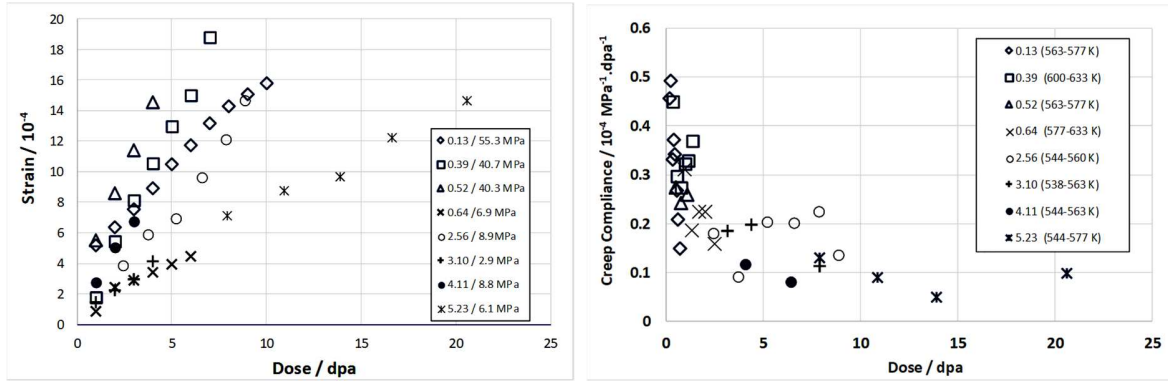


Figure 5-12. Creep as a function of dose rate for EN58E SS springs irradiated in Dounreay fast reactors at temperatures between 544 K and 633 K (271 °C – 360 °C): (a) strain as a function of dpa dose; (b) compliance as a function of dpa dose. The legend shows the dpa rate (in units of 10^{-7} dpa.s $^{-1}$) and stress for each dataset.

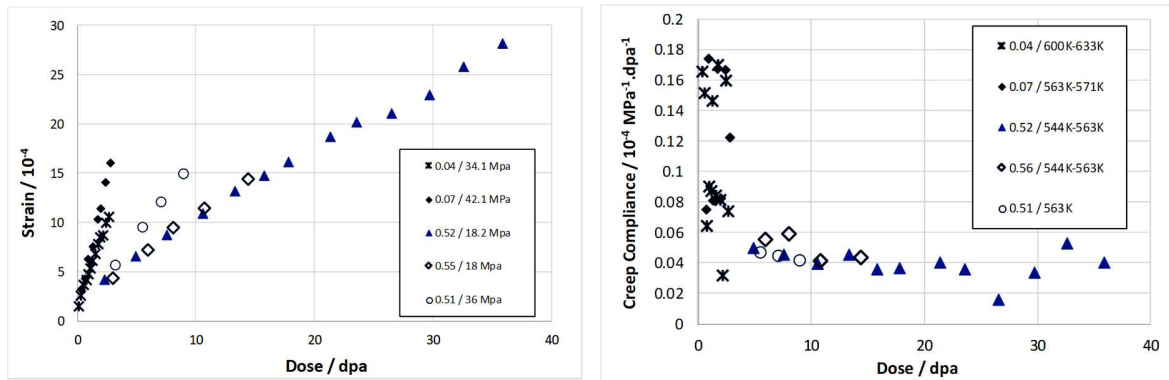


Figure 5-13. Creep as a function of dose rate for FV548 SS springs irradiated in Dounreay fast reactors at temperatures between 544 K and 633 K (271 °C – 360 °C): (a) strain as a function of dpa dose; (b) compliance as a function of dpa dose. The legend shows the dpa rate (in units of 10^{-7} dpa.s $^{-1}$) and stress for each dataset.

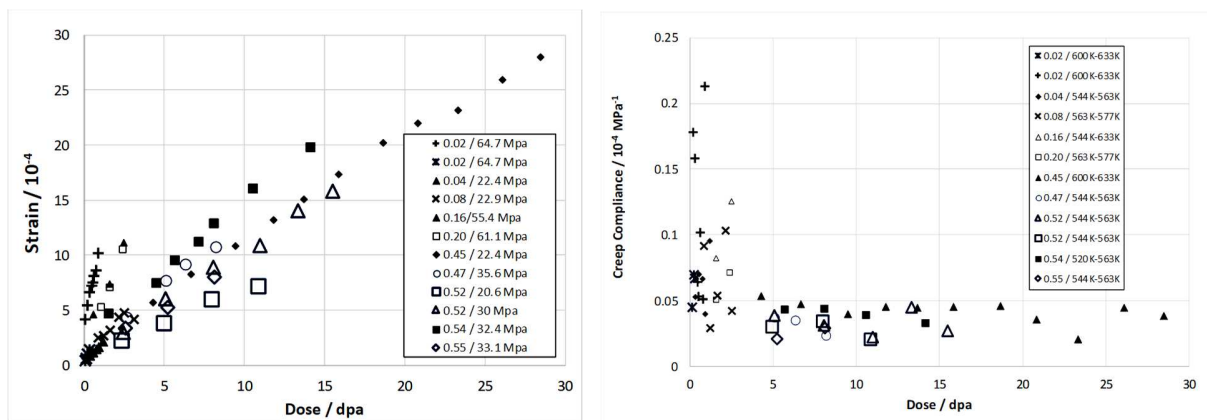


Figure 5-14. Creep as a function of dose rate for 316 SS springs irradiated in Dounreay fast reactors at temperatures between 520 K – 633 K (247 °C – 360 °C): (a) strain as a function of dpa dose; (b) compliance as a function of dpa dose. The legend shows the dpa rate (in units of 10^{-7} dpa.s⁻¹) and stress for each dataset.

The transition to true steady-state irradiation creep occurs over a dose of about 5 dpa and is separate from the primary strain transient that occurs during the first 500 hours of irradiation and is complete by about 0.1 dpa. Even though the material exhibits pseudo-steady-state creep after the initial transient there are still changes occurring in the material that are also coincidental with an increase in yield strength. The change in yield strength caused by radiation damage occurs over a dose range up to about 10 dpa and is shown in Figure 5-15 (Garnier et al., 2007). The evolution of the yield strength (a surrogate for radiation damage) can be correlated with the transition to steady-state creep shown in Figures 5-12, 5-13 and 5-14.

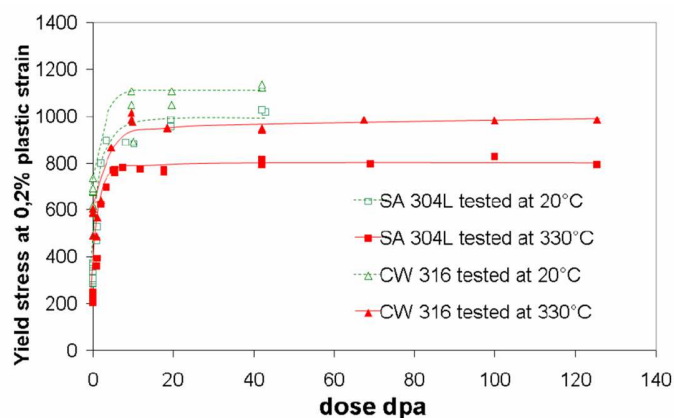


Figure 5-15. Compilation of yield stress data at 20 and 330 °C for austenitic stainless steels as a function of dose irradiated at 330 °C (Garnier et al., 2007).

5.3.5 Effect of microstructure and chemistry variables

Whereas thermal creep in the temperature and stress ranges of interest is clearly dependent on dislocation slip, there is strong evidence that irradiation suppresses dislocation slip (Griffiths et al, 2005; Griffiths et al, 2006; DeAbreu, 2018). Although the stress-induced climb and glide mechanism assumes that climb of dislocations over obstacles more than compensates for the hardening effect of irradiation, there are few data to indicate whether this is the dominant mechanism in austenitic stainless steels at power reactor conditions. At low fluences, high temperatures or high stresses one might expect slip to be more dominant. In the reactor core, one must assume that dislocation slip and diffusional mass transport are both potential mechanisms for irradiation creep. The important question is how much of

each contributes to the observed strain and under what circumstances. Clearly at the beginning of irradiation one can expect thermal creep, i.e. that from dislocation slip, to be high, transitioning to secondary irradiation creep as the material hardens. Stainless steels are no different from other alloys. The effect of cold-work seems to be mostly realised in the primary creep stage. The secondary creep rate for CW stainless steel is apparently similar to that of annealed material, Figure 5-16.

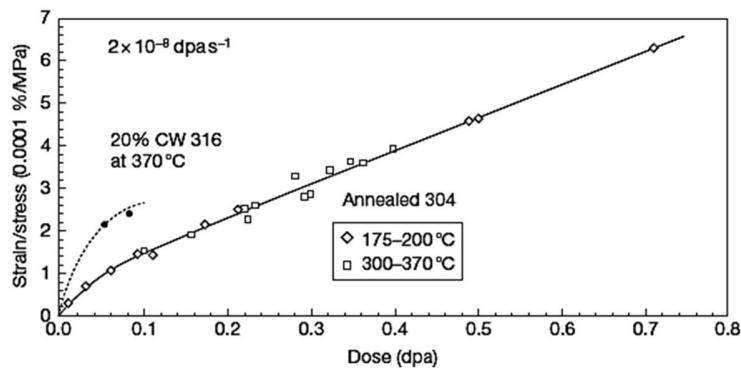


Figure 5-16. Irradiation creep of austenitic steels during uniaxial testing in the K Reactor, showing independence of creep of annealed 304 on temperature in the range 175–370 C. Reproduced from Foster, J. P.; Gilbert, E. R.; Bunde, K.; Porter, D. L. J. Nucl. Mater. 1998, 252, 89–97; Gilbert, E. R. Reactor Technol. 1971, 14, 258–285. B_0 is 0.92106 (MPa dpa). The larger transient of cold-worked 316 is due to its much higher dislocation density.

For steels it appears as though the steady-state irradiation creep is not strongly dependent on the initial dislocation structure, see Figures 5-11 and 5-16 and Table 5-1. In Figure 5-5 it is clear that the irradiation creep compliance, strain per unit stress per unit dpa, is slightly higher for annealed compared with cold-worked material, albeit for different alloys (304 SS and 316 SS).

6 Irradiation creep in Ni-based alloys

6.1 Ni-alloy usage in nuclear reactors

Ni-based alloys are used as specialised components in conventional light and heavy water reactors. Precipitation-hardened Ni-alloys are used primarily as springs and spacer grids in fuel assemblies and fasteners (bolts) in LWRs. In-reactor creep of bolts may lead to a torque decrease, which can be detrimental for safe operation. The relaxation of the spring tension due to creep also affects the ability of spring components to perform their design function. Irradiation-induced stress relaxation is therefore important for LWR fuel assembly performance as a loss of tension will mean the fuel rods are more susceptible to vibrations during service. For PWRs the discharge burnup for the fuel assemblies occurs at about 50 GWd/t and this corresponds to a fast neutron fluence of about $10 \times 10^{25} \text{ n.m}^{-2}$ ($E > 1 \text{ MeV}$), or about 15 dpa for the Inconel 718 or X-750 alloys used in such assemblies and corresponds with about 4 years at the peak flux or 6 years at the core average flux. So long as the springs retain sufficient tension up to about 15 dpa it is unlikely that stress relaxation will have a big effect on fuel assembly performance.

In CANDU reactors Inconel X-750 springs are used as tight-fitting spacers for fuel assemblies and also as tensioning springs for guide tubes. The irradiation creep stress relaxation of the springs in CANDU reactors is enhanced by the approximately three-fold higher thermal neutron flux relative to LWRs. The higher thermal neutron flux coupled with the longer duration of operation in the CANDU reactor compared with fuel assemblies in LWRs (Griffiths, 2014; Griffiths, 2019) means that irradiation creep of Ni-alloys is a more serious issue for CANDU reactors compared with LWRs. Excessive spring de-tensioning has been reported for the Inconel X-750 tensioning springs of guide tubes used in some CANDU reactors (Garner et al., 2010 ; Griffiths et al., 2013) but de-tensioning in this case did not seriously impede reactor operation. De-tensioning of Inconel X-750 tight-fitting spacers could be an issue in abnormal circumstances if they move from their design locations. Observations and calculations show that there is insufficient relaxation of the spacers, before they become pinned in position by the relative sag of the concentric pressure tubes and calandria tubes that they separate, which is a problem (Griffiths et al., 2013).

For fast reactor applications interest in Ni-alloys materials is primarily focused on their resistance to radiation-induced void swelling compared to austenitic steels, although a perceived susceptibility to irradiation embrittlement limits their application to some extent (Boothby, 2012).

Alloys with high Ni content are prone to enhanced H and He production in nuclear reactors with a high thermal neutron flux, such as the CANDU reactor. The increased gas production induces enhanced dpa rates (due to recoil ion damage), but also the He generation, in particular, means that Ni-alloys are

particularly prone to He-embrittlement. From the perspective of irradiation creep, gas bubble formation will influence the deformation processes, in part because of the role of He-bubbles as barriers to dislocation slip, but more importantly through the effect of high densities of cavities/bubbles on diffusional mass transport. At high temperatures, He helps to promote cavity growth, thus potentially increasing both creep and swelling once the cavity size is such that bias-driven cavity growth is significant. At low temperatures He bubbles have the opposite effect; high sink densities of any type effectively promotes recombination of point defects, thus potentially reducing irradiation creep.

6.2 Dose and Dose-Rate Dependence of Irradiation Creep in Ni-Alloys

One comprehensive study of the effect of dose and dose rate on creep of precipitation-hardened PE16 alloy was conducted by (Lewthwaite and Mosedale, 1979). They examined the effects of different heat-treatments on irradiation creep of springs tested at different temperatures and constant stresses (using dead weights) in the Dounreay fast reactor (DFR). Although much of the data were confounded by differences in heat treatment, which mainly affected the size of the γ' precipitates, Lewthwaite and Mosedale identified a flux dependence in which the creep compliance was higher at low fluxes. Such an effect was also identified in stainless steels irradiated in DFR (Lewthwaite and Mosedale, 1980). Boothby showed that the flux dependence for the steady-state creep compliance was similar in both PE16 and other stainless steels (Boothby, 2012). The instantaneous creep compliance is defined as the rate of change in strain per unit stress per unit dpa. In the case of a stress relaxation test, the stress is constantly changing. The analysis of the creep compliance is more complicated than for a simple creep test.

Although Lewthwaite and Mosedale studied temperature and flux variables for different heat treatments of PE16, they did not provide any definitive conclusions concerning the temperature dependence of creep, largely because most of the data at high temperatures was also for low neutron fluxes. They showed that there was a non-linear dependence of creep on damage rate for sets of specimens with mean irradiation temperatures that were either 280 °C or 343 °C. In the study of stainless steels they concluded that in the temperature range of 513 K – 633 K (240 °C - 360 °C) the creep compliance (per unit damage dose) increased with decreasing dose rate, independent of temperature. They did, however, indicate that the creep compliance increased with increasing temperature in the case of stainless steels (Lewthwaite and Mosedale, 1980).

(Gilbert and Chin, 1985) showed that irradiation creep of solution-treated PE16 increased with temperature during isothermal tests at temperatures of 425 °C - 590 °C and stresses of 100 MPa and 200 MPa. Solution-treated Inconel 706, however, exhibited the highest creep at 425 °C and a minimum in

creep rate at 540 °C for the same conditions. The difference was attributed to the complications caused by the irradiation temperature on γ'' precipitate formation in the Inconel 706, both alloys forming γ' precipitates.

Garner and Toloczko (Garner and Toloczko, 1987) pointed out that the damage rate dependence of irradiation creep in stainless steels reported by (Lewthwaite and Mosedale, 1980) is confounded by the effect of fluence. The dose dependence of the irradiation creep compliance at different damage rates is assessed here by a re-examination of the Lewthwaite and Mosedale creep data for PE16 (0). The normalised creep strain divided by the applied engineering stress reported by Lewthwaite and Mosedale is reproduced in Figure 6-1. To delineate the temperature effect the specimens irradiated in the range of 271 °C - 304 °C are shown by solid symbols; specimens irradiated in the range of 327 °C - 360 °C are shown by hollow symbols and crosses. Different states of thermo-mechanical processing and the damage rates (in units of 10^{-7} dpa.s⁻¹) are listed in the legend. The material tested is in three states: over-aged (OA), solution-treated (ST) and full heat treated (FHT). The solution treatment (ST) ensures that all γ' precipitates are dissolved; the full heat treated (FHT) corresponds to normal precipitation-hardened structure (γ' precipitates that are ~12 nm diameter); and over-aged (OA) produces γ' precipitates that are 39-46 nm diameter. Because the strain also includes the uncharacterised transients (given by the intercepts of the curves shown in Figure 6-1) the creep compliance (creep strain per unit stress per unit time or dose) cannot simply be determined by dividing the data by the dose. However, one can assume that at zero stress there is zero strain. The data show that the strain normalised for stress at a given dpa dose increases with lower damage rates for a given metallurgical condition (OA or FHT), consistent with the conclusions of Lewthwaite and Mosedale (Lewthwaite and Mosedale, 1979). There is some evidence for higher creep at the higher temperatures but the difference is not as large as the flux effect. With the additional assumption of linearity with stress the creep compliance can be determined from the slopes of the curves in Figure 6-1. Apart from the non-linear dose dependence of creep strain there is a longer transient dose with low creep rate for the FHT (optimized gamma prime precipitates) condition (i.e., lower strain), for a given dose rate.

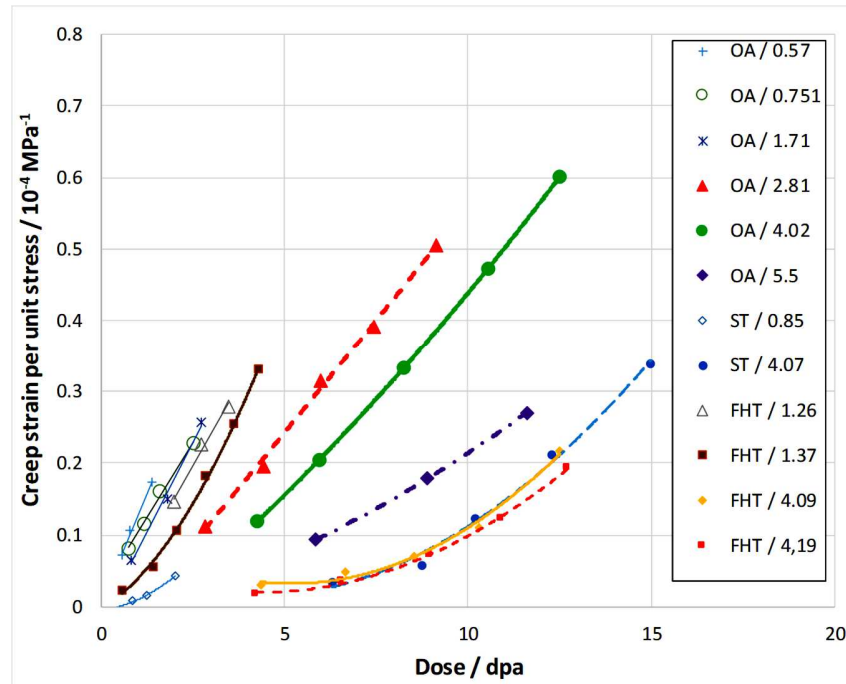


Figure 6-1. Shear strain per unit stress against dpa dose for PE16 springs irradiated in Dounreay fast reactors at temperatures between 271 °C - 360 °C. The different heat-treatments for the springs (OA, ST and FHT) and the damage rate, in units of $10^{-7} \text{ dpa}\cdot\text{s}^{-1}$, are given in the legend, see text.

The Lewthwaite and Mosedale data for the PE16 alloy don't extend to low enough doses at a given irradiation temperature to show the transition from primary to secondary creep. The primary creep is inferred from the intercept at zero dpa of the fit to the creep strain plotted against dpa. The data shown in Figure 6-1 show that the primary creep is small relative to the secondary creep strains. Lewthwaite and Mosedale concluded that there was a negative flux dependence for the steady-state irradiation creep, i.e. a higher creep compliance (per unit stress, per unit dpa) at lower damage rates. This conclusion is supported by the data plotted in Figure 6-1.

6.3 Temperature Dependence of Irradiation Creep in Ni-Alloys

Most of the available creep data for alloys used in power reactors (Inconel 718 and X-750) are largely based on stress relaxation measurements of springs or bent beams. Stress relaxation data from springs irradiated in EBR-2 at 644 K (371 °C) and bent beams irradiated in NRU at 333 K and 573 K (60 °C and 300 °C) are shown in Figure 6-2 for doses between about 0.1 and 20 dpa (Walters and Ruther, 1977 ; Allen et al. 2009). The linearity of the log plots over the range of the data indicates that the primary creep occurs at very low doses (<0.1 dpa) and the data shown correspond with steady-state creep behaviour. For Zr-alloys the transition from primary to secondary (steady-state) creep appears to be complete at low

fluences ($7.2 \times 10^{23} \text{ n.m}^{-2}$, $E > 1\text{MeV}$) and for times $<1000\text{h}$ in a fast neutron flux of $2 \times 10^{17} \text{ n.m}^{-2}.\text{s}^{-1}$ in the NRU reactor (Causey et al., 1988), which corresponds to an atomic displacement dose of about 0.1 dpa. Ni-alloys appear to have a similar dose dependence for the transition from primary to secondary steady-state creep as the Zr-alloys at about 300 °C. However, the secondary creep cannot be considered truly steady-state if the microstructure, which dictates the creep behaviour, is evolving. One can assume pseudo-steady state behaviour and compare rates at roughly the same dose levels in order to assess the effect of temperature variations.

One feature of the Inconel X-750 relaxation data is the negative temperature dependence for the relaxation/creep rate. This temperature dependence is opposite to that observed in Zr-alloys (Causey et al., 1980) but is consistent with behaviour reported for austenitic steels at relatively low temperatures (section 5).

The negative temperature dependence of irradiation creep exhibited by Ni-alloys is also opposite that observed in precipitation-hardened Nimonic 80A alloy, a Ni alloy similar to Inconel X-750 (Taylor and Jeffs, 1966), albeit for a different range of temperatures and neutron fluences. Although they showed that thermal creep was strongly dependent on temperatures, plotting the irradiation creep data from (Taylor and Jeffs, 1966) on a dpa scale (Figure 6-3) shows that the steady-state irradiation creep rate is relatively insensitive to temperature, whereas the transient, primary creep, strain has a strong positive temperature dependence. For the temperature regime in question, 325 °C – 525 °C (598 K – 798 K), a substantial fraction of the relaxation occurs in the primary regime and is consistent with the primary strain being dominated by thermal creep. For secondary creep after the initial transient the temperature dependence for irradiation creep is less obvious; the creep curve at 798 K has a similar slope to the creep curve at 598 K.

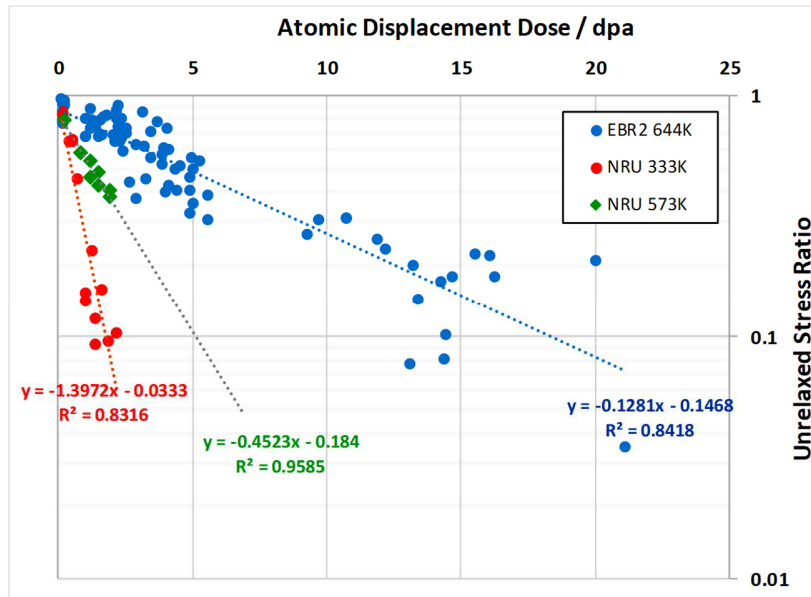


Figure 6-2. Stress relaxation data for Inconel X-750 bent beams irradiated in NRU and springs in EBR-2. The slope of the unrelaxed stress ratio plotted on a log scale against dpa is proportional to the irradiation creep compliance (see Appendix A). The higher slope at lower temperatures indicates that the creep compliance has a negative temperature dependence.

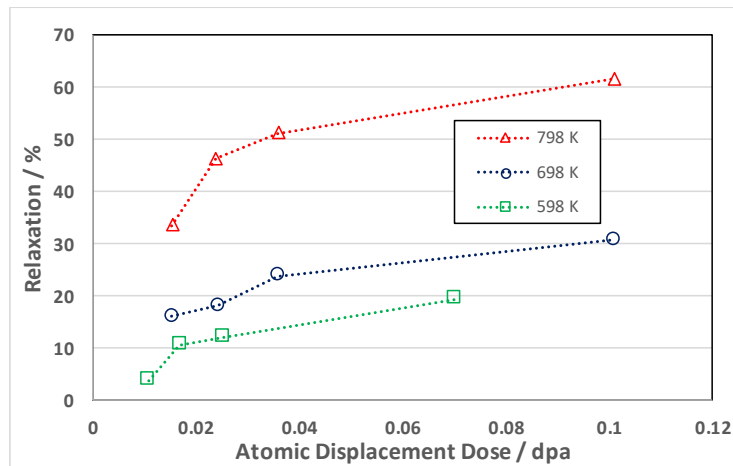


Figure 6-3. Stress relaxation data for Nimonic 80A springs irradiated in the DIDO reactor at various temperatures (K).

The apparent secondary creep in Fig. 6-3 may not correspond to steady-state behaviour given the low dose (< 0.1 dpa) and any conclusions regarding secondary creep behaviour must be restricted to the dose range applicable to the data. Unfortunately the stress relaxation data for Inconel X-750 do not overlap sufficiently with the Nimonic 80-A data in either temperature or dose range to make any meaningful comparisons of secondary creep behaviour. At the higher doses applicable to the Inconel X-750 data (Figure 6-2) one can be more confident that the creep is in a steady-state condition. The negative

dependence of steady-state irradiation creep on temperature exhibited by the Inconel X-750 appears to be a phenomenon that is also exhibited by Ni (Causey et al., 1980) and has also been observed in other austenitic alloys (Grossbeck and Mansur, 1991 ; Stoller et al., 1992).

The stress relaxation data from (Causey et al., 1980) for Inconel X-750 are consistent with stress relaxation data for Inconel 718 of (Morize et al., 1987) and (Knaab et al. 1985), Figure 6-4. The Inconel 718 data were obtained from materials with a metallurgical state assumed to be representative of the states of spring components in PWRs using the test reactors NRU and OSIRIS. The Knaab data have been converted to dpa using a conversion factor of 1.474 dpa per 10^{21} n.cm⁻² ($E > 0.82$ MeV), which is based on dpa calculations using the SPECTER code and the core spectrum for a PWR (Griffiths et al., 2017b). The dpa values for the Morize data were obtained using a ratio of 1.526 dpa per 10^{21} n.cm⁻² ($E > 1$ MeV) for the OSIRIS and SILOE reactors (Griffiths et al., 2017b).

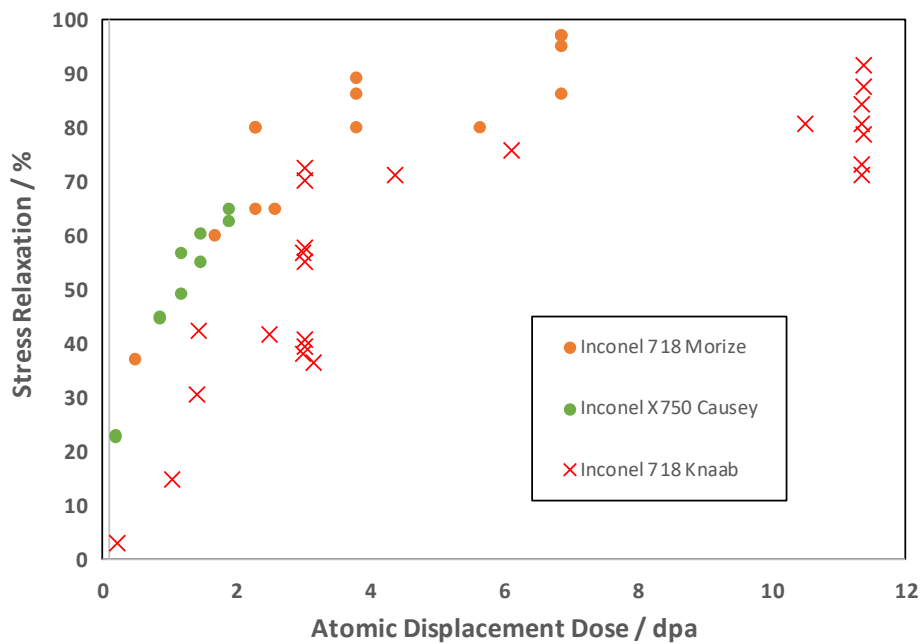


Figure 6-4. Stress relaxation derived from creep of internally pressurised tubes, springs and bent beams for Inconel X-750 and Inconel 718 irradiated at 300 °C – 315 °C compared with PWR data.

6.4 Discussion on the irradiation creep mechanisms of Ni-based alloys

6.4.1 Deformation mechanism as a function of dose and dose rate

In-reactor deformation of Ni-based alloys is the result of two competing phenomena. On the one hand, radiation enhances creep through the stress-induced climb and glide (SICG) mechanism, which only applies to perfect edge dislocations, and on the other hand irradiation suppresses creep by promoting the formation of jogs on screw or mixed dislocations by absorption of point defects. These jogs are obstacles to dislocation motion, as described in the first part. Furthermore, under irradiation point defect clusters are created that are barriers to slip. Creep due to dislocation slip can be expected to be a function of damage rate but will be suppressed by increased clustering and jog formation on mixed and screw dislocations occurring within the early stages of irradiation. In this early transient regime of creep, the slip-based mechanism dominates and can be described mostly by SICG, although mass transport giving climb of edge dislocations will also contribute to the strain.

Steady-state irradiation creep, which is the creep that is observed after an initial transient in strain that occurs within the first few thousands of hours of operation, may be attributed to the uninhibited glide of dislocations until they impinge on barriers to slip that may be already present in the material. But this pseudo-steady-state is also affected by the irradiation dose (dpa), hence the term pseudo. After the initial transient stage thermal creep due to dislocation glide slows as the dislocations encounter barriers to slip. Irradiation will add to these barriers thus shortening the time where uninhibited slip is occurring. This stage of creep can be considered similar to thermal creep in the laboratory at high temperatures. Thermal creep of unirradiated material due to dislocation slip is more rapid than thermal creep of irradiated material. It is only the enhancement of creep at high fluxes that leads to enhanced irradiation creep by either climb and glide or simple diffusional mass transport.

One can consider that irradiation creep in Ni-alloys is governed by two mechanisms: (i) involving dislocation slip that is at the same time suppressed and enhanced by irradiation through the mechanism of stress-induced climb and glide (SICG); (ii) mass transport involving climb of network dislocations as well as point defect absorption at grain boundaries (SIPA-AD on grain boundaries). The first mechanism will predominate at low fluxes/fluence when the material is not fully hardened by the irradiation damage and is likely to be responsible for the primary transient creep behaviour that is observed at very low doses ($\ll 0.1$ dpa) but may also persist up to doses of several dpa as the microstructure evolves and hardens. At higher doses (>1 dpa) if the material is hardened against dislocation slip, the secondary creep is proportional to the damage dose (dpa) and is likely dependent mostly on diffusional mass transport. At

high doses and temperatures, complications arise because of the confounding effects of the γ' and γ'' precipitate structure that may either dissolve or evolve depending on the irradiation temperature and damage rate (Nelson et al., 1972). One reason that could account for the increasing creep rate with increasing dose for the data shown in Figure 6-1 is the effect of increasing dose in modifying the precipitate structure. Precipitate dissolution could enhance irradiation creep, coherent precipitates being both barriers to slip and recombination sites for point defects. Another reason for the non-linearity could be due to differences in swelling onset but without information on the irradiated microstructure one cannot conclude anything. At low temperatures, the negative temperature dependence of irradiation creep exhibited by Ni-alloys may be attributed to the effects of increased recombination and lower radiation damage densities resulting in fewer barriers to slip (less damage) and enabling dislocation glide to occur, albeit at a lower temperature. Precipitate dissolution may also be more pronounced at lower irradiation temperatures (Nelson et al., 1972), as observed in the case of Inconel X-750 for temperatures <200 °C compared with >300 °C (Griffiths, 2019). At higher temperatures (425 °C - 590 °C) the irradiation creep is also complicated by the evolution of the precipitate structure and may either exhibit a positive or negative temperature dependence (Gilbert and Chin, 1985).

Increased recombination and corresponding lower cluster densities may be responsible for the apparent increased creep rates per unit dpa at low fluxes reported by (Lewthwaite and Mosedale, 1979). Such a flux dependence is also apparent in stainless steels but the flux effect is confounded by the effect of irradiation dose. An added complication is the effect of point-defect recombination that is significant for stainless steels and Ni-alloys at temperatures <300 °C. At low temperatures higher fluxes result in fewer point defects per unit dose (dpa) when recombination is an important factor.

6.4.2 Discussion on the negative temperature effect

One model developed to account for the anomalous temperature dependence of irradiation creep observed in some Ni-alloy materials is based on a longer transient time for vacancy point defects to reach steady-state at lower temperatures (Stoller et al., 1992). Radiation-enhanced climb and glide is assumed to be the predominant creep mechanism (Heald and Speight, 1974 ; Heald and Harbottle, 1977). An additional, or alternative, consideration that may be important is the effect of increased recombination rates at irradiation temperatures < 300 °C (Griffiths, 2014; Griffiths, 2019). The lower flux of point defects to dislocations at lower temperatures will result in less climb and the creep per unit dpa will be lower, whether by slip or mass transport. The higher creep rates observed at lower temperatures (Causey et al.,

1980; Causey et al., 1988) cannot simply be the result of enhanced point defect recombination. It is conceivable, however, that conventional thermal creep due to dislocation glide (albeit at a lower temperature) is suppressed at higher temperatures because of the increased defect cluster density (Griffiths, 2019). The higher creep rate observed at lower temperatures could simply reflect increased suppression of thermal creep at the higher temperatures because of a higher cluster density (Griffiths, 2013; Griffiths, 2019).

The negative temperature dependence of irradiation creep in Ni-alloys can be interpreted by considering that irradiation creep is comprised of two contributions: (i) dislocation slip; (ii) mass transport. The higher creep rate of cold-worked Inconel X-750 at 60 °C compared with 300 °C and 371 °C may be understood in terms of the suppression of network dislocation mobility at the higher temperature due to the higher cluster density and point defect absorption on non-edge network dislocations, and the apparent lower density of barriers and locking mechanisms allowing free mobility of dislocations at the lower temperature (Griffiths et al., 2013). Although conventional thermal creep may be slow at low temperatures, it is possible that irradiation creep due to dislocation glide could be enhanced at neutron fluxes low enough to limit point defect clustering but high enough to increase the point defect concentration in the matrix to enhance irradiation creep due to dislocation glide.

A negative temperature dependence has also been observed at high doses and high temperatures for solution-treated Inconel 706 irradiated in EBR-II (Gilbert and Chin, 1985). At temperatures of 425°C, 540°C, and 590°C the negative temperature dependence was attributed to the effect of γ'' formation at the higher temperature restricting creep. At the lower temperatures and lower doses of the stress relaxation testing of Inconel X-750 (Figure 6-2) it is unlikely that the precipitate structure will be sufficiently affected to affect the creep (Griffiths, 2019).

7 Irradiation creep of Ferritic and ferritic-martensitic Steels

Ferritic and ferritic-martensitic (FM) steels have been of special interest for advanced reactor design, for both fission and fusion, due to their demonstrated resistance to irradiation swelling. This resistance to neutron dose allows for the design of higher burnup fuel, leading to better fuel economy for the next generation reactors. FM steels are currently the leading candidate materials for sodium fast reactor core internals such as fuel claddings and wrappers (Yvon & Carré, 2009) as well as structural material for fusion applications. However, these alloys have lower thermal creep resistance compared to austenitic stainless steels and are generally not recommended for use as structural materials above 600°C. In addition, irradiation creep can occur at much lower temperature than thermal creep and often occurs simultaneously with irradiation swelling. In order to design reactor core components using these steels, analysis of their irradiation creep behavior becomes increasingly important given the complex behavior that may arise when attempting to predict creep deformation under radiation damage.

Although significant scientific progress have been made through modeling, simulation, and separate effects testing to understand irradiation creep in ferritic steels, the verification and validation of the results for reactor design will inevitably require corroborative data from neutron irradiation experiments. The lack of high dose neutron irradiation data remains the major obstacle for having a fully predictive irradiation creep mechanistic model; therefore most irradiation creep models currently used for reactor design remain largely empirical.

As nuclear reactor design continues to push materials margins to get better performance out of advanced reactors, irradiation creep and swelling is often the limiting deformation mechanism for in core materials. It can determine the design thickness of fast reactor fuel cladding, lifetime of in core components, and may even have implications on safety margins under transient conditions. Given the importance of irradiation creep of FM steels to advanced reactor development, it is worthwhile to achieve mechanistic understanding of irradiation creep to reduce the uncertainty in the empirical equation used in current nuclear design. This section will describe the general trends observed for irradiation creep of FM steels and the leading mechanisms proposed that can describe the existing observations and be used to predict irradiation creep behavior of FM steels in the future.

7.1 Neutron Irradiation Experiments

Neutron irradiation creep experiments have been performed on various FM steels of different compositions to support fast reactor programs in the past. The FM steels tested ranged from 12Cr FM

steels such as HT9, different variants of 9Cr steels such as T91 and P91, and other reduced activation FM steels intended for fusion applications (Klueh & Harries, 2001) .

Typically, neutron irradiation creep results are obtained from measuring the diametral strain of pressurized tubes in a nuclear reactor where the dose rate and temperature are well controlled. The internal pressure will cause a hoop stress and cause plastic deformation as the tube creeps. The main issue with this method is that swelling will contribute to the diametral strain measurements in addition to irradiation creep, making it difficult to separate out the different mechanisms from the strain data alone. In order to separate out the swelling contributions, swelling rates are either measured or calculated in addition to the irradiation creep data. There are many methods that can be used to account for volumetric swelling in irradiation creep analysis, including diametral strain of zero pressure tubes, immersion density measurements, or TEM analysis of the void fraction of the irradiated samples. Different scientists may employ different techniques to account for volumetric swelling in the irradiation creep analysis. In general, the following empirical description is used to describe irradiation creep of ferritic steels,

$$\dot{\epsilon} = (B_o + D\dot{S}) \sigma^n \quad 31$$

Where B_o is the creep compliance, \dot{S} is the measured irradiation swelling rate as a function of dpa, D is the creep-swelling coupling coefficient, σ is the applied stress, and n is the stress exponent. Table 7-1 summarizes the creep compliance of many neutron irradiation creep experiments as compiled by Maloy et al. (Henry & Maloy, 2017). Typically, creep compliance of ferritic steels can vary anywhere between $0.3 - 1 \times 10^{-6} \text{ MPa}^{-n}/\text{dpa}$ with stress exponents varying between 1 – 1.5.

Table 7-1: Values of B_o in Ferritic Martensitic steels irradiated below 550°C

Material	Cr (wt%)	Irradiation temperature (°C)	Stress exponent (n)	B_o ($\text{MPa}^{-n}/\text{dpa}$)	Reference
HT9	12	430-500	1.33	0.33×10^{-6}	Chin (Chin, 1983)
HT9	12	400-500	1	$0.3-1.7 \times 10^{-6}$	Toloczko & Garner, 1999)
HT9	12	330	1	0.44×10^{-6}	Grossbeck (Grossbeck, et al., 1996)

T91	9	400	1	0.5×10^{-6}	Toloczko (Toloczko, et al., 1994)
EM12	9.5	400-490	1	0.44×10^{-6}	Seran (Seran, et al., 1992)
EM10	8.8	400-490	1	0.44×10^{-6}	Seran (Seran, et al., 1992)
JLF	9	400-500	1.5	$0.6-1.0 \times 10^{-6}$	Kohyama (Kohyama, et al., 1994)
JLF	7.8	400-500	1.5	0.7×10^{-6}	Kohyama (Kohyama, et al., 1994)
9Cr-1Mo	9	325	1	0.7×10^{-6}	Alamo (Alamo, et al., 2007)
9Cr-2W1V	9	325	1	0.7×10^{-6}	Alamo (Alamo, et al., 2007)
Eurofer	9	325	1	$0.43-0.76 \times 10^{-6}$	Alamo (Alamo, et al., 2007)
PNC-FMS	11	405-550	1	0.67×10^{-6}	Uehira (Uehira, et al., 2000)

7.2 Neutron irradiation of FM Steel T91

The most comprehensive set of irradiation creep study available for T91 are those analyzed by Toloczko et al (Toloczko, et al., 1994) in FFTF. Two types of pressure tubes were fabricated from two heats of T91. The bigger pressure tube has dimensions of 6.86 mm OD x 5.76 mm ID x 28.2 mm with a wall thickness of 600 μ m. The smaller pressure tube has dimensions of 4.57 mm OD x 4.17 mm ID x 22.4 mm with a wall thickness of 200 μ m. The tubes were pressurized with helium to various stresses and irradiated in FFTF at ~400°C, ~500°C, 550°C, and ~600°C at a dose rate of 0.8-1.7 $\times 10^{-6}$ dpa/s.

At 400°C, five different stress levels were tested for their irradiation creep behavior along with two stress free tubes to quantify the irradiation swelling behavior. No clear creep transient was observed in the 400°C condition. The dose dependence of creep strain is not linear due to the effects of stress enhanced swelling, shown in Figure 7-1 (Toloczko, et al., 2006). The stress dependence of the creep rate is roughly linear at 400°C. The creep behavior at 500°C deviates from those of 400°C. A clear creep transient is observed for stresses above 100 MPa at 500°C. The creep rate at 500°C for T91 retains its linear stress dependence for stresses below 140 MPa, with some evidence suggesting that the stress dependence is slightly non-linear above 550°C.

This study provided the few in-reactor data for T91 across a wide temperature, stress, and dose range that are necessary for understanding the mechanisms behind irradiation creep behavior. Analyses of the creep strains suggest that creep rates generally have linear stress dependence, and very small temperature dependence. A recent limited irradiation of T91 in BOR60 (Alamo, et al., 2007) at 325°C confirmed a creep modulus of $0.7 \times 10^{-6} \text{ (dpa MPa)}^{-1}$, consistent with previous observations.

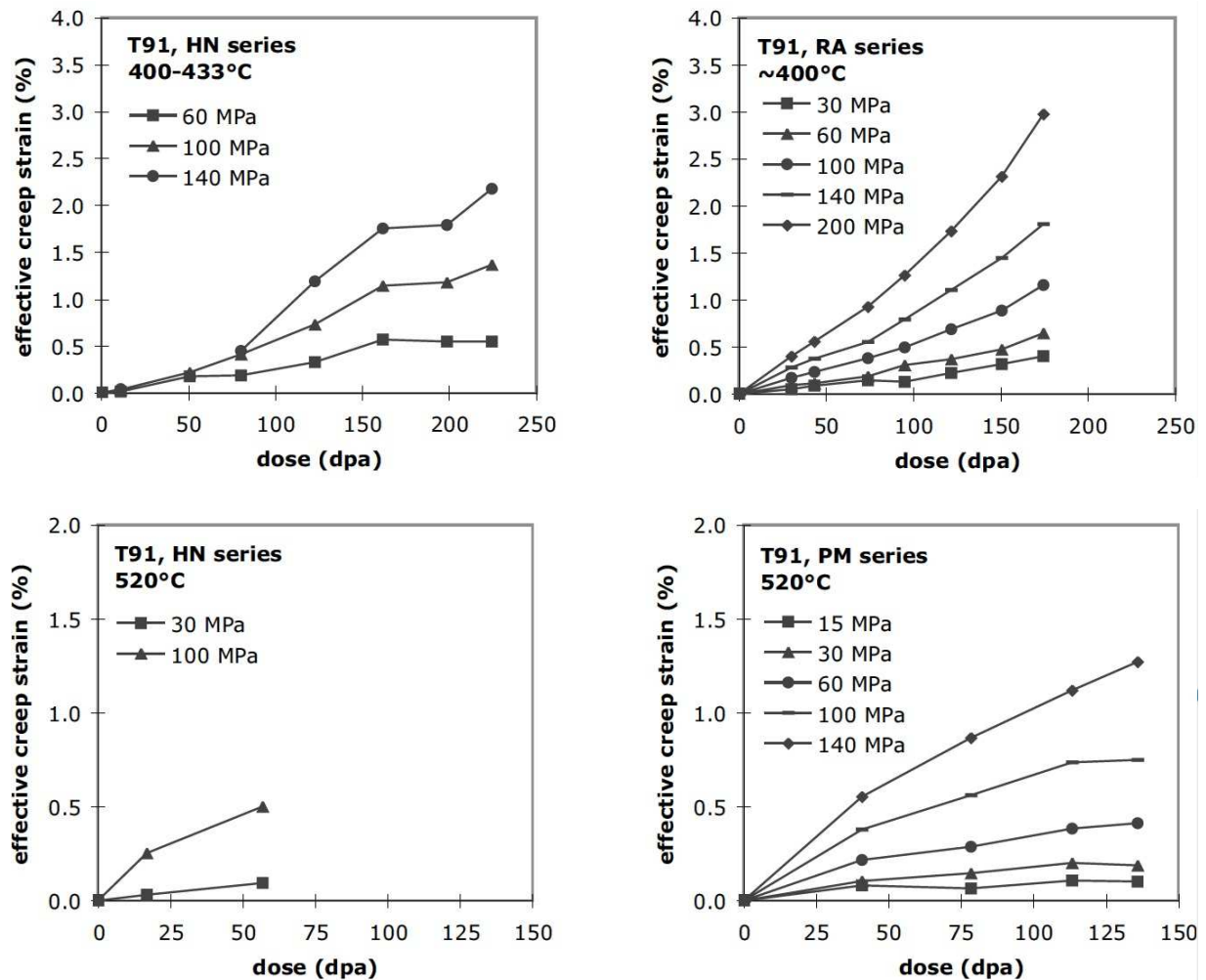


Figure 7-1. FFTF T91 irradiation creep strain as a function of dose (Toloczko, et al., 2006).

7.3 Neutron irradiation creep of HT9

HT9 was one of the first FM steels to be used and tested in fast reactor environments that showed marked improvement in swelling resistance compared to austenitic steels. HT9 is a 12Cr FM steel that has been extensively studied in FFTF to quantify its irradiation creep resistance by Toloczko, and Garner et al. (Toloczko, et al., 1994) (Garner & Toloczko, 1996) (Garner & Puigh, 1991) (Garner, et al., 2000). The HT9 creep tubes were pressurized by helium up to 200 MPa hoop stress. The irradiation temperature were

kept between 375°C to 750°C in FFTF and the samples were irradiated up to a maximum dose of 200 dpa. The pressure tubes were periodically discharged and their diameter strain was measured before reinsertion into the reactor.

A study comparing HT9 and 9Cr-1Mo to austenitic steel PCA provided a comprehensive analysis of the creep rates as a function of stress and dose (Garner & Puigh, 1991). The creep strain found for HT9 and 9Cr-1Mo were very similar, while the PCA were factors of 4-8 larger. It was also observed that the stress dependence of the creep strain increased dramatically when the temperature was above 550°C. The dramatic increase at higher temperatures could be an evidence that thermal creep is significant above 550°C. Analysis of the creep compliance at 400°C showed PCA to have a compliance of $B=9.8 \times 10^{-6} \text{ MPa}^{-1} \text{ dpa}^{-1}$, about factor of 5 greater than the compliance of $B=2.1 \times 10^{-6} \text{ MPa}^{-1} \text{ dpa}^{-1}$ found for HT9. Analysis of the creep swelling coupling coefficient found that for both austenitic PCA and HT9 the coefficient D was around $0.6 \times 10^{-2} \text{ MPa}^{-1}$. Based upon that observation, the crystalline structure is determined to be not very important in the creep-swelling relationship.

In a follow up study on the same experiment, Toloczko (Garner & Toloczko, 1996) analyzed more carefully the irradiation creep stress dependence of HT9 and 9Cr-1Mo by taking into account the stress free swelling data from both immersion density and TEM void counting. By taking into account the swelling contributions, creep compliance B and creep-swelling coefficient D were calculated for 9Cr-1Mo as $0.5 \times 10^{-6} \text{ MPa}^{-1} \text{ dpa}^{-1}$ and $0.7-1.0 \times 10^{-2} \text{ MPa}^{-1}$ respectively. However, the HT9 stress exponent dependence was found to be closer to ~ 2 instead of linear. This study confirmed the magnitude of creep compliance and stress swelling coefficient for FM steels under neutron irradiation. However, the greater than linear stress dependence of HT9 at high dose complicates mechanistic analysis since it contradicts the majority of existing theoretical irradiation creep mechanisms as well as experimental analyses (Table 7-1).

The HT9 creep samples irradiated in FFTF were also compared to those irradiated in the Prototype Fast Reactor (PFR) in a joint US/UK creep study (Toloczko, et al., 1998). It was found that the swelling behavior of the stress free HT9 tubes showed very different behavior in the two reactor environments. The HT9 tube showed positive swelling in FFTF but negative swelling in the PFR irradiations. It is recognized that swelling is dependent upon irradiation history, but no further explanation was given for the discrepancy in swelling in the two reactors. It was also found that the creep compliance and creep swelling coefficient of the HT9 irradiated in PFR fell within the range of $B=0.25-1.0 \times 10^{-6} \text{ MPa}^{-1} \text{ dpa}^{-1}$ and $D=0.6 \times 10^{-2} \text{ MPa}^{-1}$. These values are typical of those found in previous irradiation creep studies on FM steels.

The in-reactor studies on HT9 showed that FM steels share similar creep rates in different reactor environments. The irradiation creep stress dependence for HT9 is between linear and quadratic, with minimum temperature dependence below 550°C. Despite the consistent general behaviour, many studies stop short of confirming a single irradiation mechanism for HT9. For example, the EBR-II experiment on HT9 pressure tubes suggested a combination of climb induced glide and stress-induced preferential absorption mechanism, but ultimately concluded that insufficient data exists to determine the exact mechanism (Paxton, et al., 1980). The combination of stress free swelling, stress enhanced swelling, and irradiation creep complicates the analysis of in-reactor studies. Therefore, a systematic study of the irradiation creep and swelling would be valuable to help narrow down the specific irradiation creep mechanism operating in FM steels. In 2013, TerraPower initiated such a neutron irradiation program in BOR60 on a proprietary version of HT9 to support the development of its Traveling Wave Reactor (TWR) program. The results from this irradiation campaign should provide additional irradiation creep data to the existing database to confirm the HT9 irradiation behavior.

7.4 Neutron Irradiation of Ferritic ODS Alloys

Irradiation creep and swelling study have been performed on an ODS alloy MA957 by Toloczko (Toloczko, et al., 2004) (Toloczko, et al., 2012) in FFTF. MA957 is a 14Cr ferritic steel with ~5 nm yttrium oxide particles finely dispersed throughout its matrix. The stock rods of MA957 were formed from hot extruded powders followed by a combination of hot and cold working. Some of the stock rods were then swaged and annealed down to 5.84mm OD x 5.08mm ID x 6.73mm pressure tubes. The rest were drawn and annealed down to 6.86mm OD x 5.74mm ID x 28.1mm pressure tubes. The samples were irradiated in FFTF from 400°C – 600°C up to 110 dpa for six different stress levels. The diameter of the pressure tubes were measured before and after each irradiation cycle using a scanning laser profilometer.

The irradiation creep rates were calculated for MA957 as a function of temperature and stress. The stress dependence was observed to be linear with stress below 121 MPa at 400°C. At 500°C, the stress dependence was linear only at stresses below 87 MPa. At higher temperatures, the large transient in primary creep makes it difficult to draw conclusions on creep rates with only two data points for each stress condition. The creep compliance was found to be between $5 \times 10^{-7} \text{ MPa}^{-1} \text{ dpa}^{-1}$ and $1.5 \times 10^{-6} \text{ MPa}^{-1} \text{ dpa}^{-1}$.

Microstructure analysis of the ODS alloy after irradiation creep showed that creep rate was not significantly affected by the size and density of dispersed oxides. Because of this lack of creep dependence on dislocation obstacles, the authors dismissed the traditional dislocation climb and glide as the

dominating irradiation creep mechanism (Toloczko, et al., 2012). However, the ODS particles do improve the high temperature creep strength of the material.

This study provided the much needed data for in-reactor irradiation creep behavior for ODS alloys. The data set was sufficient to draw conclusions on the stress dependence, temperature dependence, and dose dependence of irradiation creep strain. However, the lack of low dose transient data caused difficulty in drawing conclusions about the creep behavior at higher temperatures. In addition, although these experiments provided evidence against the conventional dislocation climb glide as the dominating mechanism for irradiation creep, there is still insufficient data to narrow down which mechanism is dominating.

7.5 Neutron Irradiation of Reduced Activation Ferritic Steels

Low activation ferritic steels of various chromium contents were irradiated in FFTF to provide materials database for fusion reactor design. The irradiation creep data of these samples were compiled by Kohyama (Kohyama, et al., 1994), and compared to 316SS austenitic steels and 2.25Cr-1W bainitic steels. The samples were machined into pressure tubes that are 19.8 mm in length, outer diameter of 3.57 mm with a wall thickness of 0.25 mm. The creep tubes were exposed to fast neutron flux in FFTF for a total exposure time of 300.4 equivalent full power days. The total dose accumulated varied between 25 dpa ($5.8 \times 10^{22} \text{ n/cm}^2$) to 36 dpa ($8.5 \times 10^{22} \text{ n/cm}^2$).

The analysis of the creep rates of the different steels found linear stress dependence at 430°C for all stress levels. At temperatures higher than 430°C, linear stress dependence was still observed at low stress regime, but switched to weakly quadratic stress dependence at stresses higher than 60 MPa. The study claimed that 9-12% Cr steels showed the best creep resistance, while the 7-8% Cr showed the worst creep resistance. However, given the uncertainty of $\pm 0.04\%$ strain in the calculated creep strains, only the experiments at 520°C showed significant difference between strain rates of steels at different Cr content. Similar to other neutron irradiation experiments, the strain rate was fitted to the empirical creep equation with stress exponent of $n=1.5$. Creep compliance was found to be around $2 \times 10^{-6} \text{ dpa/s}$ up to $1.5 \times 10^{-6} \text{ dpa/s}$ at 600°C.

Irradiation creep of reduced activation FM steel F82H was obtained following irradiation in the High Flux Isotope Reactor (HFIR) at 573 to 773K up to a dose of 5 dpa. Ando (Ando, et al., 2007) examined the irradiation creep strain of the samples from this experiment and calculated the creep compliance for each temperature and stress conditions. The F82H creep tubes were 21.85 mm long with an inner diameter of 4.17 mm with a wall thickness of 2 mm. The tubes were pressurized with helium to achieve

hoop stresses between 0-400 MPa. The creep tubes were irradiated in HFIR for an accumulated 224 equivalent full power days, with a dose rate ranging from 2.17×10^{-7} dpa/s to 3.08×10^{-7} dpa/s. Stress free creep tubes were also irradiated in the reactor to monitor swelling in the material. The tube diameter was measured before and after irradiation by laser micrometer with a precision of ± 250 nm to obtain the diameter strain.

Irradiation creep strain appeared to be linear at stress levels below 200 MPa at 573K, but increased dramatically at higher stress levels. At 773K, creep strain was linear below 100 MPa, but deviated from linearity at higher stresses.

7.6 Engineering Implications

Although significant amount of neutron irradiation experiments have been performed on ferritic steels, the large number of variables involved in these experiments makes it difficult to analyze every aspect of the irradiation creep behavior. In general, it can be concluded that irradiation creep of FM steels is dominant over thermal creep at temperatures below 550°C, has stress exponents between 1 – 1.5, and minimal temperature dependence. Because irradiation creep occurs in the same temperature ranges as irradiation swelling, any theory on irradiation creep of ferritic steels must account for swelling as well.

Given the consistent trends observed in these irradiation creep experiments, it is clear that a mechanistic description could be developed to explain and even predict irradiation creep behavior of ferritic martensitic steels. In the 1970s, many irradiation creep mechanisms were hypothesized to explain the general behavior that is consistent with current understanding of irradiation damage in materials (Matthews & Finnis, 1988). Over the decades, numerous studies were conducted that confirmed or invalidated some detailed aspects or assumptions of each irradiation creep mechanism, but no single study has conclusively identified a single irradiation creep mechanism that is solely responsible for the irradiation creep of ferritic martensitic steels. The next section will highlight some of the leading irradiation creep mechanisms proposed and the major studies that support them.

7.7 Irradiation Creep Mechanism of Ferritic Martensitic Steels

As with most theoretical mechanisms that attempt to describe macroscopic behavior, all the leading irradiation creep mechanisms share the same fundamental description of irradiation damage behavior on the atomistic level. When neutrons damage the steel, it will create a cascade of point defects (i.e. interstitials and vacancies) that migrate to sinks such as dislocations or grain boundaries. The point defects that do not annihilate by recombination can combine into defect clusters that further migrate and

coalesce into larger microstructure features such as voids, precipitates, or dislocation loops. Irradiation enhanced microstructural features may function as new sinks that act as obstacles for dislocation motion and/or directly contribute to macroscopic deformation (Was, 2007) (Klueh & Harries, 2001). In addition, the point defects generated by the irradiation damage may also enhance dislocation motion by increasing dislocation climb velocity and enabling dislocation glide. Depending on the microstructure feature of the material, one or more of these mechanisms may be dominating at any point in time. The same irradiation creep mechanism could also manifest itself differently depending on the material crystalline structure, grain size, sink densities and the local stress state (IAEA Nuclear Energy Series No. NF-T-4.3, 2012). In order to manage the complexity of all the possible combinations of independent variables, it is useful to start from the better established creep theory for austenitic steels and highlight the differences between austenitic and FM steels.

It is generally accepted that dislocations are strong biased sinks that absorb more interstitials in favor of vacancies. In absorbing the excess interstitial concentration as the result of irradiation damage, the dislocations can climb and glide much faster compared to thermal activation and leave the remaining vacancies to coalesce into voids that drive irradiation swelling. This irradiation enhanced climb-glide mechanism (i.e. I-creep) was very successful in describing the irradiation creep and swelling of austenitic steels (Gittus, 1972). However, major challenges arise when trying to adapt this mechanism to FM steels. The observation of irradiation creep in FM steels in the absence of any observable swelling calls into question whether the inherent interstitial bias of dislocations is the main driving force for irradiation creep.

Stress induced preferred absorption (SIPA) invokes the concept that, in addition to dislocation bias for interstitials, the applied stress imposes an additional driving force on all sinks in the material (Mansur, 1979). It allows for a high creep rate in the absence of swelling that is proportional to the applied stress. However, it is difficult to account for the difference in microstructure and the sensitivity to cold-work and grain size observed in irradiation creep. To fill that gap, preferred absorption glide (PAG) is proposed as a secondary mechanism where a dislocation will climb around an obstacle by SIPA mechanism and then glide under the influence of the applied stress until it meets another obstacle. PAG has a quadratic stress dependence and may explain some of the irradiation creep data showing higher than linear stress dependence.

It is clear all irradiation creep mechanisms on FM steels need to rely on some assumptions regarding the material microstructure. Dislocation driven irradiation creep mechanisms such as SIPA and

PAG do not account for all of the observed irradiation creep microstructure features. Some studies have shown that dislocation loops will nucleate preferentially on specific crystal planes as a function of the applied stress, suggesting stress induced preferential nucleation (SIPN) (Brager, et al., 1977) (Xu & Was, 2014) (Fikar, et al., 2017) may also contribute to irradiation creep in the primary creep regime. Irradiation enhanced grain boundary diffusion may also play a role given that most observations on creep rate have a strong dependence on grain size (Closs, et al., 1977).

There is not yet a singular irradiation creep mechanism proposed that conclusively describes and predicts the irradiation creep behavior of FM steels. The leading theory suggest the dominating irradiation creep mechanism for FM steels is some form of stress induced dislocation motion with a combination of secondary irradiation effects. Verifying and validating an irradiation creep model will necessitate additional data accounting for all the observed microstructural features. Additional concentrated efforts in gathering consistent experimental data, microstructure analysis, and atomistic simulations are needed to produce a truly predictive non-empirical model for irradiation creep of FM steels.

8 Irradiation creep of graphite

The irradiation creep of graphite, unlike other materials, is a beneficial behavior because it allows for the stress relaxation of internal stresses that build up in graphite. These internal stresses are a result of the temperature and dose variations through large graphite components (Tsang and Marsden, 2006). If irradiation creep did not occur, these internal stresses would quickly surpass the graphite strength and cause the components to rip themselves apart. Irradiation creep in graphite is a difficult property to understand and quantify due to the fact that graphite undergoes significant irradiation-induced property changes (dimension/volume, elastic modulus, strength, thermal conductivity, thermal expansion (Campbell et al., 2016)). Nevertheless, irradiation creep has been extensively studied during the past 60 years (Perks and Simmons, 1964; Jenkins and Stephen, 1966 ; Gray et al., 1967; Brocklehurst and Brown, 1969; Gray, 1973 ; Oku et al., 1988; Oku et al., 1990; Campbell, 2018; Campbell and Was, 2014; Campbell and Katoh, 2018; Veringa and Blackstone, 1976). Because graphite undergoes dimensional changes without the application of stress, all irradiation creep studies should include non-stressed reference specimens to allow for the determination of dimensional changes only due to the applied stress. When this is accomplished, the apparent creep (ε_c) is given by a viscoelastic model:

$$\varepsilon_c = \frac{a\sigma}{E_0} (1 - \exp(-b\gamma)) + k\sigma\gamma$$

(32)

where a and b are constants, σ is the applied stress, E_0 is the pre-irradiation Young's modulus, γ is fast neutron fluence, and k is the steady state creep coefficient (Burchell, 2008). The primary creep saturates at low fluence while secondary/steady state creep occurs for higher fluences. There is limited high-dose irradiation creep results, but it is thought that graphite will experience "break-away" creep (Gray, 1973; Burchell, 2008) at doses where the unstressed graphite would begin to swell. An interesting phenomena observed by Brocklehurst and Brown (Brocklehurst and Brown, 1969) was that the creep strain in compression and tension was similar up to 1% strain.

Much of the historical work suggested that the primary creep would saturate around 1 elastic strain unit (ESU) equal to σ/E_0 (Perks and Simmons, 1964; Oku et al., 1988; Oku et al., 1990). But some work found that the primary creep was not always equal to 1 ESU (Jenkins and Stephen; 1966; Campbell, 2018) and even had a temperature dependence (Campbell, 2018). Kennedy performed experiments, reported in (Campbell, 2018), that changed applied stress during a single irradiation and found that the primary creep strain retained the stress dependence even after initial irradiation. Jenkins and Stephen

(Jenkins and Stephen; 1966) also observed that primary creep is recoverable when irradiated without stress. All of these results suggest that the primary creep strain is likely due to dislocation bowing (Campbell, 2018; Hesketh, 1965), but Kelly and Brocklehurst (Kelly and Brocklehurst, 1970) suggested that dislocation pins are destroyed and the transient existence of the pins allows dislocation bowing and recovery occurs from the line tension of the dislocations, or climb and glide mode where edge dislocations (with lines parallel to the c-axis) act as pins for basal dislocations, and the edge dislocations climb by absorption of point defects..

The steady state creep rate (k) dependencies on experimental conditions are more complicated. The dependence of k on the applied stress has been found to have a linear dependence (Gray et al., 1967; Gray, 1973; Oku et al., 1988; Campbell, 2018; Campbell and Was, 2014). The dose rate dependence of k from constant stress experiments (Campbell, 2018; Campbell and Was, 2014) exhibited a linear dependence on dose rate, while restrained shrinkage experiments (Veringa and Blackstone, 1976) found k to be inversely dependent on dose rate. The inverse dose rate dependence of creep rate observed by Veringa (Veringa and Blackstone, 1976) was from experiments carried out in two different regions of the reactor (in core and reflector). But Nikolaenko (Nikolaenko et al., 1970) observed that the non-stressed volumetric change of graphite is strongly dependent on the ratio of the gamma and neutron fluxes, so it is possible that when Veringa performed irradiations in different locations of the reactor that the inverse flux dependence was due to the gamma ray effects noted by Nikolaenko. Several authors observed a linear dependence of k with temperature: Jenkins (Jenkins and Stephen, 1966) in a temperature range of 350K up to 600K, Oku (Oku et al., 1988) in the temperature range of 900°C to 1200°C, Campbell (Campbell and Was, 2014) in the temperature range from 700°C up to 1200°C. However, at lower temperatures, Campbell (Campbell and Katoh, 2018) found that the creep rate at 250°C was higher than at 500°C. Kennedy provided a map of creep rate with temperature, reported by Campbell (Campbell, 2018; Campbell, 2019), finding three distinct temperature regimes (Figure 8-1).

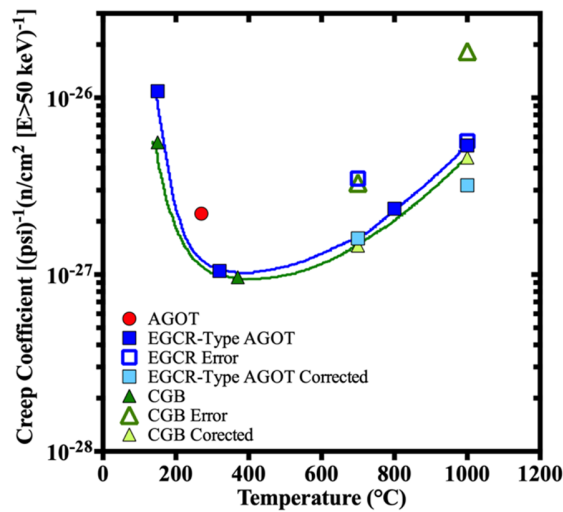


Figure 8-1. Plot of creep coefficient versus temperature [10, 18] (need to get approval to use figure).

The underlying mechanism of steady state creep is still under discussion. The first theory was postulated by Roberts and Cottrell (Roberts and Cottrell, 1956) and is the same mechanism for creep of alpha uranium. The driving mechanism is that radiation-induced anisotropic growth of the crystals cause internal stresses that approach the yield strength and the addition of an external stress results in surpassing the yield strength thus inducing creep. Kelly and Brocklehurst (Kelly and Brocklehurst, 1977) disproved this theory in graphite by adding boron to increase the dimensional change rate, by a factor of 3, but the creep rate remained unchanged at 750°C. Kelly and Brocklehurst (Kelly and Brocklehurst, 1970) postulated that irradiation creep is due to basal slip or an equivalent deformation mode, and Kelly and Foreman (Kelly and Foreman, 1974) extended this concept to result in the pinning-unpinning model. This model is driven by basal dislocation glide and the glide is hindered by pinning points that are continuously created and destroyed by irradiation. Veringa and Blackstone (Veringa and Blackstone, 1976) showed that this model should be inversely dependent on dose rate, because a lower dose rate results in a lower density of pinning points thereby increasing the creep rate. In this theory the linear stress dependence fails at low and high stresses and creep is proportional to the basal plane dislocation density. More recently researchers have discussed how the linear stress dependence of creep rate suggests that the underlying mechanism is driven by dislocation climb (Campbell and Was, 2014; Campbell and Katoh, 2018), which is a type of defect transport mechanism (Sarkar et al. 2016). The dislocation climb and defect transport mechanisms will result in a linear dose rate dependence seen in the constant stress

experiments. More detailed theoretical analyses are needed to determine the microscopic creep mechanism.

At high doses the apparent creep strain begins to deviate from linear, which is a result of the macroscopic deformation of the graphite structure that occurs without stress. Four empirical models have been developed to predict the creep rate at high doses where macroscopic changes are having an effect on the apparent creep strain. The U.K. creep model (Burchell, 1999; Kelly and Brocklehurst, 1993; Kelly, 1992) modifies the microscopic creep strain by the addition of a term that is the ratio of the Young's modulus change at high dose to the initial Young's modulus change. Kennedy (Kennedy et al., 1988) made a similar modification but utilized a parameter that is dependent on the volume change behavior. Kelly and Burchell (Kelly and Burchell, 1994 ; Burchell, 2008) modified the model by adding terms that account for the changes in the thermal expansion and a term that accounts for the crystal shape change parameter from (Simmons, 1965). The newest model is the M^2 model from Davies and Bradford (Davies and Bradford, 2007 ; Davies and Bradford, 2008). Their model is similar to the Kelly Burchell model, but removes the term for the CTE (Coefficient of Thermal Expansion) change from creep and adds in a term for the recoverable creep strain that is multiple times larger than the primary creep strain. None of these four models are able to accurately capture the high dose creep behaviour of graphite. Recent finite element modeling of irradiation creep in graphite (Fang et al., 2012) has found no significant difference between the viscoelastic (Equation **Erreur ! Source du renvoi introuvable.**), U.K. and Kennedy empirical models in the analysis of stress and life prediction. The Kennedy model was found to be most conservative while the U.K. model was the least. Another modeling effort (Erasmus et al., 2013) has also found that for components in low flux regions the inclusion of primary creep must be included in any behavior models because the primary creep strain can be an order of magnitude larger than the secondary creep strain.

The irradiation creep of graphite is complex and difficult to study because of the fact that graphite undergoes significant changes under irradiation without stress. The irradiation creep has been studied since the 1950's, but there is still a lack of mechanistic understanding of both the creep rate and the bulk dimensional changes that is preventing the ability to accurately model the graphite behavior at high neutron doses.

9 Concluding remarks and outlook

Irradiation creep is often considered to be rather simple from a macroscopic point of view. However, the deformation mechanisms at the origin of this behaviour are far from being well understood.

Many theoretical mechanisms have been proposed in the literature. There are two main categories of mechanisms: the mechanisms based on mass-transport, mainly stress induced preferred absorption, and the mechanisms based on dislocation glide, and especially climb-enhanced glide. This review has been able to clarify several important ideas. In any case the formation and regeneration of the dislocation network is necessary to understand how several percent creep strain can be achieved. It is now clear that the loop glide on their cylinder cannot bring any additional plastic strain but the coalescence of loops creating a dislocation network which can glide can indeed induce additional shear strain. Furthermore, because of the high density of loops, or more generally point defect clusters, interactions between climbing or gliding dislocations and these obstacles must occur. The overcoming of these obstacles should be considered in a complete irradiation creep theory.

Concerning the mass-transport based mechanisms, the SIPA-AD mechanism seems to be more viable, because of its higher magnitude than the SIPA-I mechanism. SIPA-AD mechanism on the dislocation network is thus most probable and for small enough grains, SIPA-AD mechanism on grain boundaries is also a possible mechanism. However, it has been pointed out that the basic properties of point defects, such as the polarizabilities at saddle point, are still poorly known. Accurate assessment of the magnitude of these phenomena thus requires additional computational work.

Concerning dislocation glide based mechanisms, several mechanisms have been discarded. The enhanced recovery mechanism does not seem to be a viable mechanism. The mobile dislocation production mechanism is not an irradiation creep mechanism in itself. Climb-enhanced glide mechanisms remain very relevant, especially when enhanced jog dragging is included, since the interaction between dislocations and point defect clusters can create jogs on screw dislocations, which are obstacles to dislocation glide. The PAG or SIPAG mechanism appears to be a second order effect and probably does not have a significant influence. For higher applied stress, dislocation unpinning mechanism may also be effective. Nevertheless, an in depth assessment of these mechanisms requires significant additional computational effort.

Experimental evidences of these mechanisms are scarce. Several authors have been able to report SIPA effect on loops. An indirect effect on loop density is sometimes observed and a direct effect on loop growth rate has been very seldom investigated. A SIPA effect on dislocations, which are the main vector

of the creep strain, has never been observed. Concerning glide based mechanisms, only one experiment clearly shows the unpinning of dislocations under ion beam at high applied stress. Dislocation glide during neutron irradiation creep experiment has never been reported. Significant effort on the experimental side is needed to assess the relevance of all these mechanisms described theoretically abundantly in the literature.

The irradiation creep studies, at the macroscopic scale, of the different materials systems discussed in this chapter show the complexity of measuring irradiation creep. In materials that undergo dimensional change under irradiation (growth or swelling) without stress, the measurements of irradiation creep are complicated by the need for reference samples at the same irradiation conditions to account for the unstressed dimensional change. Furthermore, because of the additional thermal creep rate which decreases as the irradiation hardening increases, the results are often not easy to interpret. The dependence in temperature also appears to be somewhat puzzling, depending on the material studied. Many different phenomena are often combined leading to confounded effects of the various parameters. Because of the limited amount of available consistent data obtained on the same materials, it is difficult to separate these effects and provide a clear understanding of irradiation creep behaviour.

To conclude, despite the immense research effort, irradiation creep remains a difficult subject for Materials Science, essentially because of the difficult experimental investigations. Accurate in-reactor experiments are still needed to characterize in detail the behaviour of the materials. Performing in-reactor experiments, even without in-situ dimensional measurements, are still technically challenging. In-reactor in-situ measurements should be of great interest but are even more difficult to perform. Experiments with non-monotonous loading, changing the applied stress, the neutron flux or the temperature would also be of great interest, but is the most challenging of the options.

Concerning the mechanistic understanding of irradiation creep, the most recent numerical tools (atomistic simulations, Object Kinetic Monte Carlo simulations, Dislocation Dynamics Simulations ...) should be used in a multi-scale approach to assess which mechanisms are the prevalent ones. Experiments using charged particle irradiations (electron, ion beam) should be used to design smart experiments able to distinguish the active mechanisms during irradiation creep deformation. But as is the case with charged particle irradiations, care must be taken to ensure the experiment is designed and operated to present meaningful results.

Acknowledgements: The authors want to thank Jérôme Garnier for providing valuable data concerning irradiation creep of austenitic stainless steels.

References

- Ackland, G. J., 1988. Theoretical study of the effect of point defects on the elastic constants of copper. *J. Nucl. Mater.*, Volume 152, p. 53.
- Adamson, R, Garzarolli, F., Patterson, P., 2009, In-reactor creep of zirconium alloys, ZIRAT 14 Special Topic Report, A.N.T. International, Skultuna, Sweden.
- Adamson, R. B., Coleman, C. E. & Griffiths, M., 2019. Irradiation creep and growth of zirconium alloys: A critical review. *J. Nucl. Mater.*, Volume 521, p. 167.
- Alamo, A., Bertin, J., Shamardin, V. & Wident, P., 2007. Mechanical properties of 9Cr martensitic steels and ODS-FeCr alloys after neutron irradiation at 325°C up to 42dpa. *Journal of Nuclear Materials*, Volume 80, p. 54.
- Allen T.R. and Busby J.T., Radiation damage concerns for extended light water service, *Journal of Metals*, Vol. 61, p. 29, 2009.
- Ando, M. et al., 2007. Creep behavior of reduced activation ferritic/martensitic steels irradiated at 573 and 773K up to 5dpa. *Journal of Nuclear Materials*, Volume 367-370, pp. 122-126.
- Ashby, M. F., 1972. Summary: on radiation-enhanced creep. *Scr. Metall.*, Volume 6, p. 1231.
- Ashkenazy, Y. & Averbach, R. S., 2012. Irradiation induced grain boundary flow - A new creep mechanism at the nanoscale. *Nano Lett.*, Volume 12, p. 4084.
- Atkins, T. & McElroy, R. J., 1987. The effects of applied stress on the irradiation induced microstructures of dilute nickel alloys. In *Radiation-Induced Changes in Microstructure: 13th International Symposium (Part I)*. ASTM International. p. 447.
- Barashev, A. V., Golubov, S. I. & Stoller, R. E., 2016. On the irradiation creep by climb-enabled glide of dislocations. *J. Nucl. Mater.*, Volume 477, p. 234.
- J.F. Bates, W.V. Cummings and E.R. Gilbert, 1981, Anisotropic growth of reactor fuel pin cladding, *J. Nucl. Mater.*, Vol. 99 , pp. 75-84.
- Bickel G. A., Griffiths M., Douchant A., Douglas S.R., Woo, O.T., Buyers, A., 2010, Improved Zr-2.5Nb pressure tubes for reduced diametral strain in advanced CANDU reactors, *Zirconium in the Nuclear Industry: 16th International Symposium*, P. Barb ris, M. Limb ck, Eds., American Society for Testing and Materials, ASTM STP 1529, pp.327-348.
- Boothby R., *Radiation Effects in Nickel Base Alloys*, Volume 4, *Comprehensive Nuclear Materials*, Elsevier, Amsterdam, pp. 123-150, 2012.
- Borodin, V. A. & Ryazanov, A. I., 1992. Dislocation core microstructure and its effect on irradiation creep. In *Effects of Radiation on Materials: 15th International Symposium*, ASTM STP 1125. ASTM International. p. 530.
- Borodin, V. A. & Ryazanov, A. I., 1994. The effect of diffusion anisotropy on dislocation bias and irradiation creep in cubic lattice materials. *J. Nucl. Mater.*, Volume 210, p. 258.
- Borodin, V. A., 1995. The effect of swelling on SIPA irradiation creep. *J. Nucl. Mater.*, Volume 225, p. 15.

Borodin, V., Chen, J.-C., Sauzay, M. & Vladimirov, P., 2015. Analysis and assessment of mechanisms of irradiation creep. Report Matisse European project.

Borodin, V., 2016. State-of-the-art Report on Structural Materials Modelling, Chapter 7: Radiation induced creep. Report NEA/NSC/R(2016)5.

Brager, H. R., Gilbert, E. R. & Straalsund, J. L., 1974. The effect of stress on the microstructure of neutron irradiated cold worked type 316 stainless steel. *Radiat. Eff.*, Volume 21, p. 37.

Brager, H., Garner, F. & Guthrie, G., 1977. The effect of stress on the microstructure of neutron irradiated Type 316 Stainless Steel. *Journal of Nuclear Materials*, Volume 66, pp. 301-321.

Brailsford, A. D. & Bullough, R., 1973. Irradiation creep due to growth of interstitial loops. *Philos. Mag.*, Volume 27, p. 49.

Brocklehurst, J.E. and R.G. Brown, "Constant stress irradiation creep experiments on graphite in BR-2", *Carbon*, 7, (1969) 487-497.

Brocklehurst, J.E. and B.T. Kelly, "Analysis of the dimensional changes and structural changes in polycrystalline graphite under fast neutron irradiation", *Carbon*, 31, (1993) 155-178.

Bullough, R. & Hayns, M. R., 1975. Irradiation-creep due to point defect absorption. *J. Nucl. Mater.*, Volume 57, p. 348.

Bullough, R. & Willis, J. R., 1975. The stress-induced point defect-dislocation interaction and its relevance to irradiation creep. *Philos. Mag.*, Volume 31, p. 855.

Burchell, T.D., "Fission Reactor Applications of Carbon", in *Carbon Materials for Advanced Technologies*, T.D. Burchell, Editor, 1999, Elsevier Science, Oxford.

Burchell, T.D., "Irradiation induced creep behavior of H-451 graphite", *Journal of Nuclear Materials*, 381, (2008) 46-54.

Caillard, D., Martin, J. L. & Jouffrey, B., 1980. Creep under irradiation of 316 steel in the high voltage electron microscope. *Acta Metall.*, Volume 28, p. 1059.

Caillard, D. & Martin, J. L., 2003. Thermally activated mechanisms in crystal plasticity (Vol. 8). Pergamon Materials Series, Pergamon.

Campbell, A.A. and G.S. Was, "Proton irradiation-induced creep of ultra-fine grain graphite", *Carbon*, 77, (2014) 993-1010.

Campbell, A.A., Y. Katoh, M.A. Snead, and K. Takizawa, "Property changes of G347A graphite due to neutron irradiation", *Carbon*, 109, (2016) 860-873.

Campbell, A.A., "Historical experiment to measure irradiation-induced creep of graphite", *Carbon*, 139, (2018) 279-288.

Campbell, A.A. and Y. Katoh, "Summary Report on Effects of Irradiation on Material IG-110 - Prepared for Toyo Tanso Co., Ltd.", ORNL/TM-2018/1040, (2018).

Campbell, A.A., "Corrigendum to "Historical experiment to measure irradiation-induced creep of graphite" [Carbon 139 (2018) 279–288]", *Carbon*, (2019)

Carpentier, D., Jourdan, T., Le Bouar, Y. & Marinica, M.-C., 2017. Effect of saddle point anisotropy of point defects on their absorption by dislocations and cavities. *Acta Mater.*, Volume 136, p. 323.

Causey A.R., Carpenter G.J.C., MacEwen S.R., 1980, In-reactor stress relaxation of selected metals and alloys at low temperatures, *J. Nucl. Mat.* Vol. 90, pp. 216-223.

Causey, A. R., Butcher, F. J. & Donohue, S. A., 1988. Measurement of irradiation creep of zirconium alloys using stress relaxation.. *Journal of Nuclear Materials*, 159, pp. 101-113.

Chen, Z., Kioussis, N., Ghoniem, N. M. & Seif, D., 2010. Strain-field effects on the formation and migration properties of self interstitials in α -Fe from first principles. *Phys. Rev. B*, Volume 81, p. 094102.

Chin, B., 1983. An analysis of the creep properties of a 12Cr-1 Mo-WV steel.. Snowbird, UT, In Proceedings of the topical conference on ferritic alloys for use in nuclear energy technologies.

Choudhary, B., Samuel, E.I., Rao, K.B.S., Mannan, S., 2001, Tensile stress-strain and work hardening behaviour of 316LN austenitic stainless steel. *Materials Science and Technology*, Vol. 17, pp. 223–231.

Couvant, T., Legras, L., Vaillant, V., Boursier, J., Rouillon, Y., 2005, Effect of strain hardening on stress corrosion cracking of AISI 304L stainless steel in PWR primary environment at 360_C. Proceedings of the 12th International Conference on Environmental Degradation of Materials in Nuclear Power System.

Christodoulou N. Causey A. R., Woo C. H., Tomé C. N., Klassen R. J., Holt R. A., 1993, Modelling the effect of texture and dislocation structure on irradiation creep of zirconium alloys, *Effects of Radiation on Materials: 16th International Symposium*. A.S. Kumar, D.S. Gelles, R.K. Nanstad, E.A. Little, Eds., American Society for Testing and Materials, Philadelphia, ASTM STP 1175, pp. 1111-1128.

Christodoulou N. Causey A. R., Holt R. A., Tomé C. N., Badie N., Klassen R. J., Sauvé R. and Woo C. H., 1996, Modelling in-reactor deformation of Zr-2.5Nb pressure tubes in CANDU power reactors, *Zirconium in the Nuclear Industry: Eleventh International Symposium*, ASTM 1295, E.R. Bradely and G. P. Sabol, Eds. American Society for Testing and Materials, pp. 518-537.

Closs, K., Herschbach, K., Schmidt, L. & Boorn, H. V. D., 1977. Irradiation induced creep experiments in the BR2 reactor using the resonant cavity method. *Journal of Nuclear Materials*, Volume 65, pp. 244-249.

Clouet, E. et al., 2008. Dislocation interaction with C in α -Fe: A comparison between atomic simulations and elastic theory. *Acta Mater.*, Volume 56, p. 3450.

Davies, M.A. and M. Bradford, "A revised description of graphite irradiation induced creep", *Journal of Nuclear Materials*, 381, (2008) 39-45.

Davies, M.A. and M.R. Bradford, "Modelling graphite ageing: Black art or forensic science?", in *Management of Ageing Processes in Graphite Reactor Cores*, G.B. Neighbour, Editor, 2007, RSC Publishing, Cambridge.

DeAbreu R.F., Bickel G.A., Buyers A.W., Donahue S.A., Dunn K., Griffiths M., Walters L., 2018, Temperature and flux dependence of in-reactor creep for cold-worked Zr-2.5Nb, Zirconium in the Nuclear Industry: 18th Int'l Symposium, R.J. Comstock, A.T. Motta, Eds., ASTM International, West Conshohocken, PA., ASTM STP1597, pp. 938-964.

De Almeida, L., May, I.L., Emygdio, P., 1988, Mechanistic modeling of dynamic strain aging in austenitic stainless steel, *Materials Characterization*, Vol. 41, pp. 137–150.

Dederichs, P. H. et al., 1978. Lattice theory of point defects. *J. Nucl. Mater.*, Volume 69 & 70, p. 176.

Dederichs, P. H. & Schroeder, K., 1978. Anisotropic diffusion in stress fields. *Phys. Rev. B*, Volume 17, p. 2524.

Dillon, S. J. et al., 2017. Irradiation-induced creep in metallic nanolaminates characterized by in situ TEM pillar nanocompression. *J. Nucl. Mater.*, Volume 490, p. 59.

Dollins, C. C., 1971. Irradiation creep associated with dislocation climb. *Radiation Effects*, 11(3-4), pp. 123-131.

Dollins, C. C. & Nichols, F. A., 1974. Mechanisms of irradiation creep in zirconium-base alloys. *Zirconium in Nuclear Applications*, ASTM STP 551. ASTM International.

Duffin, W. J. & Nichols, F. A., 1973. The effect of irradiation on diffusion controlled creep processes. *Journal of Nuclear Materials*, 45(4), pp. 302-316.

Ehrlich, K., 1981. Irradiation creep and interrelation with swelling in austenitic stainless steels. *Journal of nuclear materials*, 100(1-3), pp. 149-166.

Erasmus, C., S. Kok, and M.P. Hindley, "Significance of primary irradiation creep in graphite", *Journal of Nuclear Materials*, 436, (2013) 167-174.

Estrin, Y., 2007. Constitutive modelling of creep of metallic materials: Some simple recipes. *Materials Science and Engineering: A*, 463(1-2), pp. 171-176.

Fang, X., H. Wang, S. Yu, and C. Li, "The various creep models for irradiation behavior of nuclear graphite", *Nuclear Engineering and Design*, 242, (2012) 19-25.

Faulkner, D. & McElroy, R. J., 1979. Irradiation creep and growth in zirconium during proton bombardment. *Effects of Radiation on Structural Materials*, ASTM STP683. West Conshohocken, PA: ASTM International.

Fidleris, V., 1988. The irradiation creep and growth phenomena. *Journal of Nuclear Materials*, 159, pp. 22-42.

Fikar, J., Groger, R. & Schaublin, R., 2017. Effect of orientation of prismatic dislocation loops on interaction with free surfaces in bcc iron. *Journal of Nuclear Materials*, Volume 15, pp. 161-165.

Fleck, R.G., Price, E.G., Cheadle, B.A., 1984, Pressure tube development for CANDU reactors, Zirconium in the Nuclear Industry: 6th International Symposium. D.G. Franklin, R.B. Adamson, Eds., American Society for Testing and Materials, ASTM STP 824, pp. 88-105.

Flinn J.E., Garner F.A., Hall M., 2007, Anisotropic swelling observed in history effects experiments conducted in EBR-II on previously irradiated and stressed AISI 304 tubes. The 8th Russian conference on reactor material science.

Foreman, A. J. E. & Makin, M. J., 1966. Dislocation movement through random arrays of obstacles. *Philosophical Magazine*, 14(131), pp. 911-924.

Foster J., Bunde K., Gilbert E., 1998, Stress state dependence of transient irradiation creep in 20% cold worked 316 stainless steel. *J. Nucl. Mater.*, Vol. 257, pp 118–125.

Foster J.P, Bunde K., Grossbeck M., Gilbert E.R., 1999, Temperature dependence of the 20% cold worked 316 stainless steel steady state irradiation creep rate. *J. Nucl. Mater.*, Vol. 270, pp 357–367.

Foster J., Gilbert E., Bunde K., Porter D, 1998, Relationship between in reactor stress relaxation and irradiation creep. *J. Nucl. Mater.*, Vol. 252, pp 89–97.

Foster J.P, Bunde K., Porter D., 2003, Irradiation creep of annealed 304L stainless steel low dose levels. *J. Nucl. Mater.*, Vol. 317, pp 167–174.

Franklin, D. G., Lucas, G. E. & Bement, A. L., 1983. Creep of zirconium alloys in nuclear. ASTM STP 815. ASTM International.

Friedel, J., 1953. Anomaly in the rigidity modulus of copper alloys for small concentrations. *The London, Edinburgh, and Dublin Philosophical Magazine and Journal of Science*, 44(351), pp. 444-448.

Garner, F. A., Wolfer, W. G. & Brager, H. R., 1979. A reassessment of the role of stress in development of radiation-induced microstructure. *Effects of Radiation on Structural Materials*, ASTM STP 683, ASTM International, p. 160.

Garner, F. A. & Gelles, D. S., 1988. Irradiation creep mechanisms: an experimental perspective. *J. Nucl. Mater.*, Volume 159, p. 286.

Garner, F.A, Porter, D., 1988, Irradiation creep and swelling of AISI 316 to exposures of 130 dpa at 385-400C, *J. Nucl. Mater.*, Vol. 155-157, pp. 1006–1013.

Garner, F. A.; Puigh, R. J., 1991, Irradiation creep and swelling of the fusion heats of PCA, HT9 and 9Cr-1Mo irradiated to high neutron fluence, *J. Nucl. Mater.*, Vol. 179–181, pp. 577–580.,

Garner, F. & Puigh, R., 1991. Irradiation creep and swelling of fusion heats of PCA, HT9 and 9Cr-1Mo irradiated to high neutron fluence. *Journal of Nuclear Materials*, Volume 179-181, pp. 577-580.

Garner, F.A, Mitchell, M., 1992, The complex role of phosphorus in the neutron induced swelling of titanium modified austenitic stainless steels. *J. Nucl. Mater.*, Vol.187, pp. 223–229.

Garner, F. A., Hamilton, M. L., Eiholzer, C. R., Toloczko, M. B., & Kumar, A. S., 1992, Irradiation and thermal creep of a titanium-modified austenitic stainless steel and its dependence on cold work level. *Journal of nuclear materials*, Vol. 191, pp. 813-817

Garner F.A., 1994, Irradiation performance of cladding and structural steels in liquid metal reactors, Nuclear Materials, part 1. Materials Science and Technology : A Comprehensive Treatment, 10A.

Garner, F. & Toloczko, M., 1996. Irradiation creep and void swelling of two LMR heats of HT9 at ~400C and 165dpa. Journal of Nuclear Materials, Volume 237, pp. 289-292.

Garner F.A. and Toloczko M.B., "Irradiation creep and Void Swelling of Austenitic Stainless Steels at Low Displacement Rates in light Water Energy Systems", J. Nucl. Mater. 251 (1997) pp. 251-262.

Garner, F., Toloczko, M. & Sencer, B., 2000. Comparison of swelling and irradiation behavior of fcc-austenitic and bcc-ferritic/martensitic alloys at high neutron exposure. Journal of Nuclear Materials, Volume 276, pp. 123-142.

Garner F.A., Griffiths M., Greenwood L.R., Gilbert, E.R., 2010, Impact of Ni-59 (n, alpha) and (n, p) reactions on dpa rate, heating rate, gas generation and stress relaxation in Fast Reactors, LWR and CANDU reactors, Proc. 14th Intern. Conf. on Environmental Degradation of Materials in Nuclear Power Systems- Water Reactors, American Nuclear Society, pp. 1344-1354.

Garner, F.A., 2010, Void Swelling and Irradiation Creep in Light Water Reactor Environments, Chapter 10 in "Understanding and Mitigating Ageing in Nuclear Power Plants", edited by P. G. Tipping, Woodhead Publishing Limited, pp. 308-356.

Garner, F. A., Gilbert, E. R. & Neustroev, V. S., 2011. Recent insights on the parametric dependence of irradiation. Colorado Springs, 15th International Conference on Environmental Degradation.

Garner, F.A., 2012, *Radiation Damage in Austenitic Steels*, Comprehensive Nuclear Materials, Elsevier, Amsterdam, Vol. 4.02, pp. 33-95.

Garnier J., Bréchet Y., Delnondedieu M., Pokor C., Massoud J.P., 2011a, Irradiation creep of SA 304L and CW 316 stainless steels: Mechanical behavior and microstructural aspects. Part I: Experimental results, Journal of Nuclear Materials, Vol. 413, Issue 2, pp. 63-69

Garnier, J. et al., 2011b. Irradiation creep of SA 304L and CW 316 stainless steels: Mechanical behaviour and microstructural aspects. Part II: Numerical simulation and test of SIPA model. J. Nucl. Mater., Volume 413, p. 70.

Garnier J., Dubuisson P., Delnondedieu M., Massoud J-P., Bréchet Y., Leclercq S., Besson J., Scott P., Averty X. and Rozenblum F., "Deformation under irradiation of 304L and 316 austenitic stainless steels", Proceedings of the 13th Conference on Environmental Degradation of Materials in Nuclear Power Systems – Water Reactors, Canadian Nuclear Society, 2007.

Gaumé, M., Baldo, P., Mompiau, F. & Onimus, F., 2018. In-situ observation of an irradiation creep deformation mechanism in zirconium alloys. Scripta Materialia, 154, pp. 87-91.

Gelles, D., Garner, F., Brager & H.R., 1981. Frank loop formation in irradiated metals in response to applied and internal stresses. Philadelphia: in: D. Kramer, H.R. Brager, J.S. Perrin (Eds.) 10th Int. Symp. on Effects of Radiation on Materials, American Society for Testing and Materials, pp. 735-753.

Gelles, D. S., 1993. Effects of stress on microstructural evolution during irradiation. J. Nucl. Mater., Volume 205, p. 146.

Gelles, D. S., Kimura, A. & Shibayama, T., 2000. Analysis of stress-induced Burgers vector anisotropy in pressurized tube specimens of irradiated ferritic martensitic steels: JFMS and JLF-1. In: M. L. Hamilton, A. S. Kumar, S. T. Rosinski & M. L. Grossbeck, Eds. Effects of Radiation on Materials: 19th International Symposium, ASTM STP 1366. ASTM International., p. 535.

Gharbi, N. et al., 2015. Impact of an applied stress on c-component loops under Zr ion irradiation in recrystallized Zircaloy-4 and M5. Journal of Nuclear Materials, 467, pp. 785-801.

Gilbert, E. R., Kaulitz, D. C., Holmes, J. J., Claudson, T. T. , 1973, Fast reactor induced creep in 20% cold worked type 316 stainless steel. In Irradiation embrittlement and creep in fuel cladding and core components, proceedings of the conference organized by the British Nuclear Energy Society in London, 9-10 November 1972.

Gilbert, E. R.; Bates, J. F., 1977, Dependence of irradiation creep on temperature and atom displacements in 20% cold worked type 316 stainless steel. In Measurement of Irradiation-enhanced Creep in Nuclear Materials, Proceedings of an International Conference Organized by the Commission of the European Communities at the Joint Research Centre, Petten, The Netherlands, May 5-6, 1976, Elsevier Ed., pp. 204-209

Gilbert, E.R. Chin B., 1978, In-reactor creep measurements, Trans ANS 28, pp.141-142.

Gilbert, E. R., Chin, B. A., 1985, Non-Isothermal In-Reactor Creep of Nickel Alloys Inconel 706 and PE-16, in Effects of Radiation on Materials: 12th International Symposium; Garner, F. A., Perrin, J. S., Eds.; American Society for Testing and Materials: Philadelphia, PA, ASTM STP 870, Vol. 1, pp 52-60,

Gilbert E.R, Foster J.P, 2001, Dependence of the non swelling in reactor steady state creep component of austenitic phase alloys on the stacking fault energy. J. Nucl. Mater., 2001, Vol. 298, pp. 321-328.

Gittus, J., 1972. Comparison of the theoretical and actual rates of creep in a fast reactor. Journal of Nuclear Materials, Volume 45, p. 174.

Gittus, J. H., 1972. Theory of dislocation-creep due to the Frenkel defects or interstitialcies produced by bombardment with energetic particles. Philosophical Magazine, 25(2), pp. 345-354.

Gittus, J., 1975. Creep, viscoelasticity and creep fracture in solids. Vol. 16 éd. London: Applied Science Publishers.

Gray, B.S., J.E. Brocklehurst, and A.A. McFarlane, "The Irradiation Induced Plasticity in Graphite Under Constant Stress", *Carbon*, 5, (1967) 173-180.

Gray, W.J., "Constant stress irradiation-induced compressive creep of graphite at high fluences", *Carbon*, 11, (1973) 383-392.

Griffiths M., A Review of Microstructure Evolution in Zirconium Alloys, Journal of Nuclear Materials, Vol.159, pp.190-218, 1988.

Griffiths M., Davies W. G., Causey A. R., Moan G. D., Holt R. A. and Aldridge S. A., Variability of In-Reactor Diametral Deformation for Zr-2.5Nb Pressure Tubing, Zirconium in the Nuclear Industry: Thirteenth International Symposium, ASTM STP 1423, G. D. Moan and P. Rudling, Eds., ASTM International, pp. 796-810, West Conshohocken, PA, 2002a.

Griffiths M., Davies P. H., Davies W. G. and Sagat S., Predicting the In-Reactor Mechanical Behaviour of Zr-2.5Nb Pressure Tubes from Post-Irradiation Microstructural Examination Data, Proc: 13th Int. Symp. on Zr in the Nucl. Ind., ASTM-STP-1423, pp. 507-523, Annecy, 2002b.

Griffiths M., Christodoulou N., Donohue S.A., 2005, Damage dependence of irradiation deformation of Zr 2.5Nb pressure tubes, J. ASTM International, 2, Paper ID JAI 12432, ASTM STP 1467, pp. 686-708.

Griffiths M., Wang N., Buyers A., Donohue S.A., 2009, Effect of irradiation damage on the deformation properties of Zr-2.5Nb pressure tubes, Zirconium in the Nuclear Industry: 15th International Symposium, B. Kammenzind, M. Linbäck, Eds., American Society for Testing and Materials, ASTM STP 1505, pp. 541-549.

Griffiths M., Bickel G.A., Donohue S.A., Feenstra P., Judge C.D., Poff D., Walters L., Wright M.D., Greenwood L.R., Garner F.A, 2013, Degradation of Ni-alloy Components in a CANDU Reactor Core, 16th Int. Symposium on Environmental Degradation in Materials, Asheville, NC.

Griffiths M., 2013, The Effect of Irradiation on Ni-containing Components in CANDU Reactor Cores: A Review, AECL Nuclear Review, Vol. 2, No. 1, pp. 1-16; erratum AECL Nuclear Review, Vol. 3, No. 2, p.89, 2014.

Griffiths M, Walters L, Greenwood L. R, Garner F., 2017a, Accelerated materials evaluation for nuclear applications, Journal of Nuclear Materials, Vol. 488, pp.46-62.

Griffiths M., Bickel G.A., DeAbreu R., Li W., 2017b, Irradiation creep of Zr-alloys, Mechanical and Creep Behavior of Advanced Materials, The Minerals, Metals & Materials Society, I. Charit, Y.T. Zhu, S.A. Maloy, P.K. Liaw, Eds., pp. 165-182.

Griffiths M., Ni-based Alloys for Reactor Internals and Steam Generator Applications, Chapter 9 in: Structural Alloys for Nuclear Energy Applications, S. Zinkle and R. Odette, Eds., Elsevier, ISBN: 9780123970466, 2019.

Grossbeck M.L., Horak J., 1988, Irradiation creep in type 316 stainless steel and US PCA with fusion reactor He/dpa levels. J. Nucl. Mater., Vol. 155-157, pp 1001–1005.

Grossbeck M.L., Ehrlich K., Wassilew C., 1990, An assessment of tensile, irradiation creep, creep rupture, and fatigue behavior in austenitic stainless steels with emphasis on spectral effects, Journal of Nuclear Materials, Vol. 174, pp 264-281

Grossbeck M.L and Mansur L.K., 1991, Low-Temperature Irradiation Creep of Fusion Reactor Structural materials, J. Nucl. Mater. Vol. 179-181, pp. 130-134.

Grossbeck M.L., Gibson L.T., Jitsukawa S., 1996, Irradiation creep in austenitic and ferritic steels irradiated in a tailored neutron spectrum to induce fusion reactor levels of helium, Journal of Nuclear Materials, Vol. 233-237, pp 148 - 151

Hahn, J.H., Moon, H.G., 1988, Study on the effect of dynamic strain aging on the strain rate sensitivity of 304 austenitic stainless steel, Korean journal of metals and materials, vol 26, pp. 423–439.

Hausen, H., Schüle, W., Cundy, M., 1988, Fusion Technology, vol 88, pp. 905–909.

Heald P.T. and Speight M.V., 1974, Steady state irradiation creep, Phil. Mag. Vol. 29, pp. 1075-1080.

Heald, P. T. & Speight, M. V., 1975. Point defect behaviour in irradiated materials. *Acta Metall.*, Volume 23, p. 1389.

Heald, P. T. & Harbottle, J. E., 1977. Irradiation creep due to dislocation climb and glide. *Journal of Nuclear Materials*, 67(1-2), pp. 229-233.

Henager, C. H., Simonen, E. P. & Bradley, E. R., 1983. Effect of microstructure on light ion irradiation creep in nickel. *J. Nucl. Mater.*, Volume 117, p. 250.

Henry, J. & Maloy, S., 2017. Irradiation-resistant ferritic and martensitic steels as core materials for Generation IV nuclear reactors. In: *Structural Materials for Generation IV Reactors*. pp. 329-355.

Hesketh, R. V., 1963. A transient irradiation creep in non-fissile metals. *Philosophical Magazine*, 8(92), pp. 1321-1333.

Hesketh, R.V., "The mechanisms of irradiation creep in graphite", *Philosophical Magazine*, 11, (1965) 917-927.

Hesketh, R. V., 1968. Application of the generalised theory of yielding creep to irradiation creep in Zirconium alloys. *Journal of Nuclear Materials*, 26(1), pp. 77-86.

Holt, R. A., 1980. Microstructure dependence of irradiation creep and growth of zirconium alloys. *J. Nucl. Mater.*, Volume 90, p. 193.

Holt R. A., 1979, Effect of microstructure on irradiation creep and growth of Zircaloy pressure tubes in power reactors, *J. Nucl. Mater.*, *J. Nucl. Mater.* 82, pp. 419-.

Holt R.A., 2008, In-reactor deformation of cold-worked Zr–2.5Nb pressure tubes, *J. Nucl. Mater.*, 372, pp.182-214.

Holt, R. A., 2008. In-reactor deformation of cold-worked Zr–2.5 Nb pressure tubes. *Journal of Nuclear Materials*, 372(2-3), pp. 182-214.

Hull, D. & Bacon, D. J., 2001. *Introduction to dislocations*. Butterworth-Heinemann.

IAEA Nuclear Energy Series No. NF-T-4.3, 2012. *Structural Materials for Liquid Metal Cooled Fast Reactor Fuel Assemblies - Operational Behaviour*, Vienna: IAEA.

Jenkins, G.M. and D.R. Stephen, "The temperature dependence of the irradiation induced creep of graphite", *Carbon*, 4, (1966) 67-72.

Jitsukawa, S., Katano, Y. & Shiraishi, K., 1984. Effect of external stress on microstructural change during electron-irradiation in Nickel. *J. Nucl. Sci. Technol.*, Volume 21, p. 671.

Jitsukawa, S., Katano, Y., Shiraishi, K. & Garner, F. A., 1992. The Behavior of Irradiation-Produced Dislocation Loops under External Stress during Electron Irradiation. In *Effects of Radiation on Materials: 15th International Symposium*. ASTM International. p. 1034.

Jitsukawa, S. & Hojou, K., 1994. Effect of temperature and flux change on the behavior of radiation induced dislocation loops in pure aluminum. *J. Nucl. Mater.*, Volume 212-215, pp. 221-225.

Joseph, J., 1959. Stress relaxation in stainless steel during irradiation. USAEC Report DP-369.

Jostsons, A. et al., 1977. Faulted loops in neutron-irradiated zirconium. *Journal of Nuclear Materials*, 68(3), pp. 267-276.

Jyrkhama M.I., Bickel G.A., Pandey M.D., 2016, Statistical analysis and modelling of in-reactor diametral creep of Zr-2.5Nb pressure tubes, *Nucl. Eng. Design*, Vol. 300, pp. 241-248.

Kashyap, B.P., McTaggart, K., Tangri, K., 1987, Study on the substructure evolution and flow behaviour in type 316L stainless steel over the temperature range 21-900 °C. *Phil. Mag. A*, Vol. 57, pages 97–114.

Kelly, B.T. and J.E. Brocklehurst, "Analysis of Irradiation Creep in Reactor Graphite", Presented at *Proceedings of the Third Conference on Industrial Carbons and Graphite*, London, April 14-17, 1970.

Kelly, A. & Nicholson, R., 1971. *Strengthening Methods in Crystals*. London: Applied Science Publishers Ltd.

Kelly, B. T. & Foreman, A. J. E., 1974. The theory of irradiation creep in reactor graphite - The dislocation pinning-unpinning model. *Carbon*, 12(2), pp. 151-158.

Kelly, B.T. and J.E. Brocklehurst, "UKAEA Reactor Group studies of irradiation-induced creep in graphite", *Journal of Nuclear Materials*, 65, (1977) 79-85.

Kelly, B.T., "Irradiation creep in graphite--some new considerations and observations", *Carbon*, 30, (1992) 379-383.

Kelly, B.T. and T.D. Burchell, "The analysis of irradiation creep experiments on nuclear reactor graphite", *Carbon*, 32, (1994) 119-125.

Kennedy, C.R., M.R. Cundy, and G. Kleist, "The Irradiation Creep Characteristics of Graphite to High Fluences", *Proceedings of the Carbon '88*, Tyne, United Kingdom, 1988, 443-445.

Kirsanov, V. V., Pyatiletov, Y. S. & Tyupkina, O. G., 1981. Irradiation creep due to dislocation glide. *Physica Status Solidi. A, Applied Research*, 64(2), pp. 735-740.

Kishimoto, N., Shiraishi, H. & Yamamoto, N., 1988. Irradiation creep of Fe-25Ni-15Cr during 10 MeV deuteron bombardment. *J. Nucl. Mater.*, Volume 155-157, p. 1014.

Klueh, R. L. & Harries, D. R., 2001. High-chromium ferritic and martensitic steels for nuclear applications. Monograph 3 in ASTM's Monograph Series, West Conshohocken, PA (USA): ASTM International.

Knaab H and von Jan R., 1985, Fuel Performance Evaluation and Improved Fuel Utilization by Pool-Site Fuel Services, *Proc. ANS LWR Fuel Performance Conference*, pp. 1 36 to1-51, Orlando, FL.

Kohyama, A. et al., 1994. Irradiation creep of low-activation ferritic steels in FFTF/MOTA. *Journal of Nuclear Materials*, Volume 215, pp. 751-754.

Konobeevsky, S. T., Pravdyuk, N. F. & Kutaitsev, V. I., 1955. Effect of irradiation on structure and properties of fissionable materials. In: *Proc. First UN Conference*, Geneva (Vol. 7, p. 433).

Krasnoselov, V.A., Kolesnikov, A. N., Prokhorov, V.I., 1987, Study of the radiation changes of the shape of a hexahedral jacket of a materials science assembly of the BOR-60 reactor, *Atomic Energy*, Vol. 63, No. 4, pp. 240–242.

Kreyns P. H. and Burkhart M. W., 1968, Radiation Enhanced Relaxation in Zircaloy-4 and Zr/2.5wt%Nb/0.5wt.%Cu Alloys, *Journal of Nuclear Materials*, Vol. 26, p. 87.

Lehmann, J., Dupouy, J. M., Broudeur, R., Boutard, J. L., & Maillard, A. (1979). Irradiation creep of 316 and 316 Ti steels (No. CEA-CONF--4645). In *Proc. Int. Conf. On Irradiation behaviour of metallic materials for Fast Reactor Core Components*, Ajaccio, Corsica, France; Jun 1979 (pp. 409-414).

- Leibfried, G. & Breuer, N., 1978. Point Defects in Metals I. In: Springer Tracts in Modern Physics. Springer-Verlag, Berlin.
- Lemaire E., Massoud J.P., Ligneau N., 2004, Ageing management of reactor vessel internals in EDF PWRs, in: International Atomic Energy Agency Technical Meeting on Reactor Core Internals Behavior and Technology for Repair and Replacement in Nuclear Power Plants.
- Lewthwaite, G. W., Mosedale, D., & Ward, I. R., 1967. Irradiation creep in several metals and alloys at 100° C. *Nature*, 216(5114), pp. 472-473.
- Lewthwaite, G. W., 1973. Irradiation creep produced by the effect of stress on the nucleation of dislocation loops. *Philos. Mag.*, Volume 28, p. 1287.
- Lewthwaite, G. W. & Proctor, K. J., 1973. Irradiation-creep in a materials testing reactor. *Journal of Nuclear Materials*, 46(1), pp. 9-22.
- Lewthwaite, G. W., and Mosedale, D., 1979, Irradiation creep of Nimonic PE16 alloy in the Dounreay fast reactor, in *Proceedings of International Conference on Irradiation Behaviour of Metallic Materials for Fast Reactor Core Components*, Ajaccio, Corsica, June 4–8, 1979; Poirier, J., Dupouy, J. M., Eds.; Le Commissariat à l'Energie Atomique (CEA): Saclay, France, pp 399–405.
- Lewthwaite G.W., Mosedale, D., 1980, The Effects of Temperature and Dose-Rate Variations on the Creep of Austenitic Stainless Steels in the Dounreay Fast Reactor, *J. Nucl. Mater.*, Vol. 90, pp. 205-215.
- Ma, P.-W. & Dudarev, S. L., 2019. Effect of stress on vacancy formation and migration in body-centered-cubic metals. *Phys. Rev. Mater.*, Volume 3, p. 063601.
- MacEwen, S. R. & Fidleris, V., 1977. Irradiation creep in Zr single crystals. *J. Nucl. Mater.*, vol. 65, p. 250–257.
- Mansur, L. K., 1979. Irradiation creep by climb-enabled glide of dislocations resulting from preferred absorption of point defects. *Philosophical Magazine A*, 39(4), pp. 497-506.
- Mansur, L. K. & Reiley, T. C., 1980. Irradiation creep by dislocation glide enabled by preferred absorption of point defects—Theory and Experiment. *Journal of Nuclear Materials*, 90(1-3), pp. 60-67.
- Mardon J.P., Charquet D., Senevat J., 1994, Development of new zirconium alloys for PWR fuel rod cladding, *Proc. ANS Int. Topical Meeting on LWR Fuel Performance*, West Palm Beach, Florida, pp. 643-649.
- Martin, G. & Poirier, J. P., 1971. Considérations sur la relation entre le fluage sous irradiation et les dommages créés par l'irradiation en l'absence de contrainte. *J. Nucl. Mater.*, Volume 39, p. 93.
- Massoud J.P., Dubuisson P., Scott P., Ligneau N., Lemaire E., 2002, The effects of neutron radiation on materials for core internals of PWRs. A joint research program, Fontevraud 5, paper 62, p 417.
- Matthews, J. R. & Finnis, M. W., 1988. Irradiation creep models - An overview. *Journal of Nuclear Materials*, 159, pp. 257-285.
- McSherry, A. J., Patel, M. R., Marshall, J., & Gilbert, E. R., 1978, Irradiation creep in bending of CW AISI 316 at low fluence. *Transactions of the American Nuclear Society* 28, p. 146.

Michel, D. J., Hendrick, P. L., & Pieper, A. G., 1978. Transient irradiation-induced creep of nickel during deuteron bombardment. *J. Nucl. Mater.*, Volume 75, pp. 1-6.

Morize P., Baicry J. and Mardon J. P., 1987, Effect of Irradiation at 588K on Mechanical Properties and Deformation Behaviour of Zirconium Alloy Strip, *Zirconium in the Nuclear Industry: Seventh Int'l Symposium*, ASTM STP 939, R. B. Adamson and L. F. P. Van Swam, Eds., American Society for Testing and Materials, Philadelphia, 101-119.

Mosedale, D., 1962. Influence of Irradiation on Creep. *J. Appl. Phys.* 33 (10), p. 3142.

Mosedale, D., Lewthwaite, G. W. & Ramsay, I., 1972. Further creep experiments in the Dounreay fast reactor. Technical Report TRG-Report-2385; CONF-721115-5.

Mosedale, D., Harries, D. R., Hudson, J. A., Lewthwaite, G. W., & McElroy, R. J., 1977. Irradiation creep in fast reactor core component materials, In: *Conference on Radiation effects in breeder reactor structural materials*. Scottsdale, AZ, USA; 19 - 23 Jun 1977, pp. 209–218.

Mott, N. F., 1952. A theory of work-hardening of metal crystals. *The London, Edinburgh, and Dublin Philosophical Magazine and Journal of Science*, 43(346), pp. 1151-1178.

Nelson R. S., Hudson J. A. and Mazey D. J., 1972, The Stability of Precipitates in an Irradiation Environment, *J. Nucl. Mater.*, Vol. 44, pp. 318-330.

Neustroev V., Shamardin V., 2000, Irradiation creep of austenitic steels irradiated up to high damage dose. *Effects of radiation on materials : 19th international symposium ASTM STP 1366*, pp 645–654.

Nichols, F. A., 1969. Theory of the creep of zircaloy during neutron irradiation. *Journal of Nuclear Materials*, 30(3), pp. 249-270.

Nichols, F. A., 1970. On the mechanisms of irradiation creep in zirconium-base alloys. *J. Nucl. Mater.*, vol. 37, no. 1,, p. 59–70.

Nichols, F. A., 1979. On the SIPA contribution to radiation creep. *J. Nucl. Mater.*, Volume 84, p. 207.

Nichols, F. A., 1987. Mechanistic modeling of Zircaloy deformation and fracture in fuel element analysis. *Zirconium in the Nuclear Industry*, ASTM STP 939. ASTM International.

Nikolaenko, V.A., V.I. Karpukhin, V.N. Kuznetsov, P.A. Platonov, V.M. Alekseev, O.K. Chugunov, Y.I. Shtrombakh, V.D. Baldin, B.S. Rodchenkov, Y.I. Smirnov, A.V. Subbotin, Y.É. Khandomirov, and I.G. Lebedev, "Effect of the composition of radiation on the radiation damage to graphite", *Atomic Energy*, 87, (1999) 480-484.

Okamoto, P. R. & Harkness, S. D., 1973. Stress-biased loop nucleation in irradiated type 316 stainless steels. *J. Nucl. Mater.*, Volume 48, p. 204.

Oku, T., K. Fujisaki, and M. Eto, "Irradiation creep properties of a near-isotropic graphite", *Journal of Nuclear Materials*, 152, (1988) 225-234.

Oku, T., M. Eto, and S. Ishiyama, "Irradiation creep properties and strength of a fine-grained isotropic graphite", *Journal of Nuclear Materials*, 172, (1990) 77-84.

Pan, Z.L., Lawrence, S. St., Davies, P.H., Griffiths, M., Sagat, S., 2005, Effect of irradiation on the fracture properties of Zr-2.5Nb pressure tubes after irradiation to the end of design life, *Zirconium in the Nuclear*

Industry: 14th International Symposium, P. Rudling, B. Kammenzind, Eds., American Society for Testing and Materials, ASTM STP 1467, pp. 759-782.

Pakarinen, J., Tähtinen, S., & Singh, B. N. (2013). A comparative TEM study of in-reactor and post-irradiation tensile tested copper. *Journal of Nuclear Materials*, 442(1-3), S821-S825.

Perks, A. J. & Simmons, J. H. W., 1964. Radiation-induced creep in graphite. *Carbon*, 1(4), pp. 441-449.

Piercy, G. B., 1968. Mechanisms for the in-reactor creep of zirconium alloys. *Journal of Nuclear Materials*, 26(1), pp. 18-50.

Porter D., Hudman G, Garner F., 1991, Irradiation creep and swelling of annealing type 304L stainless steel at 309_c and high neutron fluence. *J. Nucl. Mater.*, Vol. 179-181, pp 581– 584.

Puigh, R.J., 1986, The in-reactor deformation of the PCA alloy, *Journal of Nuclear Materials*, Vol. 141–143, pp. 954-959.

Renault-Laborne, A. et al., 2016. Evolution of microstructure after irradiation creep in several austenitic steels irradiated up to 120 dpa at 320° C. *Journal of Nuclear Materials*, 475, pp. 209-226.

Roberts, A. C. & Cottrell, A. H., 1956. Creep of alpha uranium during irradiation with neutrons.. *Philosophical Magazine*, 1(8), pp. 711-717.

Saka, H., Kawamura, K. & Hashimoto, M., 1989. High-voltage electron microscopy observation of stress-induced preferential absorption of interstitials. *Philos. Mag. A*, Volume 59, p. 687.

Sarkar, A., J. Eapen, A. Raj, K.L. Murty, and T.D. Burchell, "Modeling irradiation creep of graphite using rate theory", *Journal of Nuclear Materials*, 473, (2016) 197-205.

Savino, E. J., 1977. Point defect-dislocation interaction in a crystal under tension. *Philos. Mag.*, Volume 36, p. 323.

Savino, E. J. & Tomé, C. N., 1982. Irradiation creep by stress-induced preferential attraction due to anisotropic diffusion (SIPA-AD). *J. Nucl. Mater.*, Volume 108 & 109, p. 405.

Schober, H. R., 1984. Polarizabilities of point defects in metals. *J. Nucl. Mater.*, Volume 126, p. 220.

Schoeck, G., 1958. Influence of Irradiation on Creep. *Journal of Applied Physics*, 29(1), pp. 112-112.

Séran J.L., Touron H., Maillard A., Dubuisson P., Hugot J., LeBoulbin E., Blanchard P., Pelletier M., 1990, The swelling behavior of titanium stabilized austenitic steels used as structural materials of fissils subassemblies in Phenix. ASTM STP 1046, pp 739–752.

Seran, J. et al., 1992. In: *Effects of Radiation on Materials: 15th International Symposium ASTM STP 1125*. Philadelphia, PA: American Society for Testing and Materials, p. 1209.

Siems, R., 1968. Mechanical interactions of point defects. *Phys. Stat. Sol.*, Volume 30, p. 645.

Simmons, J.H.W., "Radiation damage in graphite", *International Series of Monographs in Nuclear Energy*, Vol. 102, 1965, Oxford, New York, Pergamon Press.

Simonen, E. P. & Hendrick, P. L., 1979. Light ion irradiation-induced creep mechanisms in nickel. *J. Nucl. Mater.*, Volume 85 & 86, p. 873.

Simonen E. P., Garner F.A., Klymyshym N.A. and Toloczko M.B., Response of PWR Baffle-Former Bolt Loading to Swelling, Irradiation Creep and Bolt Replacement As Revealed Using Finite Element Modelling, Proc. 12th International Conference on Environmental Degradation of Materials in Nuclear Systems-Water Reactors, 2005.

Singh, B. N., Foreman, A. J. E. & Trinkaus, H., 1997. Radiation hardening revisited: role of intracascade clustering. *Journal of nuclear materials*, 249(2-3), pp. 103-115.

Singh, B. et al., 2004. Final Report on In-Reactor Tensile Tests on OFHC –Copper and CuCrZr Alloy, Roskilde, Denmark: Risø-R-1481(EN).

Skinner, B. C. & Woo, C. H., 1984. Shape effect in the drift diffusion of point defects into straight dislocations. *Phys. Rev. B*, Volume 30, p. 3084.

Soniak A., L'Hullier N., Mardon J.-P., Rebeyrolle V., Bouffioux P. and Bernaudat, C., Irradiation Creep Behaviour of Zr-base Alloys, Zirconium in the Nuclear Industry: 13th Int'l Symposium STP 1423, ASTM, pp. 837-862, 2002.

Stoller, R. E. & Odette, G. R., 1987. A composite model of microstructural evolution in austenitic stainless steel under fast neutron irradiation. ASTM International. In: *Radiation-Induced Changes in Microstructure: 13th International Symposium*. ASTM STP 955.

Stoller R.E., Grossbeck M.L. and Mansur L.K., 1992, A Theoretical Model of Accelerated Irradiation Creep at Low Temperatures by Transient Interstitial Absorption, 15th International Symposium on Effects of Radiation on Materials; ASTM STP 1125, pp. 517-529.

Straalsund, J., 1977. Irradiation creep in breeder reactor structural materials. s.l., In *Radiation effects in breeder reactor structural materials*, p. 191.

Tanigawa, H., Kohyama, A. & Katoh, Y., 1996. A modeling of radiation induced microstructural evolution under applied stress in austenitic alloys. *J. Nucl. Mater.*, Volume 239, p. 80.

Taylor, G. I., 1934. The mechanism of plastic deformation of crystals. Part I. - Theoretical. *Proceedings of the Royal Society of London. Series A*. 145(855), pp. 362-387.

Taylor, R. & Jeffs, A. T., 1966. The effect of irradiation on stress relaxation in Nimonic 80A. *Journal of Nuclear Materials*, 19(2), pp. 142-148.

Toloczko, M., Garner, F. & Eiholzer, C., 1994. Irradiation creep and swelling of the US fusion heats of HT9 and 9Cr-1Mo to 208 dpa at ~ 400°C. *Journal of Nuclear Materials*, vol. 212, p. 604.

Toloczko, M., Garner, F. & Eiholzer, C., 1998. Irradiation creep of various alloys irradiated at ~400C in the PFR and FFTF reactors. *Journal of Nuclear Materials*, Volume 258-263, pp. 1163-1166.

Toloczko, M. & Garner, F., 1999. In: *Effects of Irradiation on Materials: 18th International Symposium*. ASTM STP 1325. West Conshohocken, PA: American Society for Testing and Materials, p. 765.

Toloczko M., Garner F.A., 2002, Stress and temperature dependence of irradiation creep of selected FCC and BCC steels at low swelling, *Effects of Radiation on Materials*, ASTM STP 1447.

Toloczko, M. et al., 2004. Irradiation creep and swelling from 400 to 600C of the oxide dispersion strengthened ferritic alloy MA957. *Journal of Nuclear Materials*, Volume 329-333, pp. 352-355.

- Toloczko, M., Garner, F. & Maloy, S., 2006. In-reactor Creep of Two Heats of T91 from ~400C to 600C, Los Alamos: Los Alamos National Laboratory Technical Report.
- Toloczko, M., Garner, F. & Maloy, S., 2012. Irradiation creep and density changes observed in MA957 pressurized tubes irradiated to doses of 40-110 dpa at 400-750C in FFTF. *Journal of Nuclear Materials*, Volume 428, pp. 170-175.
- Tomé, C. N., Cecatto, H. A. & Savino, E. J., 1982. Point-defect diffusion in a strained crystal. *Phys. Rev. B*, Volume 25, p. 7428.
- Tomé C.N., So C.B., Woo C.H., 1993, Self-consistent calculation of steady-state creep and growth in textured zirconium, *Phil. Mag. A*, Vol. 67, pp. 917-930.
- Trinkaus, H., 1972. On the investigation of small dislocation loops in cubic crystals by diffuse X-ray scattering. *Phys. Stat. Sol. b*, Volume 54, p. 209.
- Trinkaus, H., 1975. Theory of polarization induced elastic interaction of point defects. Gatlinburg, Tennessee, USA, International conference on radiation damage in metals, p. 254.
- Tsang, D.K.L. and B.J. Marsden, "The development of a stress analysis code for nuclear graphite components in gas-cooled reactors", *Journal of Nuclear Materials*, 350, (2006) 208-220.
- Uehira, A., Mizuta, S., Ukai, S. & Puigh, R., 2000. Irradiation creep of 11Cr–0.5Mo–2W,V,Nb ferritic–martensitic, modified 316, and 15Cr–20Ni austenitic S.S. irradiated in FFTF to 103–206 dpa. *Journal of Nuclear Materials*, Volume 283, p. 396.
- Uehira A., Ukai S., Mizuta S., Puigh R., 2001, Irradiation creep deformation of modified 316 and 15Cr-20Ni base austenitic fuel elements irradiated in FFTF. *Effects of radiation on materials : 20th international symposium ASTM STP 1405*, pp 487–499.
- Varvenne, C. & Clouet, E., 2017. Elastic dipoles of point defects from atomistic simulations. *Phys. Rev. B*, Volume 96, p. 224103.
- Vattré, A. et al., 2016. Non-random walk diffusion enhances the sink strength of semicoherent interfaces. *Nat. Commun.*, Volume 7, p. 10424.
- Veringa, H.J. and R. Blackstone, "The irradiation creep in reactor graphites for HTR applications", *Carbon*, 14, (1976) 279-285.
- Walters, L. C., McVay, G. L. & Hudman, G. D., 1977. Irradiation-induced creep in 316 and 304L stainless steels. (No. CONF-770641-3). Argonne National Lab., IL (USA). Conference: Conference on radiation effects in breeder reactor structural materials, Scottsdale, AZ, USA, 19 Jun 1977
- Walters L.C. and Ruther W.E., 1977, In-reactor stress relaxation of Inconel X750 springs, *Journal of Nuclear Materials*, Vol. 68, pp. 324-333.
- Walters L., Bickel G. A., Griffiths M., 2015, The effects of microstructure and operating conditions on irradiation creep of Zr-2.5Nb pressure tubing, *Zirconium in the Nuclear Industry: 17th International Symposium*, R.J. Comstock, P. Barberis, Eds, ASTM International, West Conshohocken, PA, ASTM STP 1543, pp. 693-725.

- Walters L., Douglas S.R., Griffiths M., 2018, Equivalent radiation damage in zirconium irradiated in various reactors, *Zirconium in the Nuclear Industry: 18th International Symposium*, R. J. Comstock and A. T. Motta, Eds., ASTM International, West Conshohocken, PA, ASTM STP 1597, pp. 676–690.
- Was, G. S., 2007. *Fundamentals of Radiation Material Science*. New York: Springer.
- Wassilew, C., Ehrlich, K. & Bergmann, H.-J., 1987. Analysis of the in-reactor creep and rupture life behavior of stabilized austenitic stainless steels and the nickel-base alloy Hastelloy-X. s.l., *Influence of Radiation on Material Properties: 13th International Symposium (Part II)*. ASTM International., p. 30.
- Weertman, J., 1955. Theory of steady-state creep based on dislocation climb. *Journal of Applied Physics*, 26(10), pp. 1213-1217.
- Weertman, J., 1957. Steady-state creep through dislocation climb. *Journal of Applied Physics*, 28(3), pp. 362-364.
- Williams J., Spellward P, Walmsley J., Mager T., Koyama M., Mimaki H., Suzuki I., 1997, Microstructural effects in austenitic stainless steel materials irradiated in a pressurized water reactor. Eighth international symposium on environmental degradation of materials in nuclear power systems, pp 725–733.
- Wire, G., Straalsund, J., 1977, Irradiation induced stress relaxation previously irradiated 304 stainless steel in a fast flux environment. *J. Nucl. Mater.*, Vol. 64, pp. 254–264.
- Wolfer, W. G., Foster, J. P. & Garner, F. A., 1972. The interrelationship between swelling and irradiation creep. *Nucl. Technol.*, Volume 16, p. 55.
- Wolfer, W. G., 1975. Prediction of irradiation creep from microstructural data. *Scr. Metall.*, Volume 9, p. 801.
- Wolfer, W. G. & Ashkin, M., 1975. Stress-induced diffusion of point defects to spherical sinks. *J. Appl. Phys.*, Volume 46, p. 547.
- Wolfer, W. G. & Ashkin, M., 1976. Diffusion of vacancies and interstitials to edge dislocations. *J. Appl. Phys.*, Volume 47, p. 791.
- Wolfer, W. G., Mansur, L. K. & Sprague, J. A., 1977. Theory of swelling and irradiation creep. No. CONF-770641-7. Wisconsin Univ., Madison (USA). Dept. of Nuclear Engineering; Oak Ridge National Lab., TN (USA); Naval Research Lab., Washington, DC (USA). Conference on radiation effects in breeder reactor structural materials, Scottsdale, AZ, USA, 19 Jun 1977.
- Wolfer, W. G., 1980. Correlation of radiation creep theory with experimental evidence. *J. Nucl. Mater.*, Volume 90, p. 175.
- Woo, C. H. & Gösele, U., 1983. Dislocation bias in an anisotropic diffusive medium and irradiation growth. *J. Nucl. Mater.*, Volume 119, p. 219.
- Woo, C. H., 1984. Irradiation creep due to elastodiffusion. *J. Nucl. Mater.*, Volume 120, p. 55.
- Woo, C. H. & Puls, M. P., 1985. PODSIP: a computer program for the evaluation of point-defect properties in metals. No. AECL--8392. Atomic Energy of Canada Ltd.

- Woo, C. H., 1988. Theory of irradiation deformation in non-cubic metals: effects of anisotropic diffusion. *Journal of Nuclear Materials*, 159, pp. 237-256.
- Woo, C. H., Garner, F. A. & Holt, R. A., 1993. Irradiation creep due to SIPA under cascade damage conditions. *Effects of Radiation on Materials: 16th Int. Symp. ASTM STP 1175*. ASTM International, p. 27.
- Woo, C. H., 1995. Correlation between void swelling and SIPA creep. *J. Nucl. Mater.*, Volume 225, p. 8.
- Woo C. H., Causey A.R., Holt R.A., 1999, Methods of analysis and measurement of irradiation creep in non-cubic metals, *Phil. Mag. A*, Vol. 79, pp. 59-84.
- Woo, C.H., So, C.B., 2000, Effect of stress on point defect diffusion in HCP metals and irradiation creep, *Phil. Mag. A*, Vol. 80, pp. 1299-1318.
- Xu, C. & Was, G., 2014. Anisotropic dislocation loop distribution in alloy T91 during irradiation creep. *Journal of Nuclear Materials*, Volume 454, pp. 255-264.
- Xu, C. & Was, G. S., 2015. Proton irradiation creep of FM steel T91. *J. Nucl. Mater.*, Volume 459, p. 183.
- Yvon, P. & Carré, F., 2009. Structural materials challenges for advanced reactor systems.. *Journal of Nuclear Materials*, 385(2), pp. 217-222.
- Zinkle, S. J., 1992. Anisotropic dislocation loop nucleation in ion-irradiated MgAl₂O₄. *Journal of nuclear materials*, 191, pp. 645-649.
- Zinkle, S. J. M. P. J. & Stoller, R. E., 1993. Dose dependence of the microstructural evolution in neutron-irradiated austenitic stainless steel. *Journal of Nuclear materials*, 206(2-3), pp. 266-286.
- Zuppiroli, L. et al., 1977. Fluage de molybdène sous irradiation par les fragments de fission à 20 K. *Philos. Mag.*, Volume 35, p. 853.